
# DENSITY FUNCTIONAL THEORY STUDY OF COPPER ZINC TIN SULPHIDE ($Cu_2ZnSnS_4$) DOPED WITH CALCIUM AND BARIUM

By

MLOTSHWA THOKOZANE MXOLISI

(11628059)

**DISSERTATION**

PRESENTED IN FULFILMENT FOR THE REQUIREMENTS OF THE MASTER OF SCIENCE (M.Sc.) DEGREE

IN

**PHYSICS**

SCHOOL OF MATHEMATICAL AND NATURAL SCIENCES

AT THE

**UNIVERSITY OF VENDA**

SUPERVISOR: DR N.E. MALUTA (UNIVEN)

CO-SUPERVISORS: PROF R.R. MAPHANGA (CSIR)

: DR J.K. KIRUI (UNIVEN)

YEAR: 2020

## Declaration

I, Mlotshwa Thokozane Mxolisi, declare that the dissertation titled “Density functional theory study of copper zinc tin sulphide ($Cu_2ZnSnS_4$) doped with calcium and barium” for the Master of Science degree in Physics at the University of Venda hereby submitted by me has not been previously submitted for a degree at this or any other university. I further declare that it is my own work in design and in execution and that all referenced material contained therein have been duly acknowledged.

Signed by  at_THOHOYANDOU on the 24 day of August__2020

## Dedications

I would like to dedicate this dissertation to my family more especially my parents, Busisiwe and Jacob Mlotshwa, not forgetting my siblings Thembi, Sonto, Sfiso, Sphesihle, Mduduzi and Zanele for their continuous patience and support as I carry on with my studies. Lastly my lovely niece and nephews, Tsepiso, Palisa, Nhlanhla, Thabiso and Amahle:

## Acknowledgements

I would like to acknowledge the University of Venda and the department of Physics for granting me the opportunity to continue with my studies. My supervisor, Dr NE Maluta for his continuous guidance and supervision, not forgetting my co-supervisors Prof RR Maphanga and Dr JK Kirui for their valuable inputs. My lab co-workers for their tireless efforts during discussions. I would also like to acknowledge financial support from the National Research Foundation (NRF) and UNIVEN through the directorate of research and innovation.

## Abstract

The sun is the most important source of renewable energy today. Producing energy from sunlight using cheap, abundant and non-toxic materials is considered a major challenge in the field of solar-electrical energy conversion. Fossil fuel combustion, depletion of non-renewable sources, global warming and environmental degradation are some of the push factors towards clean, non-toxic and environmentally friendly methods of producing electrical energy. To harvest solar energy, a thin film solar cell composed of the $Cu_2ZnSnS_4$ (CZTS) semiconductor is a candidate, which can harvest useful amounts of energy. Some of its advantages are the optical direct band gap and high absorption coefficients. In this study, CZTS is investigated as a material for solar cells using first principle method. Thus, structural, electronic and optical properties of pure CZTS and doped CZTS (112) surface were investigated using the density functional theory as implemented in the Cambridge Serial Total Energy Package code. Alkali earth metals, Calcium (Ca) and Barium (Ba) were adsorbed on the CZTS (112) surface using the adsorption locator module. The results suggest that doping with barium rather than calcium could improve the photocatalytic activity on the CZTS based solar cells. Doping using different elements yielded improved optical and electronic properties of the CZTS based solar cells.

**Key words:** $Cu_2ZnSnS_4$, density functional theory, electronic properties, optical properties, doped and undoped $Cu_2ZnSnS_4$

# Contents

## List of abbreviations

| | | |
|---|---|---|
| Ba | - | Barium |
| BIPV | - | Building Integrated Photovoltaic |
| CASTEP | - | Cambridge Serial Total Energy Package |
| Ca | - | Calcium |
| CBM | - | Conduction Band Minimum |
| CdTe | - | Cadmium Telluride |
| $CO_2$ | - | Carbon Dioxide |
| CO | - | Carbon Monoxide |
| CIGS | - | Copper Indium Gallium Selenide |
| CZTS | - | Copper Zinc Tin Sulphide |
| DFT | - | Density Functional Theory |
| DOS | - | Density of States |
| GGA | - | Generalized Gradient Approximation |
| GGA+U | - | Generalized Gradient Approximation with Hubbard Potential |
| HSE | - | Heyd-Scuseria-Ernzerhof |
| HEG | - | Homogenous Electron Gas |
| LDA | - | Local Density Approximation |
| Na | - | Sodium |
| OPVC | - | Organic Photovoltaic Cell |
| PCE | - | Power Conversion Efficiency |
| PV | - | Photovoltaic |

| | | |
|---|---|---|
| SAREC | - | South African Renewable Energy Council |
| STASA | - | Solar Thermal Association of South Africa |
| SAPVIA | - | South African Photovoltaic Association |
| SASTELA | - | Southern Africa Solar Thermal and Electricity Association |
| SAWEA | - | South African Wind Energy Association |
| SESSA | - | Sustainable Energy Society of Southern Africa |
| UV | - | Ultra-violet |
| VASP | - | Vienna Ab-initio Simulation Package |
| VBM | - | Valence Band Maximum |
| $V_{Cu}$ | - | Vacancies of copper |
| WZ-KT | - | Wurtzite-derived Kesterite |
| WZ-ST | - | Wurtzite-derived Stannite |
| ZB-KT | - | Zincblende-derived Kesterite |
| ZB-ST | - | Zincblende-derived Stannite |
| $Zn_{Cu}$ | - | Zinc replacing copper |

## List of figures

## List of tables

# CHAPTER ONE

## 1. Introduction

### 1.1. Renewable energy

Renewable energy is energy that is collected from renewable resources that are naturally restored on a human timescale. The most emerging renewable sources of energy are wind, solar and hydroelectricity. These energy sources will always be available for utilization by human activities because they are re-occurring over a period of time [1]. Renewable energy plays an important role in reducing greenhouse gas emissions. Currently, in South Africa there is only one major provider of electricity that we all depend upon and that is using fossil fuels such as coal. Diversifying energy supply will bring competition in the market and thus resulting in lower costs of electrical energy while providing alternatives to the energy supply.

Industries, factories, power plants, various government institutions, scientific institutions and private organizations are growing vastly based on available natural energy sources. Conventional energy sources based on oil, coal and natural gas have proven to be highly effective drivers of economic progress but at the same time polluting the environment and damaging human health. These traditional fossil fuel-based energy sources are facing increasing pressure from a host of environmental conversation, with the most serious challenge confronting the future use of coal being the Kyoto protocol greenhouse gas reduction targets [2]. Currently, a wide range of strategies are implemented in different countries to increase the share of electricity from renewable energy sources [3]. Hence, developed countries are searching for new alternative energy sources to minimize the pressure on natural sources such as gas, oil, coal, etc. [4].

Reducing energy consumption and protecting the environment have gradually gained attention from countries worldwide. To keep sustainable development, governments, research institutes and industries have been working on the problems caused by the shortage of available energy sources. It is well known that the best way is to exploit renewable energy resources. The potential of renewable energy sources is enormous

as they can in principle meet many times the world's energy demand. The development and use of renewable energy sources can enhance diversity in energy supply markets, contribute to securing long term sustainable energy supplies, help reduce local and global atmospheric emissions, provide commercially attractive options to meet specific energy service needs particularly in developing countries and rural areas hence helping to create new employment opportunities there [2].

In general, renewable energy is more expensive to produce and use than fossil fuel energy. Favorable renewable resources are often located in remote areas and it can be expensive to build power lines from the renewable energy source to the cities that need electricity. Renewable sources are not always available, clouds reduce electricity from solar plants, days with low wind reduce electricity from wind farms and drought reduce the water available for hydropower. However, coming up with cheaper, efficient and easy technology could solve the problem.

### 1.1.1. Types of renewable energy sources

There are many forms of renewable energy: most of them depend in one way or another on sunlight. Different types of technologies are used in many ways to harvest energy from renewable sources. The types of renewable energy include geothermal, hydropower, solar energy, tidal power, wave power and wind power.

### 1.1.2. Solar energy

Solar energy is the radiant energy emitted by the sun, it is created by nuclear fusion that takes place in the sun and about $3.86 \times 10^{26}$ Watts of energy is produced [5]. This energy is harnessed using a range of ever-evolving technologies such as solar heating, photovoltaics and solar thermal energy. Solar energy is inexhaustible and it has already been theoretically and experimentally proven that the earth would not be polluted if solar energy was utilized effectively [6]. The sun (source of earth's solar power) is the most important source of renewable energy today, producing energy from sunlight using cheap, abundant and non-toxic materials is considered a major challenge in the field of solar-electrical energy conversion. Solar energy is freely available, and it is used by almost all forms of life on earth. Silicon solar cell technology is presently the most widely

used technology in commercial solar cells capturing more than 80% of the photovoltaic market; however high efficiency silicon solar cells require single crystal silicon wafers that are quite expensive [7]. The thin film technology is taking some market share from the dominant silicon wafer technology. Solar cells are regarded as one of the key technologies towards a sustainable energy supply and a solution to the energy crisis.

### 1.1.3. South African solar energy development

South Africa has introduced a policy document known as white paper on renewable energy to ensure that the implementation of renewable technologies is a practical aspect. The purpose of white paper on renewable energy is to set out government's principles, goals and objectives for renewable energy. It further commits government to a number of enabling actions to ensure that renewable energy becomes a significant part of its energy portfolio over the next ten years [8].

There are number of organisations that seek to ensure the implementation of renewable energy technologies, for example South African Renewable Energy Council (SAREC) whose main objectives includes the removal of barriers to the development of renewable energy. Other organizations include the Solar Thermal Association of South Africa (STASA), South African Photovoltaic Association (SAPVIA), South African Wind Energy Association (SAWEA), Sustainable Energy Society of Southern Africa (SESSA) and the Southern Africa Solar Thermal and Electricity Association (SASTELA) [9]. Renewable energy in South Africa has the potential to create thousands of long-term sustainable jobs in manufacturing, installation as well as maintenance and ensure energy security in the future.

Eskom generates 95 % of the electricity used in South Africa and 45 % of the electricity used in Southern Africa [10]. Figure 1 illustrate the sources of energy supply in South Africa, which shows that about 70 % of energy comes from coal. Most areas in South Africa average more than 2500 hours of sunshine per year and average daily solar radiation levels ranging between 4.5 kWh/m$^2$ and 6.5 kWh/m$^2$ in one day. The Southern African and in fact the whole of Africa has sunshine all year around. The annual 24-hour global solar radiation average is about 220 W/m$^2$ for South Africa [10].

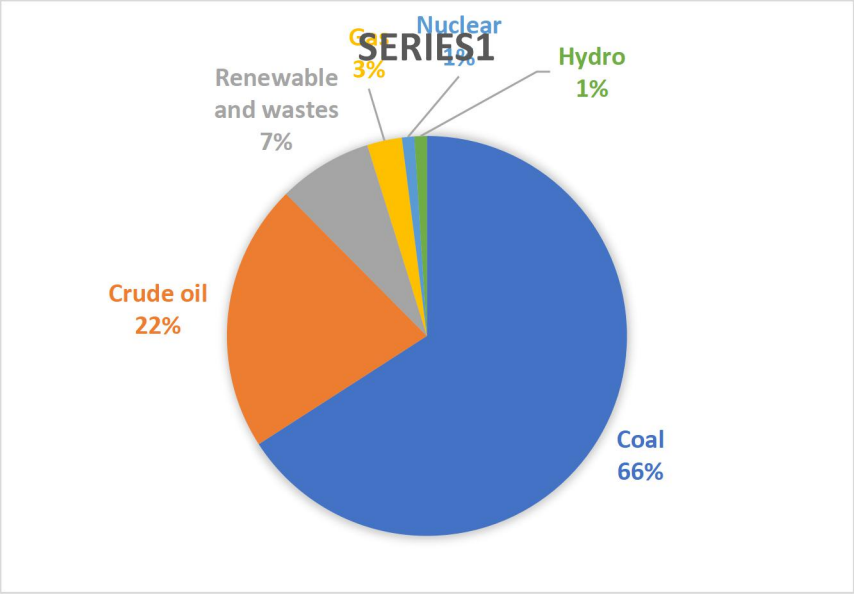


Figure 1. South African energy supply sources [10].

Currently, the dominating energy supply source in SA is using coal, bringing problems to the environment as it releases more carbon dioxide ($CO_2$), which is a greenhouse gas that is partly responsible for global warming. Carbon monoxide (CO) may also be released during the combustion of coal, which is toxic to human if inhaled. The use of renewable sources releases none of the harmful gases to both the human and environment. Essentially, renewable sources are all environmentally friendly, sustainable and reliable. A material that can be able to exploit the availability of renewable sources should be affordable, abundant, environmentally friendly and reliable to be able to compete with the current dominant energy supplying sources. Hence, it is important to develop renewable technologies to be able to produce affordable clean energy.

### 1.1.4. Barriers to renewable energy

There are many factors preventing the development of renewable energy in South Africa and developing countries. Some of the factors may arise due to political influence and economical status of the country in general. The key issues include the following [11]:

- Many renewable energy technologies remain expensive compared to the current dominant energy supply method.
- Implementation of renewable energy technologies needs significant initial investment and support for a long period before reaching profitability.
- There is a lack of consumer awareness on benefits and opportunities of renewable energy.
- Current renewable energy technologies have very low efficiencies compared to their capabilities and it is not enough to supply on the national electricity grid.
- Currently installed solar panels are suffering from degradation and a short period of optimal performance of their lifespan due to materials unable to withstand harsh weather conditions such as wind, heat, etc. leading to module failure.

Although renewable energy technologies often have very high investments costs, their operation and maintenance costs are generally lower than conventional fossil based energy technologies [8]. The African continent has an abundance of renewable energy resources; hence it is vitally important that the resources are used optimally.

Renewable energy sources have not reached their full potential for energy production and sustainability. Photovoltaic (PV) solar cells have the potential to be the largest contributor to the renewable energy sources as the most of South Africa has long sunshine hours and hot climate regions. They have the potential to improve up to their maximum optimal level based on material development and modifications.

### 1.2. Photovoltaic cell

A photovoltaic cell (PV) is an electrical device that converts the energy of light directly into electricity by the photovoltaic effect. It is defined as a device whose electrical properties such as current and resistance vary when exposed to light. It is the direct conversion of sunlight using panels or collectors. Photoelectric effect causes the materials to absorb photons of light and release electrons, when these electrons are captured, the resulting electric current can be used as electricity. PV systems are capable of directly converting sunlight into electrical energy. The theoretical conversion

efficiency of PV systems is relatively higher than other power generators and they do not contain movable parts, they can work continuously free from maintenance longer than other power generation technologies [12].

### 1.2.1. Working principle of PVs

Light is made up of packets of energy called photons. When they hit a solid surface, they excite the electron bound into solid up to a higher energy level in which they are freer to move but these electrons relax and come back to the ground state after dissipating the energy. Light shining on the PV cell produces both a current and a voltage to generate electric power. This process requires firstly, a material in which the absorption of light raises an electron to a higher energy state and secondly the movement of this higher energy electron from the solar cell into an external circuit. The electron then dissipates its energy in the external circuit and returns to the solar cell [12].

A variety of materials and processes can potentially satisfy the requirements for photovoltaic energy conversion but in practice nearly all photovoltaic energy conversion uses p-n junction semiconductor materials. When light energy strikes, the solar cell shown in Figure 2, electrons are knocked loose from the atoms in the semiconductor material. If electrical conductors are attached to the positive and negative sides, forming an electric circuit, the electrons can be captured in the form of an electric current. Electrons are the only moving parts in a solar cell, at the end they all go back to where they came from [13].

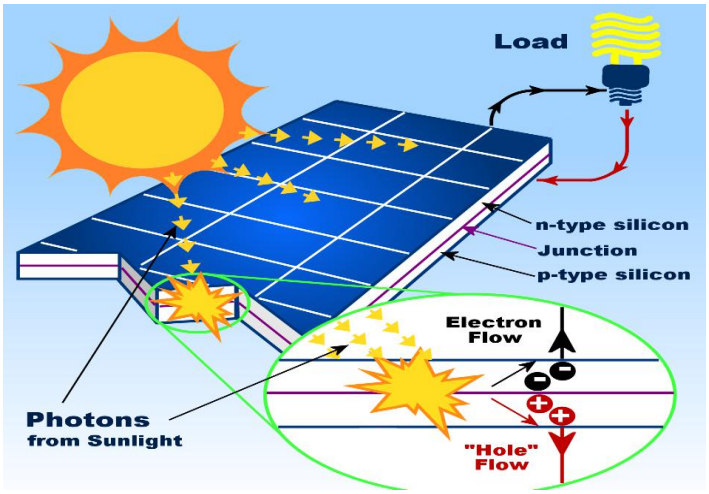


Figure 2. Diagrammatic representation of the working principle of PV cells [14].

When light shines on a PV cell, it may be reflected, absorbed or pass right through it. The PV cell is composed of semiconductor material, which combines some properties of metals and those of insulators. That makes it uniquely capable of converting light into electricity. When light is absorbed by the semiconductor, photons of light can transfer their energy to electrons, allowing the electrons to flow through the material as electrical current. The current flow out of the semiconductor to metal contacts and then makes its way out to the electric grid.

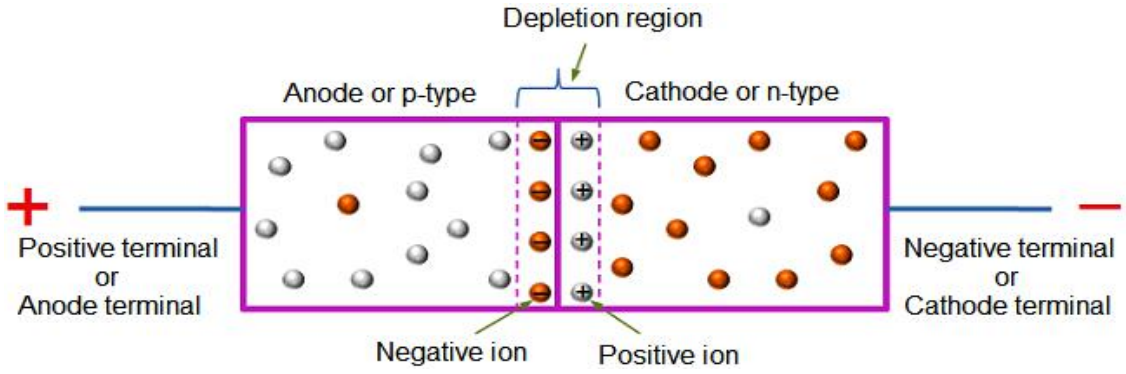


Figure 3. Working principle of a p-n junction in solar cells like silicon solar cells [15]

Most common PV devices use a single junction or interface to create an electric field within a semiconductor such as a PV cell. In a single-junction PV cell, only photons

whose energy is equal or greater than the band gap of the cell material can free an electron for an electric circuit as depicted by Figure 3. The photovoltaic response of single-junction cells is limited to the portion of the sun's spectrum whose energy is above the band gap of the absorbing material and lower energy photons are not used. The most efficient solar cell yet still only converts 46 % of the available sunlight to electricity and most commercial systems are currently converting between 15 and 26 % [13]. To increase efficiency, a material which has proper band gap needs to be used and to ensure full absorption of photon, the use of anti-reflective material on the solar cell is required.

The merits of photovoltaics are countless some of which being that it is silent and renewable. Ideal PV system for developing countries needs to employ solar panels with very low production cost, high efficiency and a good design that enables easy and low-cost installation. Very low production cost and limited lifetime may give similar results as higher production cost and very long lifetime. Depending on the site for the photovoltaic installation, different amounts of energy could be produced. Amount of electric energy depends both on the latitude of the installation as well as on the microclimate, tilt angle and possible shadowing problems [13].

### 1.2.2. Types of PV technologies

Solar cell technologies are traditionally divided into four generations, namely; first, second, third and fourth generation solar cells. There are several types of semiconductor technologies currently in use for PV solar panels.

#### 1.2.2.1. First generation

The first generation of PV cells are made from silicon. Single crystalline silicon is called monosilicon while the polycrystalline silicon is called polysilicon. Beginning in 2006, over half of the world's supply of polysilicon was being used for production of solar panels. Monosilicon has higher efficiency and thus higher cost. Crystalline silicon devices have theoretical limiting efficiency of about 29 % and can achieve an energy pay-back of 1-2

years. Most low-end manufactures are producing PV cells with efficiency of 7-8 %. They are rigid and require a lot of energy in production [16].

#### 1.2.2.2. Second generation

The second-generation PV cells apply amorphous, procrystalline and nanocrystalline (black silicon on glass) to a plastic or metal surface by chemical vapour deposition. Thin film silicon is opposed to wafer silicon (also called bulk or crystalline silicon) by making use of amorphous silicon. Overall thin film solar cells have lower efficiency and are less expensive than crystalline silicon. Most thin film cell technology have an efficiency of 12-20 %. State of the art thin film cells can reach an efficiency of 10-16 % with the highest reported efficiency being 18 % [17].

Thin film technology has been developed for building integrated photovoltaic (BIPV). These are semi-transparent solar cells that can be applied as window glazing thus, BIPV technology can be used for window tinting while generating electricity. However, as the production of second generation solar cells still include vacuum processes and high temperature treatments, there is still a large energy consumption associated with the production of these solar cells [18]. The copper zinc tin sulphide ($Cu_2ZnSnS_4$), also known as CZTS based thin film solar cell is a second-generation photovoltaic solar cell and is shown in Figure 4. With its many advantages, such as environmentally friendly and largely available materials on the earth surface, it thus becomes one of the promising solar cell technologies. CZTS material has attracted researchers in recent years and is investigated extensively to improve its efficiency.

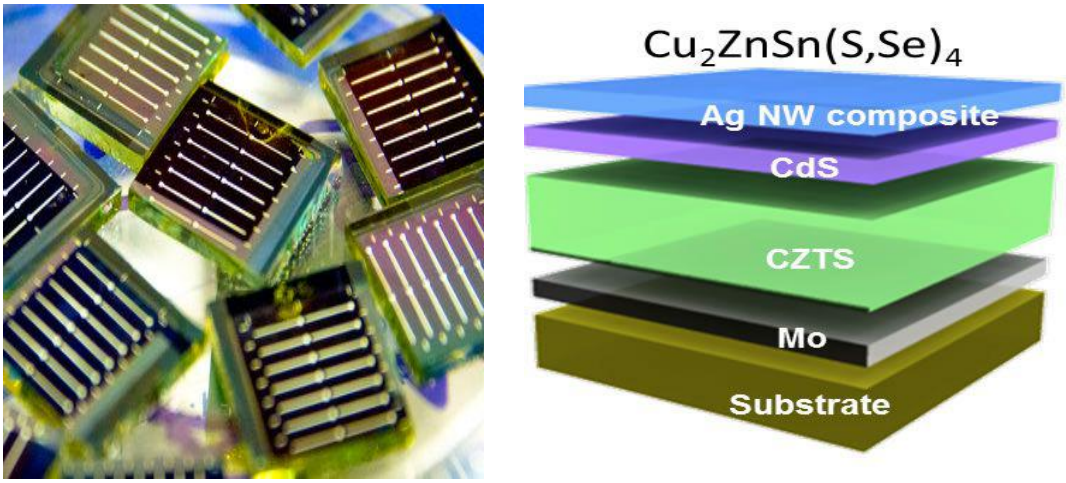


Figure 4. Thin film photovoltaic cells [18] with an indication of its layers on the right [19]

#### 1.2.2.3. Third generation

The third-generation PV cell technology uses organic, electronic conductive polymers or small molecules for light absorption and electric charge transport. The benefits are low cost and large-scale production capability with flexibility. The disadvantages are low efficiency, low stability and low strength compared to traditional non-organic PV cells. For the most part, organic photovoltaic cells (OPVCs) are still not ready for mass commercialization. In 2009, about 85 % of the PV solar cell market was dominated by crystalline silicon cells while only 15 % was represented by thin film solar cells [20].

#### 1.2.2.4. Fourth generation

The fourth generation of PV technology was introduced to combine the low cost, flexibility of polymer thin films with the stability of novel inorganic nanostructures with the aim of improving the optoelectronic properties of the low-cost thin film PVs. These devices architectures are meant to maintain the inexpensive nature of a solution processable PV structure while incorporating inorganic components to improve on energy harvesting cross-sections, the charge dissociations and charge transport within the PV cells [20].

## 1.3. Copper zinc tin sulphide

The quaternary chalcogenide $Cu_2ZnSnS_4$ gained attraction as a prospective absorber material for thin film photovoltaic applications in recent years. As it consists merely of earth-abundant, non-toxic environmentally friendly and low-cost elements, it would be a suitable alternate to other chalcogenide-based absorber materials such as CdTe or CIGS that are currently used in thin films. It is a direct band gap p-type semiconductor with an optical band gap energy value of 1.5 eV which fits well the solar irradiation spectrum and is almost equal to the optimal band gap energy of 1.45 eV with very small differences for solar cell materials [21].

Semiconductors with direct band gap are characterized by a high absorption coefficient in the relevant energy range for photovoltaics, most of the sunlight is absorbed within a small range beneath the surface and thus the need to fabricate thin film solar cells. In addition, CZTS has a high absorption coefficient above $10^{-4}$ $cm^{-1}$, which is sufficient for light absorption in thin film solar cells. The intrinsic p-type conductivity of CZTS makes it an ideal absorber material in solar cells due to the fast transfer of photo-generated holes at the front of illuminated side [22]. Up to now record efficiencies of CZTS-based thin films reached values up to 8.4 %. The conversion efficiency of CZTS reported so far is relatively low, yet compared to the currently used chalcopyrite materials, efficiencies are significantly lower [23, 24].

The wide application of CZTS cells is restricted because their photoelectric conversion efficiency is still much lower than that of chalcopyrite cells although their theoretical conversion can be as high as 32.2 %. CZTS-based thin film solar cells generally have multi layered structure of glass/Mo/CZTS/CdS/ZnO. Material CdS is an n-type semiconductor with a band gap of 2.4 eV and has always been used as the buffer layer for CZTS-based solar cells. To enhance the quality and the efficiency of CZTS thin film photovoltaics it is necessary to gain a deeper insight into the absorber material.

### 1.3.1. CZTS development

CZTS was first discovered in 1966 and was later shown to exhibit the photovoltaic effect in 1988 [25]. The first CZTS-based thin film solar cells with an efficiency of 0.66 % were reported in 1997 [26]. Shimada *et al*. fabricated the Cu/Sn/Zn stacked precursor by the deposition method and Cu/SnS/ZnS stacked precursor by sputtering technique. Using these precursors, they prepared CZTS thin films and reported the cell conversion efficiency of 4.02 % and 2.69 %, respectively [27]. The solar cell efficiency was increased to 5.7 % in 2005 by optimizing the deposition process.

Since then, numerous synthesis approaches have been implemented to fabricate the CZTS precursors including electroplating deposition, sol-gel, magnetron sputtering, thermal evaporation etc. To date, the best efficiency of CZTS-based thin film solar cells is up to 8.4 % by thermal evaporation technique [28]. Very recently, a CZTS thin film solar cell with a conversion efficiency of 9.2 % was reported, which is the new efficiency record for such solar cells [29]. Through knowledge of basic properties, synthesis and growth mechanisms, CZTS will be a priority and guarantee for the excellent photo-electronic performance.

### 1.3.2. CZTS structural aspects

The low cost, harmless CZTS-based thin film solar cells are composed of abundant materials. CZTS film possesses promising characteristic for optical properties, i.e. band-gap energy of about 1.5 eV and large absorption coefficient in the order of $10^4$ $cm^{-1}$. All constituents of CZTS film (copper, zinc, tin and sulphur) are naturally occurring and non-toxic. Therefore, using CZTS film as an absorber of solar cells will result in natural resource preservation and reduce environmental pollution [27].

The CZTS structure has copper (Cu) atoms placed in two separate positions, 2a (0, 0, 0) and 2c (0, 0.5, 0.25). Zinc (Zn) atoms placed at position 2d (0.5, 0, 0.25), tin (Sn) atom at position 2b (0.5,0.5,0) and sulphur (S) in position 8g (0.7560, 0.7566, 0.8722) [30]. CZTS appears to exist in two phases, i.e. kesterite (a sulphide mineral with a formula $Cu_2(Zn,Fe)SnS_4$) and stannite (a sulphide of copper, iron, and tin), with kesterite being the more stable phase than the stannite phase.

## 1.4. CZTS for application in PVs

CZTS is a very good alternative as an absorber layer for thin film solar cells to CIGS which are known for their optimal efficiencies but containing toxic and expensive materials such as indium and gallium [31]. An improved power conversion efficiency of 9.6 % has been demonstrated for CZT(S, Se) solar cells using hydrazine based precursor solutions for its preparation in experimental studies [31]. Better understanding of the properties of CZTS is encouraged by improving efficiencies and has drawn interest in the development of these cells through experimental and theoretical means. This study seeks to investigate photovoltaic properties of CZTS material using computer modelling techniques for application in solar cells.

## 1.5. Factors affecting conversion efficiency of solar cells

Not all the sunlight that reaches a PV cell is converted into electricity, most of it is lost due to multiple factors such as reflectivity and scattering, which must be considered when designing solar cells to achieve higher efficiencies [32]. Factors affecting the conversion efficiency of solar cells include wavelengths of sunlight reaching the earth's surface, electron recombination therefore cancelling out their contributions to the electrical current, temperature as solar cells generally work best at low temperatures and reflection [33]. A cell's efficiency can be increased by minimizing the amount of sunlight reflected away from the cell's surface i.e. untreated silicon reflects more than 30 % of incident light. Anti-reflection coatings and textured surfaces help decreases reflection. A high efficiency cell will appear dark blue or black.

## 1.6. The solar spectrum

The sun releases solar energy or sunlight by electromagnetic waves over a wide range of wavelengths, known as the solar spectrum. In a solar cell preparation, different layers are stacked together to form a complete solar cell. Each layer is used to absorb specific wavelength of light while allowing others to pass through to be collected further down. Most of the solar energy falling on earth has wavelengths of 250 nm to 2500 nm [34].

The visible spectrum, which is the portion of the electromagnetic spectrum that is visible to the human eye lies between wavelengths ranging from 380 nm -740 nm as indicated by solar spectrum in Figure 5. On the right of the visible region, there are shorter wavelengths and on the left there are longer wavelengths. The spectral energy distribution of solar light has a maximum value in the visible region.

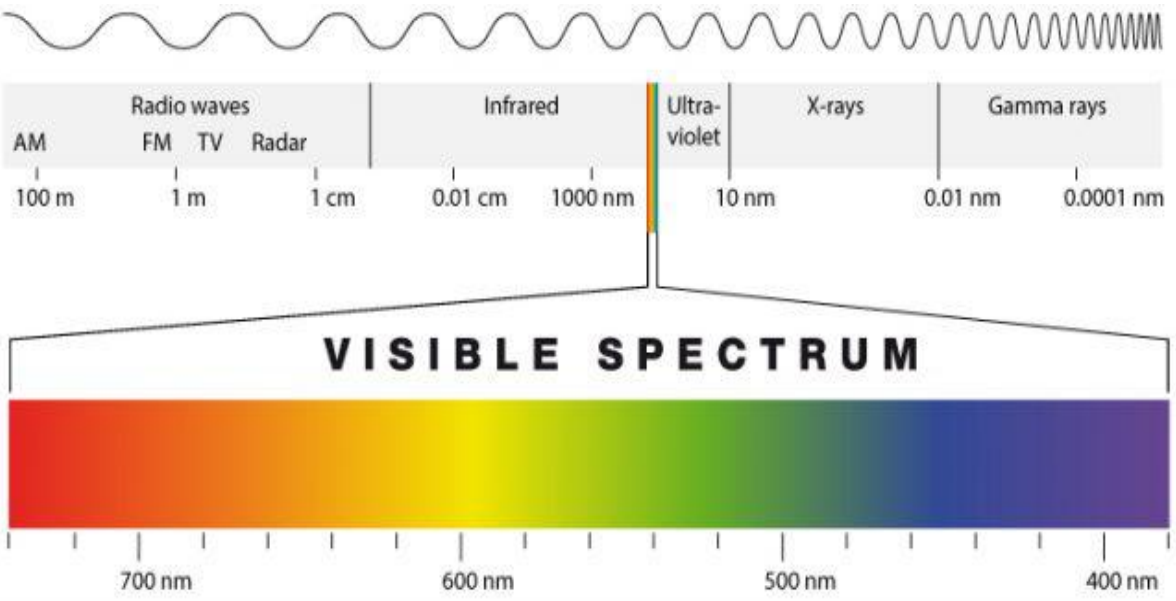


Figure 5. The solar spectrum wavelengths classifications [35].

Light having energy more than the band gap of semiconductors produce electron-hole pairs and hence desirable for photovoltaic application. If the semiconductor has band gap in the energy range of visible light, infrared region will not be useful for photovoltaic application [21].

### 1.7. Objectives of the study

The objectives of this study were to:

- develop models for undoped and doped CZTS systems
- determine the convergence parameters for the systems
- calculate structural properties of the system by geometrically optimizing the CZTS systems

- perform calculations of electronic properties for Ba and Ca and undoped CZTS (i.e. density of states and band structure)
- calculate optical properties for the CZTS systems i.e. absorbance, reflectivity, conductivity, dielectric function, refractive index and loss function.

# CHAPTER TWO

## 2. Literature review

### 2.1. Copper zinc tin sulphide

The quaternary CZTS is a promising material for the thin film solar cell application [11]. It has been intensively examined as an alternative PV material due to its similarity in material properties with CIGS, which has reached the conversion efficiency of 20 % and its relative abundance of raw materials. Although GIGS has reached a very high

efficiency amongst thin film solar cells, it contains expensive materials (indium and gallium) and the band gap is usually not optimal, hence there is a strong desire to discover novel, high efficiency, low cost solar cell absorber materials to replace GIGS [36]. CZTS is a compound semiconductor of $(I_2)(II)(IV)(VI_4)$ with a high absorption coefficient (>104 $cm^{-1}$) and a desirable band gap (  1.45 eV), it is considered an excellent PV material. The cost of raw materials for CZTS PV technology is much lower than that of the existing thin film PV technologies. Theoretical calculations have shown that conversion efficiency as high as 32 % was possible for CZTS thin film solar cell, with a CZTS layer of several micrometres [37].

In addition, CZTS as a promising candidate for efficient solar cell materials, it inherits all the merits of CIGS and has other significant features such as only being composed of abundant, non-toxic and economic elements in the earth crust [26, 38]. CZTS film has gained much interest in recent years since its optical property is optimum for photovoltaic application. Current thin film technologies are not as effective as crystalline silicon, but they are cheaper to manufacture and have several other important advantages as well and they include good performance in incident light, less sensitive to temperature related efficiency reduction and can be flexible.

The main advantage with CZTS is the high absorption coefficient for the solar spectrum, it's added advantage is the ability to tune the band gap to make an optimum match to the solar spectrum [40]. It is self-doped through the formation of intrinsic defects vacancies or point defects, these defects are formed during the growth of CZTS. Its formation energy of acceptor is lower than the donor defects [41].

Initial attempts to fabricate photovoltaic devices with $Cu_2ZnSnS_4$ or $Cu_2ZnSn(S,Se)_4$ thin films led to promising results with the efficiencies of up to 6.7 % and 9.66 % [31]. The vacancy formation energies are larger in the CZTS compared with the corresponding vacancies in the $Cu_2ZnSnSe_4$ [42]. In CZTS a temperature dependent phase transition from the kesterite (tetragonal) type structure to the cubic structure occurs at ~876 ℃, which was shown by in-situ high temperature diffraction experiments using synchrotron X-rays [43]. It was reported that to fabricate CZTS-based solar cells, the grain growth is

one of the key points for further efficiency improvements and doping CZTS films is an effective way to achieve this purpose. It was reported that the enhancement of the grain growth, improvement of the crystalline and electrical conductivity of the CZTS films can be achieved by adjusting the concentration of dopants [44].

The basic substance of a photovoltaic cell shown in Figure 6 is the semiconductor materials. The doped semiconductor develops an excess of free electrons (usually called n-type material) or develops vacancies (called holes) giving rise to a p-type material. These n-type and p-type materials combine to form a photovoltaic cell. During the absence of light, a very small number of atoms is excited and move across the junction. This causes a small voltage drop across the junction. In the presence of light, more atoms are excited and flow through the junction and cause a large current at the output. This current can be stored in a rechargeable battery and used for several applications based on requirement.

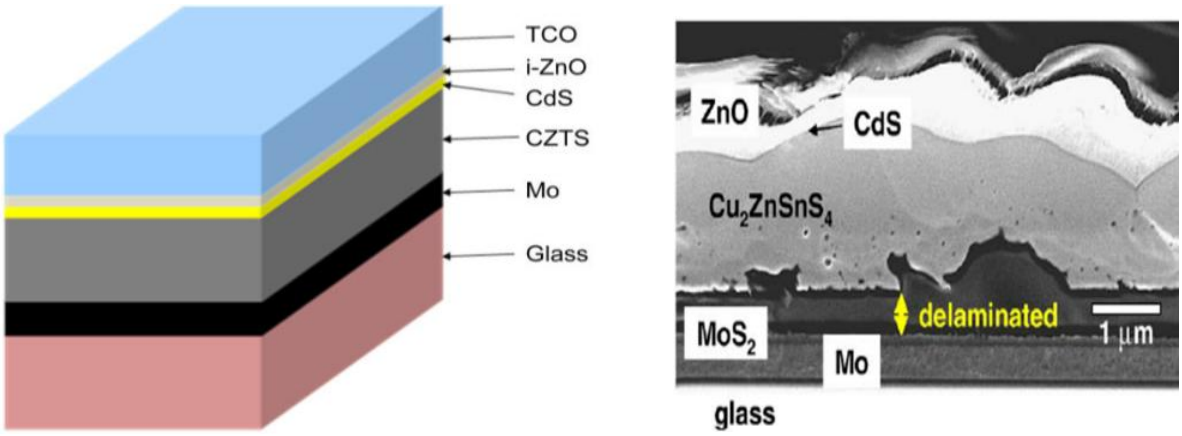


Figure 6. Schematic representation and the cross section of typical CZTS solar cell [12].

### 2.2. CZTS structural enhancement through doping

One way to improve material property is to modify one of its parts, whereby methods such as doping can be used. Xiao *et al.* performed a density functional theory investigation on the intrinsic defects, defects complexes and Na doping in CZTS system in 2015. The first principle calculations were performed with a density functional theory using Vienna Ab-initio Simulation Package (VASP) [24]. Calculations showed that the disorder and non-stoichiometry in the Cu-Zn plane could induce a band gap shrinkage

of the material. Furthermore, the experiments obtained high conversion efficiencies for the thin film solar cells under the Cu-poor and Zn-rich conditions and the most possible defects which fulfil the experimental Cu-poor and Zn-rich conditions are vacancies of copper ($V_{Cu}$) rather than zinc replacing copper ($Zn_{Cu}$).

It is necessary to keep the tin (Sn) chemical potential moderate during the CZTS thin film solar cell growth because the Sn-involved defects are harmful [24]. It was reported that any doping that improves the photovoltaic properties must not create deep transition levels and should improve the conductivity of the solar cell absorbers. The $Na_{Zn}$ (sodium replacing zinc) defect have a low formation energy and is a shallow acceptor and contributes to the conductivity of the CZTS absorbers, therefore it benefits the conversion efficiency of the solar cells [45]. Removing a Cu atom to form a vacancy weakens the orbital hybridization and causes a small enlargement of the band gap, which is consistent with previous studies.

Zong-Yan Zhao and Xiang Zhao in 2014 studied the doping effects of sodium in kesterite CZTS [46]. The study was focused on the crystal structure, electronic structure and optical properties of Na occupying different lattice sites or interstitial sites of kesterite CZTS where they were systematically calculated by density functional theory within the GGA+U method in the CASTEP code [46]. It was reported that Na impurity favours occupation of the interstitial sites. If Na impurity occupies the cation lattice sites, the band gap of CZTS would be will be broadened, which is opposite to the situation of a Na impurity occupying the interstitial sites.

The doping effects of Na in CZTS are mainly exhibited by energy band shifting, energy band broadening or narrowing and effective mass of holes at the top of valence band reduction. The doping effects of Na could improve the photovoltaic performance by influencing crystallinity, affecting grain growth, increasing hole density, shifting the acceptor level closer to the conduction band, increasing carrier concentration, elongating minority carrier lifetime etc. The study showed that even with the implantation of the Na impurity, kesterite CZTS could still maintain its exceptional

photovoltaic performance. Na doping elongates the lattice constants and causes the crystal volume to expand [47].

Zhao *et al.* investigated the electronic, optical and mechanical properties of CZTS with four crystal structures namely the zincblende-derived kesterite (ZB-KT), zincblende-derived stannite (ZB-ST), wurtzite-derived kesterite (WZ-KT) and wurtzite-derived stannite (WZ-ST) [26]. In the zincblende structure, two tetrahedrons are connected to each other by one covalent bond and the projections of other covalent bonds are respectively coincided on the plane perpendicular to the shared covalent bond. Meanwhile in the wurtzite structure, the projections of other covalent bonds are respectively staggered by $60°$ on the plane perpendicular of the shared covalent bond [46]. It was reported that there was no significant difference observed between the calculated optical and mechanical properties of the considered four crystals. For all the four structures, the valence band maximum (VBM) and the conduction band minimum (CBM) indicated that CZTS is a direct band gap semiconductor in the four crystal structures. The electronic parameters of the four crystal structures are similar, except for the fundamental band gap values. The fundamental band gap of CZTS is mainly determined by the bandwidth of the isolated conduction band. The optical properties of ZB-KT, ZB-ST and WZ-ST structures have similar general features whereas those of WZ-KT exhibit different features from them [46].

Nagaoka *et al.* reported about the effects of sodium doping on electrical properties of CZTS single crystal by using temperature dependence of Hall-effect measurement. The study reported that the sodium substitution on the cation site in CZTS was observed from the increasing of unit-cell size by powder X-ray diffraction. Sodium increased the effective hole concentration and made the thermal activation energy smaller. The degree of compensation decreased with sodium incorporation thus the hole mobility was enhanced [48].

The challenges associated with kesterite structures CZTS and CZTSe as materials for solar cells were studied by Siebentritt *et al.* back in 2012 [49]. The study reported that the equilibrium structure of both CZTS and CZTSe is the kesterite structure and the

band gaps of CZTS and CZTSe are 1.5 and 1.0 eV respectively. Theoretically, the CuZn antisite acceptor is predicted as the most probable defect. This makes secondary phases a serious challenge in the development of solar cells. So far solar cell efficiencies of 10 % have been achieved with these new materials [49]. For kesterite solar cells to present a commercially viable solution it will certainly be necessary to reach 15 % efficiency. It will be essential to grow pure kesterite phase, without any admixture of the stannite structure, because of the lower band gap of the stannite.

Another challenge for the solar cells is certainly the choice of the correct contact materials. The interfacial properties are not discussed because information is scarce, and experimental [50] and theoretical [51] data are contradictory. The control of recombination and doping will depend on the control of the native defects. However, in chalcopyrites the physicochemical nature of the doping defects is still not known and optimization of solar cells has been quite empirical.

The study of the CZTS with four crystalline structures done by Zhao *et al.* reported that in the visible light region of the solar spectrum the CZTS has better absorption properties for the application of solar energy [26]. The effective mass of charge carriers in CZTS is smaller than those of typical oxide semiconductors, which is favourable for improved photoelectric conversion efficiency. In the visible light region, zincblende-derived CZTS has better absorption properties for the application of solar energy [26].

### 2.2.1. Structural properties

CZTS thin films are usually in a polycrystalline form consisting of kesterite crystal structures. In 1974, detailed lattice data of a CZTS single crystal was reported by Stewart *et al.* [30]. Thereafter the data was frequently referenced in the literature when seeking to determine CZTS phase. The symmetry (space) group of the pure kesterite is I-4. CZTS has highly similar crystal structure with chalcopyrite copper indium gallium selenide (CIGS), which is another semiconductor like the CZTS with a very high conversion efficiency but very expensive and not environmentally friendly as it is made up of toxic elements. CZTS is a tetragonal structure with space group I-4 and angles on

the vertex are all $90.00°$. Sulphur atoms are concentrated within the structure while copper occupies all the vertices as indicated in Figure 7. Tin is positioned on the edges while zinc has at least one atom within the structure. One copper atom is located at the centre of the structure and is surrounded by sulphur atoms.

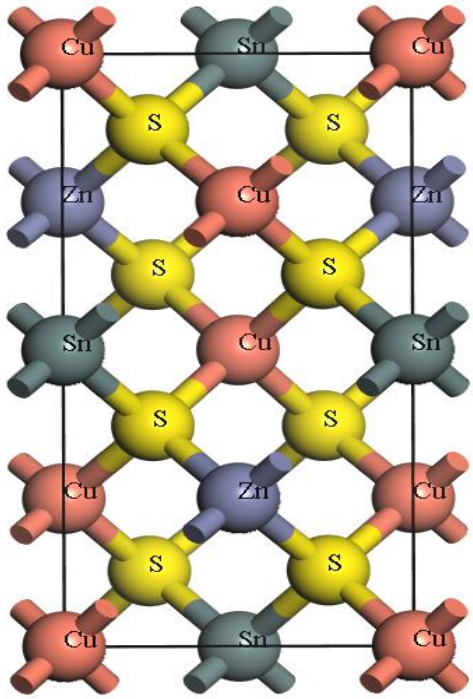


Figure 7. Crystal structure of the CZTS semiconductor material [52].

### 2.2.2. CZTS surfaces

CZTS shows the ability to improve its efficiency through the manipulation of parts or all of its components; one way this can be done is through doping one of its surfaces. Surface modifications are appealing in the growth of semiconductors. Currently very little is known about the electronic structure of CZTS surfaces, although the kesterite-based solar cells have reached efficiencies of over 11% [53]. Based on understanding of surface thermodynamics and kinetics, surface growth techniques can be used to alter the surface morphology and modify the surface electronic structures. Swami *et al.* prepared CZTS films by spin coating and indicated the formation of kesterite phase with

peaks corresponding to (112), (220) and (312) planes and confirmed the formation of good quality CZTS film [54]. By surface (i.e. 112) we refer to the Miller indices, which give the notation in crystallography for planes in a crystal normally indicated by *h*, *k* and $\ell$. Investigations on CZTS surfaces suggest that the vast majority of the low index surfaces are dipolar and that only the (112), (010) and (101) surfaces have low surface energies. In this study, (112) CZTS surface properties are investigated using density functional theory.

### 2.3. Doping

Doping is an intentional introduction of impurities into an intrinsic semiconductor for the purpose of modulating its electrical properties. The doped material is referred to as extrinsic semiconductor. A semiconductor doped to very high levels acts more like a conductor than a semiconductor. Doping a semiconductor in a good crystal allows the introduction of energy states within the band gap. Dopants also have the important effect of shifting the energy bands relative to the Fermi level. It can change the electrical conductivity of the lattice and therefore vary the efficiency of the semiconductor [55]. Figure 8 shows different ways of doping crystalline structures for properties enhancement, (a) dopants can fill empty spaces, (b) move in between atoms or (c) exchange places with atoms.

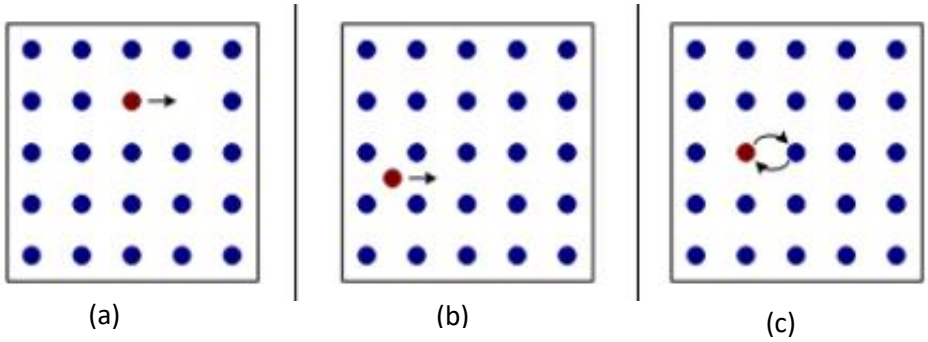


Figure 8. Different ways of doping crystal structures, (a) dopants can fill empty spaces, (b) move in between atoms or (c) exchange places with atoms [56].

Sodium is an important dopant in CZTS semiconductor that is used to control the electrical properties. There are acceptor dopants (group three elements) and donor

dopants (group five elements) [57]. An intrinsic defect occurs when a particle isn't where it should be, it is formed when an atom is missing from a position that ought to be filled in the crystal creating a vacancy or when an atom occupies an interstitial site where no atom would ordinarily appear [58].

Atom arrangements in real materials do not follow perfect crystalline patterns; the preferred structures of solids at low temperature are those that minimize the energy. The extrinsic defects are foreign atoms which are intentionally added to the material. Some of these defects are temperature dependent, they increase with increasing temperature. Defects concentration depends upon impurity concentration, which is constant and independent of temperature [58]. The minimization of defects in absorber material is essential.

### 2.3.1. CZTS doping

There is ample literature on first principle studies on doping CZTS with different atoms. Some of the atoms used to enhance the efficiency of CZTS through doping include cadmium (Cd) [59], sodium (Na) [24] [60], chromium (Cr) [61], oxygen ($O_2$) [62], antinomy (Sb) [63], potassium (K) [64], etc. Of all the dopants that have been used in literature, generally, there is no viable improvement on the efficiency of CZTS-based photovoltaic solar cells reported so far.

The results for Sb showed that low concentration doping of Sb at Sn site possesses the lowest formation energy at the Cu-poor growth condition and produces a 1.1 eV deep defects level above the valence band maximum, which is disadvantageous to solar cell applications [63]. Tablero analyzed the substitutions of Cu, Sn and Zn in CZTS by Cr, which introduced deeper bands into the energy band gap and opens more photon absorption channels that could increase the solar energy absorption [61].

A variety of dopants for CZTS have been studied so far and the highest reported power conversion efficiency (PCE) is 12.6 % for sulphur selenide-based technology [65]. Bi-doped CZTS synthesized by solution process could alter structural properties by enlarging grain size from 0.1 to 0.4 $\mu$m. Ga doped CZTS modifies electrical properties by increasing carrier concentration and mobility consequently resulting in an increased

conductivity from 0.04 to 12.2 $cm^{-1}$. Cd-doped CZTS shows enhanced optical properties by altering the bandgap from 1.54 eV to as low as 1.36 eV for optimum absorption. For alkaline metals doping, K doping reforms chemical composition by reducing ZnS secondary phase formation due to the inhibition of Sn loss, whereas Na doping improves the lifetime of photo carriers by passivating defects.

## 2.4. Band gap

Band structure of a solid describes the range of energies that an electron within the solid may have (also called energy bands, allowed bands or simply bands) and ranges of energy it may not have (called band gaps or forbidden bands). Band theory derives these bands and band gaps by examining the allowed quantum mechanical wave functions for an electron in a large periodic lattice of atoms or molecules [29].

In crystalline solids, electrons can take on any energy within an unfilled band. Energy levels are grouped in bands, separated by energy band gaps. The important energy levels in a crystal are the top of the valence band, the bottom of the conduction band, the Fermi level, the vacuum level and the energy levels of any defect states in the crystal. At zero Kelvin, the lower band is filled with electrons and labelled as the valence band, the upper band is empty and labelled as the conduction band. Semiconductors have a small energy gap between the valence band and the conduction band. Electrons can jump to the conduction band but not with the same ease as they do in conductors [66].

The valence and conduction bands are the bands closest to the Fermi level and thus determine the electrical conductivity of the solid. In non-metals, valence band is the highest range of electron energies in which electrons are normally present at absolute zero temperature, while the conduction band is the lowest range of vacant electronic states. Valence band is located below Fermi level while the conduction band is located above it. The electrical conductivity of a solid depends on its capability to allow the flow of electrons from the valence band to the conduction band.

An intrinsic semiconductor is a semiconductor in its pure state. For every electron that jumps into the conduction band, the missing electron will generate a hole that can move freely in the valence band. The number of holes will equal the number of electrons that have jumped. In extrinsic semiconductors, the band gap is controlled by purposefully adding impurities to the material which is called doping [29] [66]. The number of holes will not equal the number of electrons that jumped to the conduction band.

Theoretically, pure kesterite CZTS is a direct band gap semiconductor with a band gap of 1.495 eV between maximum of the valence band and the minimum of the conduction band which is very close to the experimental measurements of 1.49 eV [46]. This band gap is very close to the optimal band gap of semiconductors of 1.5 eV for achieving maximum conversion efficiencies. The effect of the CZTS composition on the optical properties was investigated by Marleba *et al.* [67], optical measurements showed that the band gap is not influenced by the zinc content while it increases steeply from 1.48 eV to 1.63 eV with the increase of the Sn/Cu ratio.

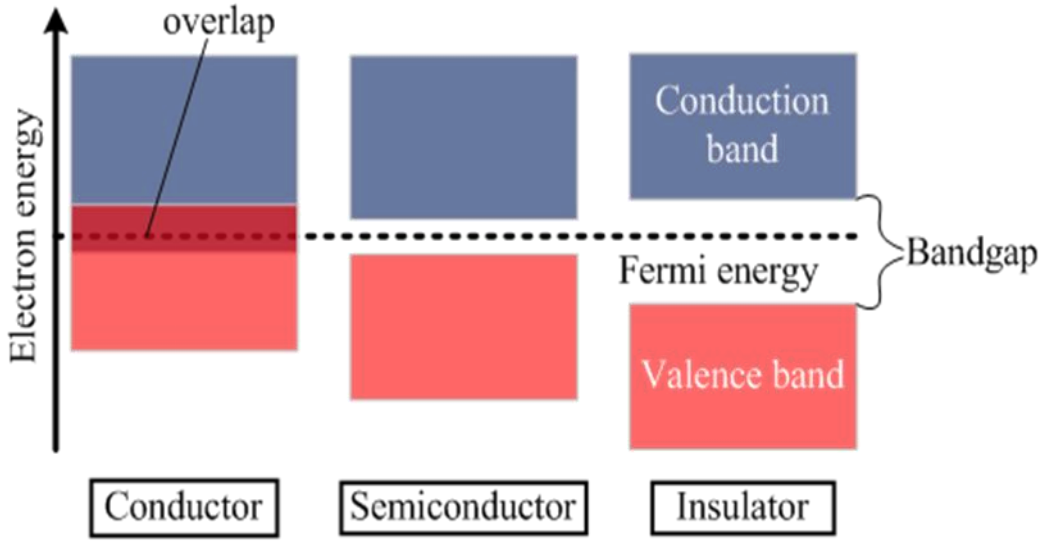


Figure 9. Illustration of the band gap for a conductor, semiconductor and insulator [66]

Figure 9 shows the difference between the conductor, semiconductor and an insulator respectively. The semiconductor has a smaller band gap, which requires less electron

energy for the electrons to move from the valence band to the conduction band, thus decreasing the band gap of semiconductors will enable the material to use less electron energy for more ease of electron flow. Decreasing the band gap of semiconductors would also improve the efficiency of solar cell technologies that uses semiconductors as it would be able to transfer electrons with even lower energies.

The best CZTS solar cells are Cu-poor and Zn-rich. The material class of kesterites to which CZTS belongs has a crystal structure very similar to that of chalcopyrite's structure therefore similar electronic properties are expected. The CZTS films showed a tetragonal structure with preferential orientation along the (112) plane. They also showed p-type semiconducting behaviour with carrier concentration ~$10^{17}$ $cm^{-3}$, optical absorption coefficients ~$10^{4}$ $cm^{-1}$ and direct optical band gap ~1.45 eV [44].

# CHAPTER THREE

## 3. Methodology

### 3.1. Theoretical methodology

A set of one-electron Schrodinger (Kohn-Sham) equations are solved using the plane wave pseudopotential approach [51]. The wave functions are expanded in a plane wave basis set defined by periodic boundary conditions and Bloch's theorem. The electron-ion potential is described by means of ab-initio pseudopotentials within both norm-conserving and ultra-soft formulations. Cambridge Serial Total Energy Package (CASTEP) which uses density functional theory with a plane wave basis set is employed to perform the structural calculations and analysis of the structures. Physical properties of materials that can be calculated using CASTEP include total energies, electronic structure, geometry, molecular dynamics, transition states, phonons, electric field response, exchange correlation etc. [68].

## 3.2. Density functional theory

Density functional theory is a computational quantum mechanical modelling method used in physics, chemistry and material science to investigate the electronic structure principally the ground state of many body system atoms, molecules and the condensed phase.

Using this theory, the properties of a many-electron system can be determined by using functionals i.e. functions of another function, which in this case is the spatially dependent electron density, hence the name density functional theory comes from the use of functionals of the electron. The original density functional theory has been generalized to deal with many different situations, spin polarized systems, multicomponent systems such as nuclei and electron hole droplets, free energy at finite temperatures, superconductors with electronic pairing mechanics, relativistic electrons, time-dependent phenomena and excited states, bosons etc. [69].

### 3.2.1. First principle calculations

A wave function in quantum mechanics describes the quantum state of a set of particles in an isolated system. The ground state for a collection of atoms can be obtained by solving the Schrödinger equation [70]

$$H\Psi = E\Psi \quad \ldots\ldots\ldots\ldots\ldots\ldots\ldots\ldots\ldots\ldots\ldots\ldots\ldots\ldots \quad (3.1)$$

Knowledge from the Born-Oppenheimer approximation which indicates that the dynamics of atomic nuclei and electrons can be separated is used,

$$m_{nuclei} \gg m_e \quad \ldots\ldots\ldots\ldots\ldots\ldots\ldots\ldots\ldots\ldots\ldots\ldots\ldots\ldots \quad (3.2)$$

where $m_{nuclei}$ is the mass of the nuclei and $m_e$ is the mass of the electron. The nuclei are heavy and slow while the electron is small and fast. The dynamics of nuclei and electrons are decoupled into two wave functions.

$$\Psi\{(r_i),(R_I)\} = \Psi_N\{R_I\} * \Psi_e\{r_i\} \quad \ldots\ldots\ldots\ldots\ldots\ldots\ldots\ldots$$

(3.3)

For many particle problems in solid state, the Schrödinger equation is solved for electrons in the form

$$H\Psi(r_1,r_2,r_3,\ldots,r_N) = E\Psi(r_1,r_2,r_3,\ldots,r_N) \quad \ldots\ldots\ldots\ldots\ldots\ldots\ldots (3.4)$$

The electron Hamiltonian consist of three important terms which include electrons.

$$H = -\frac{\hbar^2}{2m_e}\sum_i^{N_e} \nabla_i^{\,2} + \sum_i^{N_e} V_{ext}(r_i) + \sum_{i=1}^{N_e}\sum_{j>1} U(r_i,r_j) \quad \ldots\ldots\ldots\ldots\ldots (3.5)$$

where the first term of Equation 3.5 represents the kinetic energy term, the second term is the potential energy term indicating the electrons interacting with the nuclei and the third term is the electron-electron repulsion term. $V_{ext}$ is the external potential energy due to the positively charged nuclei. The term functional means a function of a function, i.e. operation on a function gives another function [69].

$$F[f] = \int_{-1}^{1} f(x)dx \quad \ldots\ldots\ldots\ldots\ldots\ldots\ldots\ldots\ldots\ldots\ldots$$

(3.6)

Equation 3.6 is an example of a functional. For the density functional theory, it is possible to move from the wave functions to electron density.

The electron density is defined in the form,

$$n(r) = \Psi^*(r_1,r_2,r_3,\ldots,r_N)\Psi(r_1,r_2,r_3,\ldots,r_N) \quad \ldots\ldots\ldots\ldots\ldots (3.7)$$

Electron density is only 3 dimensional. One of the electrons is treated as a point charge in the field of all the other electrons, which simplifies the many-electron problem to many one electron problems:

$$\Psi(r_1,r_2,r_3,\ldots,r_N) = \Psi(r_1) * \Psi(r_2) * \Psi(r_3) * \ldots * \Psi(r_N) \quad \ldots\ldots\ldots\ldots\ldots$$

(3.8)

Equation 3.8 is known as the Hartree product.

Now the electron density is defined in terms of the individual electron wave functions

$$n(r) = 2\sum_i \Psi_i^*(r)\Psi_i(r). \quad (3.9)$$

### 3.2.2. Hohenberg and Kohn theorems

The theorems constitute the basis of the Kohn-Sham density functional theory. The fundamental proposition of density functional theory is that the ground and excited state properties of a many-electron system in the presence of some external field can all be determined exactly from the ground state density. There are two fundamental theorems [71].

Theorem 1

The ground state energy $E$ is a unique functional of the electron density is given by [72]

$$E = E[n(r)] \quad (3.10)$$

Thus, the electron density is all that is required to define the total ground state energy.

Theorem 2

The electron density that minimizes the energy of the overall functional is the true ground state electron density. This theorem brings knowledge of how to find the ground state energy.

$$E[n(r)] > E_0[n_0(r)] \quad (3.11)$$

The energy functional consist of two main parts, the known and the unknown energy and given by:

$$E[\{\Psi_i\}] = E_{known}[\{\Psi_i\}] + E_{XC}[\{\Psi_i\}] \quad \ldots\ldots\ldots\ldots\ldots\ldots \quad (3.12)$$

The known energy term is given by:

$$E_{known}[\{\Psi_i\}] = -\frac{\hbar}{m_e}\sum_i \int \Psi_i^* \nabla^2 \Psi_i d^3r + \int V(r)n(r)d^3r + \frac{e^2}{2}\int\int \frac{n(r)n(r')}{r-r'} d^3r d^3r' + E_{ion} \quad \ldots\ldots \quad (3.13)$$

The unknown energy term $E_{XC}[\{\Psi_i\}]$ is known as the exchange-correlation functional and it takes care of all the quantum mechanical interactions between electrons. It includes all quantum mechanical terms and it is not known because it needs to be approximated.

### 3.2.3. The Kohn-Sham scheme

Kohn and Sham introduced a method based on the Hohenberg-Kohn theorem that enables one to minimize the functional $E[n(r)]$ by varying $n(r)$ over all densities containing $N$ electrons [51]. This constraint is introduced by the Lagrange multiplier $\mu$ chosen so that $\int n(r)dr = N$.

$$\frac{\delta}{\delta n(r)}\left[E[n(r)] - \mu \int n(r)dr\right] = 0 \quad \ldots\ldots\ldots\ldots\ldots \quad (3.14)$$

$$\Rightarrow \mu = \frac{\delta E[n(r)]}{\delta n(r)} \quad \ldots\ldots\ldots\ldots\ldots\ldots \quad (3.15)$$

Kohn and Sham chose to separate $F[n(r)]$ into three parts, so that $E[n(r)]$ becomes:

$$E[n(r)] = T_s[n(r)] + \frac{1}{2}\int\int \frac{n(r)n(r')}{|r-r'|} dr dr' + E_{XC}[n(r)] + \int n(r)V_{ext}(r)dr \quad \ldots \quad (3.16)$$

where $T_s[n(r)]$ is defined as the kinetic energy of a non-interacting electron gas with density $n(r)$ and is given by,

$$T_s[n(r)] = -\frac{1}{2}\sum_{i=1}^{N}\int \Psi_i^*(r)\nabla^2\Psi_i(r)dr \quad \ldots\ldots\ldots\ldots\ldots\ldots \quad (3.17)$$

Equation 3.16 also acts as a definition for the exchange correlation energy functional $E_{XC}[n(r)]$. We can rewrite Equation 3.15 in terms of an effective potential $V_{eff}(r)$ as follows

$$\frac{\delta T_s[n(r)]}{\delta n(r)} + V_{eff}(r) = \mu \quad \ldots\ldots\ldots\ldots\ldots\ldots\ldots\ldots \quad (3.18)$$

where

$$V_{eff}(r) = V_{ext}(r) + \int \frac{n(r')}{|r-r'|}dr' + \frac{\delta E_{XC}[n(r)]}{\delta n(r)} \quad \ldots\ldots\ldots\ldots\ldots \quad (3.19)$$

Now, if one considers a system that contains non-interacting electrons moving in an external potential equal to $V_{eff}(r)$ as defined by Equation 3.17, then the same analysis would lead to the same equation. Therefore, to find the ground state energy and density, $E_0$ and $n_0(r)$ all one must do is to solve the one-electron equations,

$$\left(-\frac{1}{2}\nabla_i^2 + V_{eff}(r) - E_i\right)\Psi_i(r) = 0 \quad \ldots\ldots\ldots\ldots\ldots\ldots\ldots\ldots \quad (3.20)$$

As the electron density is constructed per the equation

$$n(r) = \sum_{i=1}^{N}|\Psi_i(r)|^2 \quad \ldots\ldots\ldots\ldots\ldots\ldots\ldots\ldots \quad (3.21)$$

These equations must be solved with self-consistency scheme [51], which is discussed in the next subsection.

### 3.2.4. Self-consistency scheme

This scheme determines the electron density, it consist of 4 steps and are as follows:

Step 1. Guess the electron density: trial $n(r)$

Step 2. Solve the Kohn-Sham equations with $n(r)$, obtain single electron wave functions $\Psi_i(r)$

Step 3. Calculate the electron density based on the single-electron wave functions

$$n(r) = 2\sum_i \Psi_i^*(r)\Psi_i(r) \quad \ldots\ldots\ldots\ldots\ldots\ldots\ldots\ldots\ldots\ldots \quad (3.22)$$

Step 4. Compare the new electron density $n(r)$ with the initially approximated electron density $n(r)$ from step 1. The steps are illustrated in Figure 10.

There are two conditions to consider before concluding about the electron density, namely,

a. If the new density is different from the approximated density, begin with the new electron density as the approximated and repeat the whole procedure from step 1.
b. If they are both the same, then that means the true ground state electron density has been obtained.

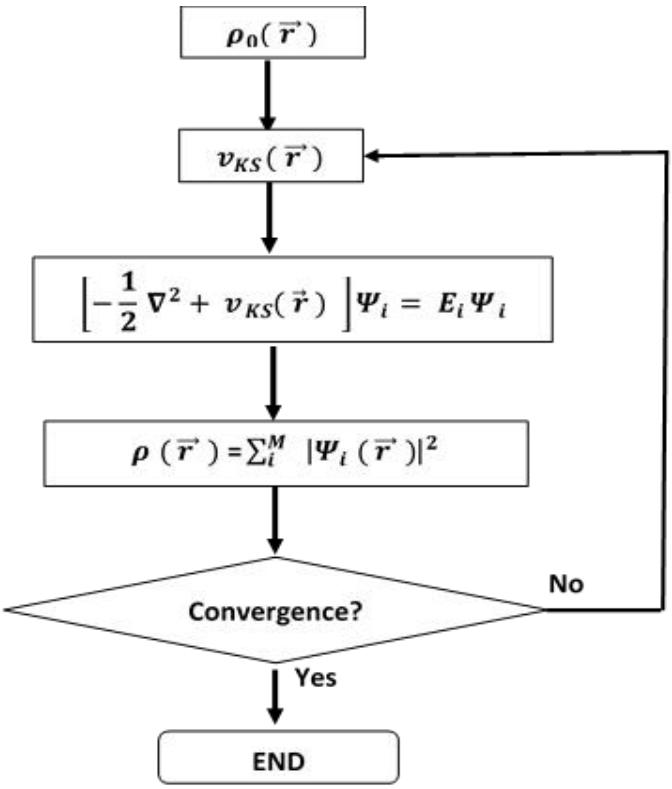


Figure 10. Flow chart of a typical DFT calculation within the Kohn-Sham method [73].

The above formulation assumes that the exchange-correlation functional is known. At present, numerical exchange correlation potentials have only been determined for a few simple model systems, and so most current density functional calculations use the local density approximation. The LDA approximates the exchange ($XC$) functional to a simple function of the density at any position $\mathrm{r}$. The value of this function is the $XC$ energy per electron in a uniform homogeneous electron gas of density $n(r)$. The LDA expression for $E_{XC}[n(r)]$ is given by:

$$E_{XC}[n(r)] \approx \int E_{XC}(n(r))n(r)\,dr \quad \ldots\ldots\ldots\ldots\ldots\ldots\ldots\ldots \quad (3.23)$$

The LDA is remarkably accurate, but often fails when the electrons are strongly correlated as in systems containing $d$ and $f$ orbital electrons [51, 74].

### 3.2.5. Correlation functionals

The mostly used functionals include the LDA, GGA and PBE functionals whereas the HSE06 functional is used for better band gap approximations. GGA functional is based on the gradients of the electron density while LDA is based on the local electron density, it depends only on one variable (the density). PBE belongs to the class of GGA functionals for the exchange correlation energy.

### 3.2.6. Exchange correlation functionals

Several functionals are used based on the area of interest in the results of the calculations, some are used because they are better in one property than the other. The mostly used functionals include the local density approximation (LDA) and generalized gradient approximation (GGA) functionals, HSE06 functional for better band gap approximations. Local density approximation is based on the local electron density, it depends only on one variable (the density). Generalized gradient approximation takes into consideration the gradient of the electron density, it requires knowledge of two variables (the density and its gradient). Other functionals include the local functionals

PBE, PW91, WC of GGA. There are also ab initio non-local HF, sX, the empirical non-local B3LYP, HSE and the DFT+U among others.

#### 3.2.6.1. Local density approximations

Local density approximations are a class of approximations to the exchange-correlation (XC) energy functional in density functional theory [75]. They depend exclusively upon the estimation of the electronic density at every point in space. Numerous methodologies can yield local approximations to the XC energy. Overwhelmingly effective nearby approximations can be defined as those that have been established from the homogeneous electron gas (HEG) [76]. In such manner, LDA is for the most part synonymous with functional considering the HEG estimate, which are then connected to practical frameworks.

The exchange-correlation functional is approximated as [77]:

$$E_{xc}^{LDA}[\rho] = \int \rho(r)\varepsilon_{xc}(\rho)dr \quad \ldots\ldots\ldots\ldots\ldots\ldots\ldots\ldots \quad (3.24)$$

where ρ is the electronic density and $\varepsilon_{xc}$ is the exchange-correlation energy per molecule of a homogeneous electron gas. The exchange-correlation energy is decayed into exchange and correlation terms linearly and can be expressed as [77]:

$$E_{xc} = E_x + E_c \quad \ldots\ldots\ldots\ldots\ldots\ldots\ldots\ldots\ldots\ldots\ldots\ldots \quad (3.25)$$

so that different expressions for $E_x$ and $E_c$ are looked for. The exchange term goes up against a straight forward systematic frame for the HEG.

Local density approximations are imperative in the development of more complex approximations to the exchange-correlation energy, for example, generalized gradient approximations or hybrid functionals, as an attractive property of any exchange-correlation functional, is that, it duplicates the correct consequences of the HEG for non-differing densities. In that capacity, LDAs are frequently an express segment of such functionals.

#### 3.2.6.2. Generalized gradient approximation

As the LDA approximates the energy of the genuine density by the energy of a local constant density, it falls flat in circumstances where the thickness experiences quick changes, for example, in atoms. A remedy to this can be made by considering the slope of the electron density, the alleged generalized gradient approximation. The LDA exchange-correlation is an inhomogeneous system in non-local density as for electrons it encompasses, and this is alluded to as inclination amendment. The GGA exchange-correlation energy is given by [77]:

$$E_x^{GGA}c(n) = \int dn(r)\varepsilon_{xc}^{GGA}[n(r), \|\nabla n(r)\|] \ldots\ldots\ldots\ldots\ldots (3.26)$$

where $\varepsilon_{xc}$ is the exchange correlation energy and $n(r)$ is the gradient term of the electron density. The GGA has been broadly utilized and has turned out to be very fruitful in remedying a portion of the inadequacies of the LDA. In many cases, GGA is used concurrently with LDA as it provides improvements to certain feature of LDA such as reduction in the over binding.

### 3.2.7. Plane-wave pseudopotentials method

The plane-wave pseudopotential method has become a powerful and reliable tool to study properties of a broad class of materials. The main idea of the method is to simplify the DFT problem by considering only valence electrons. This approximation is well understood and gives a number of computational advantages such that there are fewer electronic states in the solid-state calculations, the resulting pseudo-wave functions are smooth and node-less in the core region, both pseudopotentials and pseudo-wave functions can be efficiently represented using a plane wave basis set. The pseudopotential is much weaker in the core region that the true Coulomb potential of the nucleus and it does not have a singularity at the position of the nucleus [78].

#### 3.2.7.1. Plane-wave basis set

The plane-wave pseudopotential approach uses the plane-wave basis set to represent the orbitals. The wave function can be written as the product of the cell periodic part and a wavelike part:

$$\Psi k_i(r) = e^{ik.r} f_i(r) \quad \ldots\ldots\ldots\ldots\ldots\ldots\ldots\ldots \quad (3.27)$$

The first term is the wavelike part and the second term is the cell periodic part of the wave function. This can be expressed by expanding it into a finite number of plane waves whose wave's vectors are reciprocal lattice vectors of the crystal, given by:

$$f_i(r) = \sum_G G_{i,G}\ e^{iG.r} \quad \ldots\ldots\ldots\ldots\ldots\ldots\ldots\ldots \quad (3.28)$$

where $\mathrm{G}$ represents reciprocal lattice vectors given by $\mathrm{G}.I = 2m\pi$ for $I$, where $I$ is the lattice of the crystal and $m$ is an integer [29].

#### 3.2.7.2. Pseudopotential method

The plane-wave pseudopotential approach uses pseudopotentials to represent the nuclei and core electrons. The pseudopotential is an attempt to replace the complicated effects of the motion of the core electrons of an atom and its nucleus of the effective potential, or pseudopotential, so Schrödinger equation contains a modified term for core electrons normally found in the Schrödinger equation [79]. Figure 11 illustrates the ionic potential $(Z/r)$, the valence wave function $\Psi_{(Z/r),}$ the corresponding pseudopotential $V_{pseudo}$ and pseudo-wave function $\Psi_{\mathrm{pseudo}}$ respectively [80]. First principles pseudopotentials are derived from an atomic reference state, requiring that the pseudo- and all-electron valence eigenstates have the same energies and amplitude outside a chosen core cut-off radius.

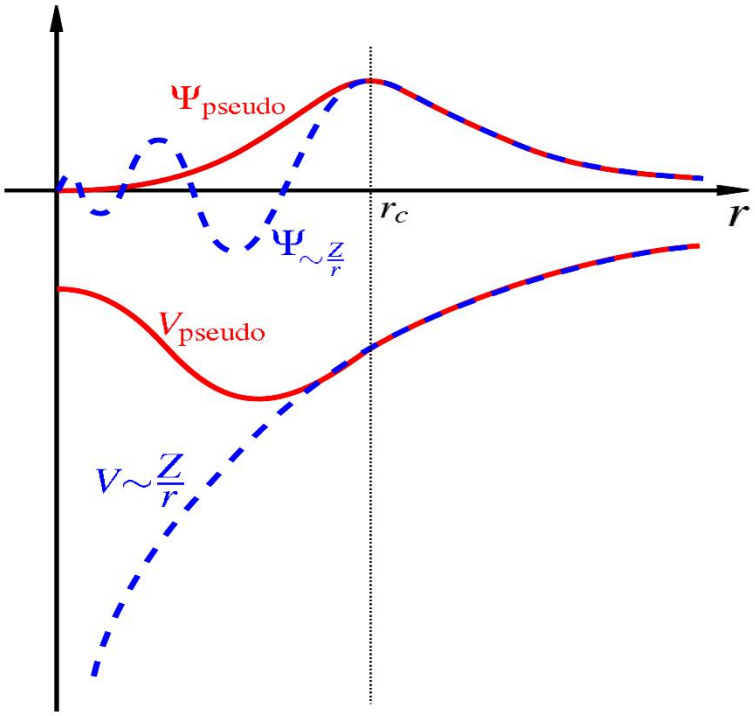


Figure 11. Comparison of wave function in the Coulomb potential of the nucleus (blue) to the one in the pseudopotential (red). The real and the pseudo wave functions and potentials match above a certain cut-off radius $r_{cut}$ [80].

The advantage of using the pseudopotential approximation is that it allows the electronic wave function to be expanded using a much smaller number of plane wave basis states, so that a smaller amount of computational time would be required for convergence of the energies.

A pseudopotential that uses the same potential for all the angular momentum components of the wave function is called a local pseudopotential. A local pseudopotential is a function that only exhibits distance dependence of the potential. The norm-conserving potential (NCP) by Kleinmann and Bylander is an example of a non-local pseudopotential, using a different potential for each angular momentum component of the wave function [81].

## 3.3. Materials studio

Materials studio is a complete modelling and simulation environment designed to allow researchers in various fields to predict and understand the relationships of a material's atomic and molecular structure with its properties and behaviour. Using Materials studio, researchers in many industries are engineering better performing materials of all types including pharmaceuticals, catalysts, polymers and composites, metals and alloys, batteries and fuel cells and more [68]. Within the Materials studio software, we have Cambridge Serial Total Energy Package (CASTEP) which enables us to perform density functional theory calculations.

### 3.3.1. Cambridge serial total energy package

CASTEP is a commercial software which uses density functional theory with a plane wave basis set to calculate the electronic properties of crystalline solids, surfaces, molecules, liquids and amorphous materials from first principles. Properties of any material that can be thought of as an assembly of nuclei and electrons can be calculated with the only limitation being the finite speed and memory of the computers being used.

Typical applications involve studies of surface chemistry, structural properties, band structure, density of states and optical properties. CASTEP can also be used to study the spatial distribution of the charge density and wave functions of a system. It can also be used efficiently to study properties of both point defects (vacancies, interstitials and substitutional impurities) and extended defects (for example grain boundaries and dislocations) in semiconductors and other materials [68].

### 3.3.2. Adsorption locator

Adsorption is a consequence of attractive interactions between the surface of the adsorbent and the species being adsorbed. The molecules at a surface of a material experience imbalanced forces of intermolecular interaction which contribute to the surface energy. Adsorption locator identifies possible adsorption configurations by

carrying out Monte Carlo searches of the configurational space of the substrate-adsorbate system as the temperature is slowly decreased. This process is repeated to find additional local energy minima.

The adsorption locator was used to determine the optimum location of the dopants Na, Ca and Ba on the CZTS (112) surface since adsorption is a surface phenomenon. It gives the best adsorption site for materials by determining low energy adsorption sites. It can also be used to generate configurations automatically, which can in turn be used as starting points for further DFT studies and to use the force field method to obtain a ranking of the energies for each generated configuration thereby indicating the preferred adsorption sites [82]. The CZTZ (112) surface was optimized by making use of the Forcite module as it takes into considerations the force fields associated with the atoms available from the Materials Studio modules. This allows the surface calculation to load the atom to be adsorbed on the surface and give different fields of adsorption and corresponding low energy regions on the surface.

## 3.4. Computational method

In this work, first principle calculations were implemented in the framework of density functional theory within the generalized gradient approximation using the PBE exchange correlation potential and utilizing the plane wave total energy pseudopotential method as implemented in CASTEP code [68]. HSE06 functional was used for better band gap approximations. The structure was modelled in Materials Studio of BIOVIA using the 3D Atomistic window and space group representing the tetragonal structure of I-4 was used. Lattice parameters of a = b = 5.430 Å and c = 10.890 Å were used to draw the external skeleton of the structure. The copper (Cu) atoms were placed in two separate positions, 2a (0, 0, 0) and 2c (0, 0.5, 0.25). Zinc (Zn) atoms placed at position 2d (0.5, 0, 0.25), tin (Sn) atom at position 2b (0.5,0.5,0) and sulphur (S) in position 8g (0.7560, 0.7566, 0.8722) [30].

### 3.4.1. Creating CZTS (112) surface

The surface of interest was cleaved from the bulk CZTS crystal structure with the Miller indices ($h$, $k$, $\ell$) taking the numbers (112). The thickness of the surface was set to 9.507

Å to account for all atoms of the structure to be on the surface. The surface vectors were U(1, -1, 0) and V(1, 1, -1). A 2x2x2 supercell was created to increase the (112) plane surface area. The vacuum thickness was set to 10.00 Å while the crystal thickness was 13.940 Å. An adsorption locator module was used to absorb dopants onto the surface by giving fields of low energy and adsorption locations on the surface.

For optical and electronic properties calculations, the band energy tolerance was set to $1.0X10^{-5}$ eV with respect to the energy tolerance per atom while the separation was 0.025 / Å. The relativistic treatment was set to Koelling-Harmon with the on the fly generated (OTFG) ultrasoft used as the pseudopotential treatment.

The surface structure was then doped with three different elements separately, the first element being sodium (group one element), which was used as a basis to validate the developed models at it has been studied extensively both experimentally and theoretically. Thus, the results of the study were validated by using sodium as a benchmark. The other two dopants which would give identity to the study were the two alkaline earth metals, calcium and barium (they exhibit low toxicity, combines with several metals, abundant, environmentally friendly and they have very high chemical reactivity). The results obtained from doping with these elements were compared with those obtained for sodium doped CZTS systems from the literature. The dopants were chosen because of their electronic configuration that is like that of Na, except that Ca and Ba have a charge of plus 2. Sodium is regarded as a promising element that it could improve the efficiency of CZTS based solar cells.

All the calculations for the unit cell were performed using a Monkhorst-Pack mesh. The geometry optimization of the structure to minimize the energy or to obtain the ground state energy of the structure was determined by performing the convergence test whereby the cut off energy was varied from 50 eV to 1000 eV by increments of 50 eV, followed by k-points variation and convergence parameters are discussed in detail in the next chapter. Based on the optimized crystal structure, once the ground state energy was obtained, the (112) surface structure was then cleaved from the bulk system, thereafter the surface was doped with Na, Ca and Ba. The structural, electronic

and optical properties, and conversion efficiency of CZTS surfaces were calculated using Centre for High Performance Computing (CHPC) facilities from Council for Scientific and Industrial Research (CSIR), Pretoria.

# CHAPTER FOUR

## 4. Results and discussions

### 4.1. Bulk CZTS

The focus is on analyzing the optical and electronic properties of copper zinc tin sulfide doped with two alkaline earth metals, calcium and barium while doping with sodium is used as a reference and a way of validating the doped model results, since there is significant literature on doping CZTS with Na. This will clearly show the differences between doping with alkali metals and alkaline earth metals. Shown in Figure 12 are the

structural models for CZTS, presented along different orientations. The copper (Cu) atoms are in two separate positions (coordinates), 2a (0, 0, 0) and 2c (0, 0.5, 0.25). Zinc (Zn) atoms are at position 2d (0.5, 0, 0.25), tin (Sn) atom at position 2b (0.5,0.5,0) and sulphur (S) in position 8g (0.7560, 0.7566, 0.8722) [30]. Sulphur atoms are the most central ones in the structure while most of copper is on the edges and only a few within the structure. Tin atom appears on all the edges.

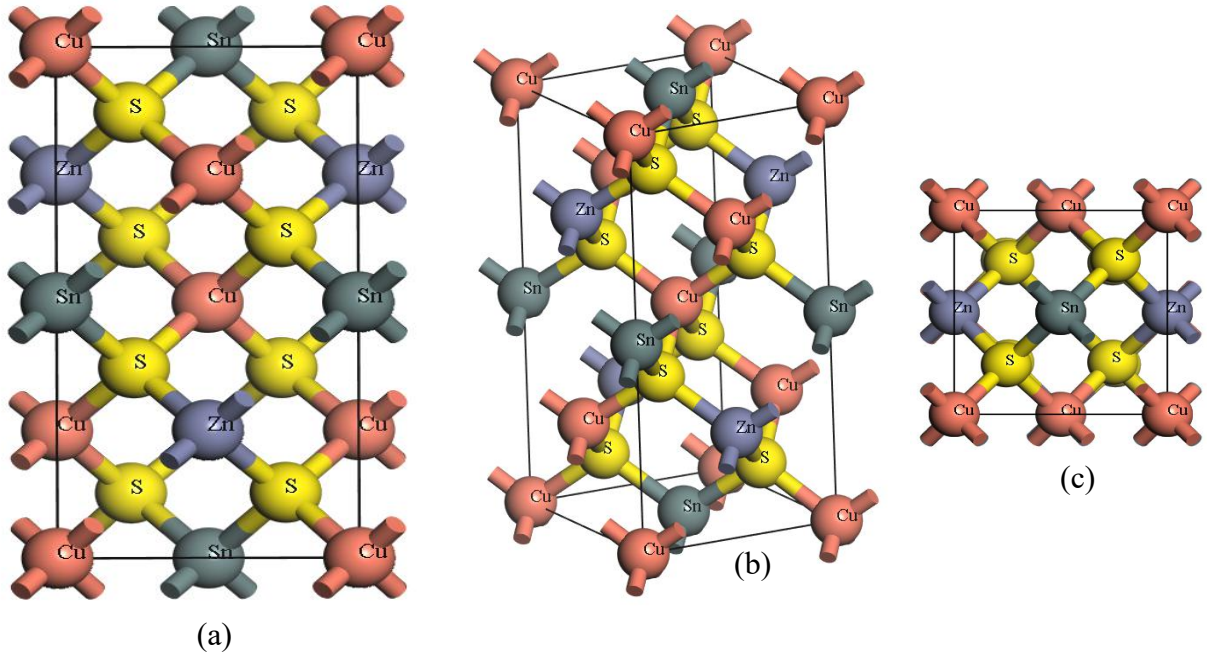


Figure 12. Different views of CZTS crystalline structure modeled in Materials Studio. (a) shows the side view, (b) shows the three-dimensional view and (c) showing top view. Different atoms are represented by various colours as depicted.

### 4.1.1. Geometry optimization

The present quantum-mechanical calculations were performed based on the application of the density functional theory and pseudopotential methods as implemented in the first principle calculation program CASTEP code [68]. Electronic exchange correlation energy was treated under generalized gradient approximation with the Perdew, Burke and Ernzerhof (PBE) [83].

To find optimal conditions at which CZTS structure would be more stable i.e. ground state conditions, we first determined suitable cut-off energy and corresponding k-points. The k-points (reciprocal space) are sampling points in the first Brillouin zone of the

material i.e. the specific region of reciprocal-space which is closest to the origin (0,0,0) [84].

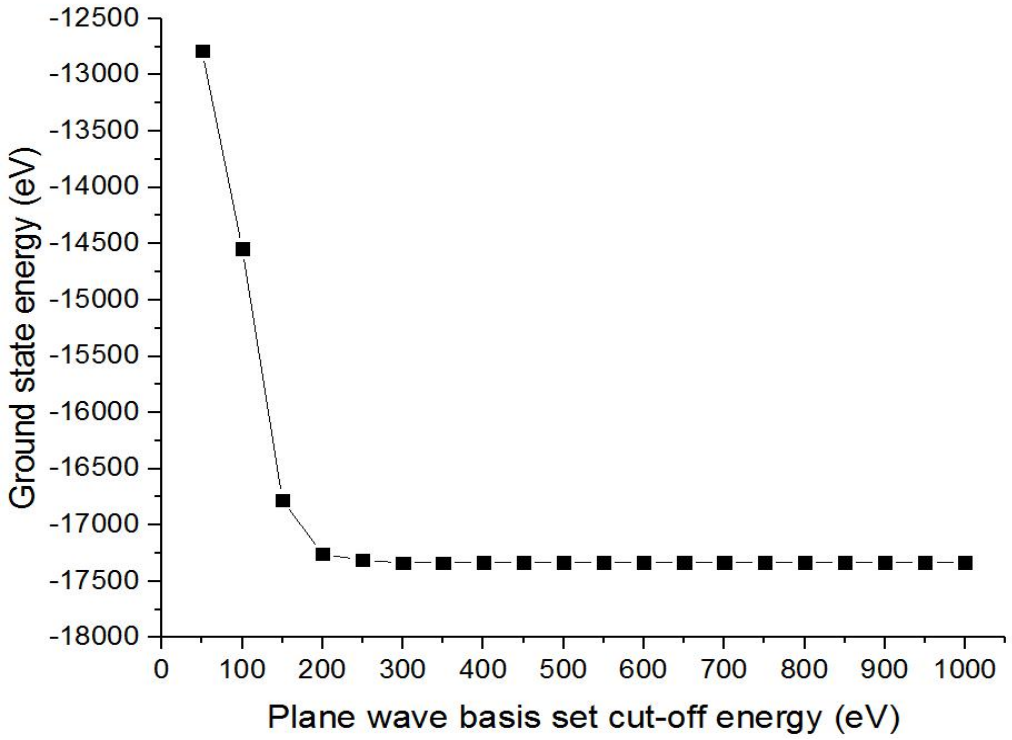


Figure 13. Total energy against plane wave basis set cut-off.

Figure 13 shows a graph of total energy against the plane wave basis set cut-off energy varied from 50 to 1000 eV with increments of 50 eV; the energy obtained from each chosen cut-off energy was recorded. The graph shows that the ground state energy becomes stable at -17331.72 eV and gives a constant value for energies starting from 400 eV, therefore the cut-off energy of 400 eV corresponding to the total energy of -17331.72 eV was chosen as the ground state energy and was used to calculate all properties for the bulk system in the study. An energy cut-off of 440 eV was used to expand the Kohn-Sham wave functions by Zongyang *et al.,* which is not far from the determined cut-off energy [26]. The wave functions were expanded in plane waves up to an energy cutoff of 380 eV by Kim *et al.* using the VASP code and the hybrid exchange-correlation functional of Heyd-Scuseria-Ernzerhof (HSE06) [85] while Maeda *et al.* applied the plane wave energy cut-off of 350 eV using CASTEP [59]. This

suggests that the energy cut-off calculations in this study are reasonable and justifiable compared to those of similar studies from the literature.

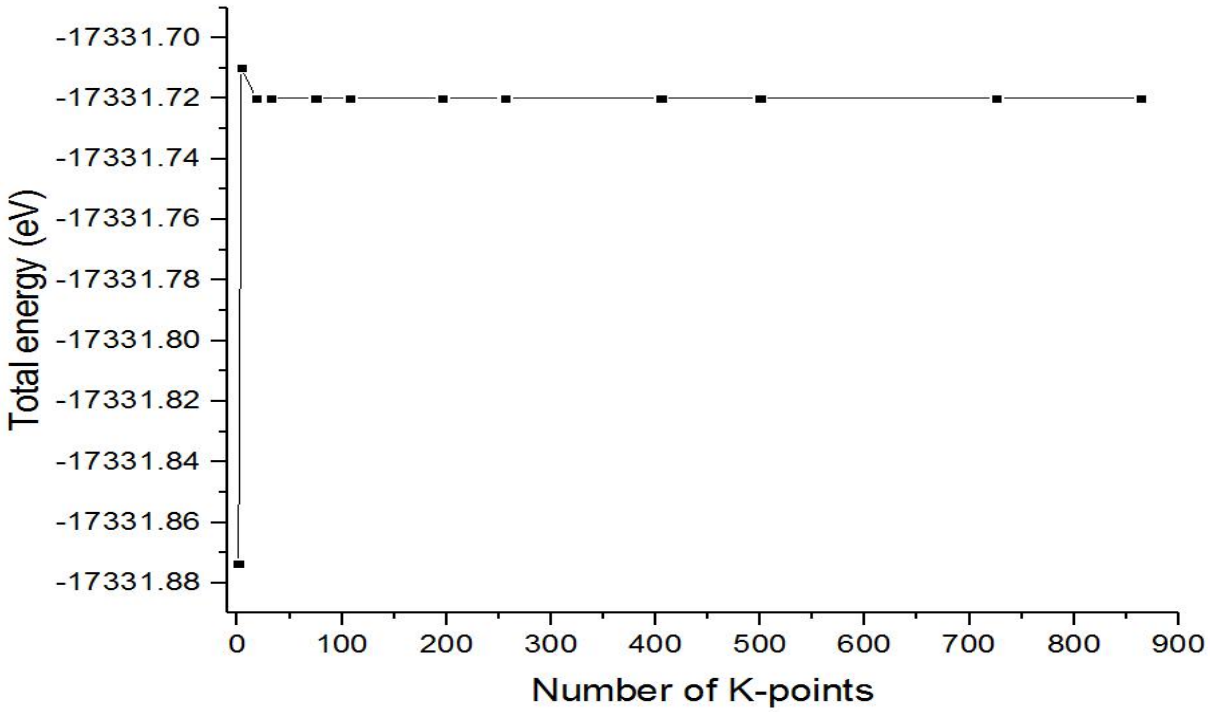


Figure 14. Graph of energy formation versus the number of k-points.

Figure 14 shows the determination of the number of k-points that gave the lowest total energy. In this work, 18 k-points were obtained to be corresponding to 4x4x2 for the Brillouin zone integration and results in a stable graph starting from that point. Therefore, all the geometry optimization and properties calculations for the bulk system were performed using 400 eV cut-off energy and 4x4x2 of k-points.

The Brillouin zone integration using a Monkhorst-Pack mesh of 4x4x2 k-points was used by Xiao *et al.* investigating intrinsic defects and sodium doping in CZTS [24]. Possible k-points that can be used include 6x6x3, 8x8x4 etc. as they all lie on the linear part of the curve indicating their usability for the Brillouin zone sampling. Dun *et.al.* used the k-points sampling of 8x8x4 to study the structure and stability of $Cu_2ZnSnS_{x-4}O_{4-x}$ and $Cu_2ZnSnS_xSe_{4-x}$ alloys for $0 \leq X \leq 4$ where pure $Cu_2ZnSnO_4$ was found to have the lowest heat of formation followed by $Cu_2ZnSnS_4$ and then $Cu_2ZnSnSe_4$ [86].

The calculated lattice parameters for the tetragonal kesterite structure of CZTS were compared with literature results and are presented in Table 1. In other CZTS studies, Chen *et.al* obtained lattice parameters of a = b = 5.630 Å and c = 11.150 Å, which are comparable with our findings [87]. After geometry optimization, the structure calculations converged after 7 iterations giving lattice parameters a = b = 5.470 Å and c = 10.920 Å which are comparable to the experimental value of a = b = 5.430 Å and c = 10.890 Å determined by Shay *et.al.* [88]. The deviation from the experimental work is very small (< 5 %). This implies that the computational methods and parameters employed in the present work are reasonable and comparable to similar previous studies.

Table 1. Lattice parameters for optimized bulk CZTS compared with experimental studies on CZTS

| | This work | Literature [26] | Deviation (%) | Literature [24] | Deviation (%) |
|---|---|---|---|---|---|
| A (Å) | 5.470 | 5.353 | 2.186 | 5.460 | 0.183 |
| B (Å) | 5.470 | 5.353 | 2.186 | 5.460 | 0.183 |
| C (Å) | 10.920 | 10.728 | 1.790 | 10.910 | 0.092 |

The angles between the lattice values were found to be 90.00° as expected for our tetragonal structure while the ratio of c/a which confirms that the magnitude of c is two times the magnitude of a is 1.996.

### 4.1.2. Electronic properties

In this section, the calculated electronic properties of the bulk system are analyzed. The CZTS bulk structure was optimized using GGA in the Perdew-Burke-Ernzerhof (PBE) scheme, allowing the atoms and the unit cell parameters to relax until the forces on all atoms had converged [83].

The band gap that we obtained for the bulk structure was 1.413 eV as visible from Figure 15, which is not far off from the expected experimental value of 1.5 eV for CZTS kesterite structure [89]. A value of 1.47 eV was obtained by Kumar *et al*. using density

functional theory on CZTS and CZTSe as absorber materials [45]. The band gap was obtained accurately by making use of the scissors operator of 1 eV, since the internal structural parameters were relaxed with the GGA functional that generally underestimates the band gap. The scissors operator describes the difference between the theoretical and experimental values of the band gap. It is applied to make the theoretical band gap match the experimental value.

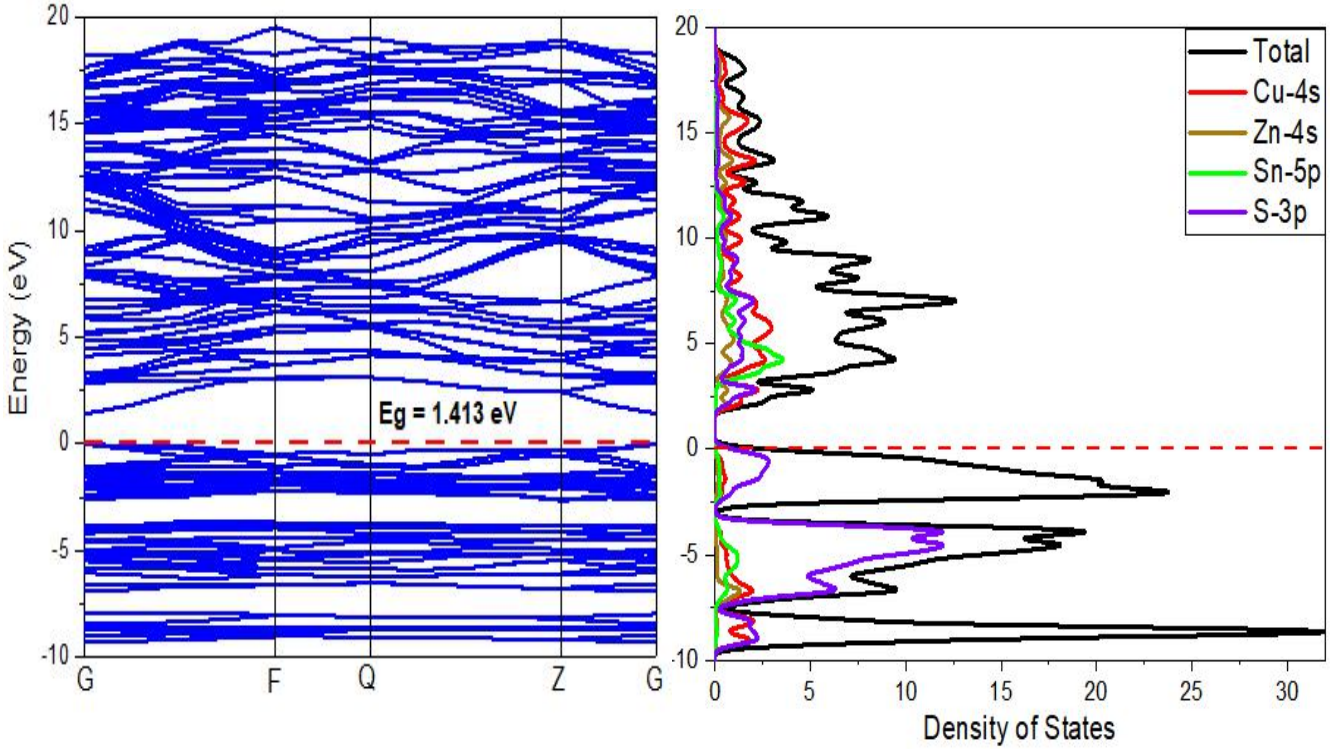


Figure 15. Band structure and density of states for bulk CZTS.

To further justify the use of scissors operator, the Heyd−Scuseria−Ernzerhof (HSE06) hybrid density functional was used to determine the band gap energy because of its accuracy for typical semiconductors. The hybrid HSE06 functional gives most certainly a better account for the band gap. HSE06 functional includes short-range exact Hartree-Fock exchange, it shifts the conduction band to higher energies like a scissor correction. The band gap obtained by using HSE06 functional is 1.495 eV, which agrees very well with the experimental value. As seen in Figure 16, CZTS possess a direct band gap as it is visibly shown on the G Brillouin zone; this is because the conduction band minimum

(CBM) and the valence band maximum (VBM) are located at the G point of the brillouin zone. Direct band gap semiconductors are the best in photon absorption and have a lower effective mass of electrons (electrons travel faster). The band gap calculated by GGA-PBE functional are obviously underestimated while the band gap calculated by HSE06 functional is very comparable to other computational results.

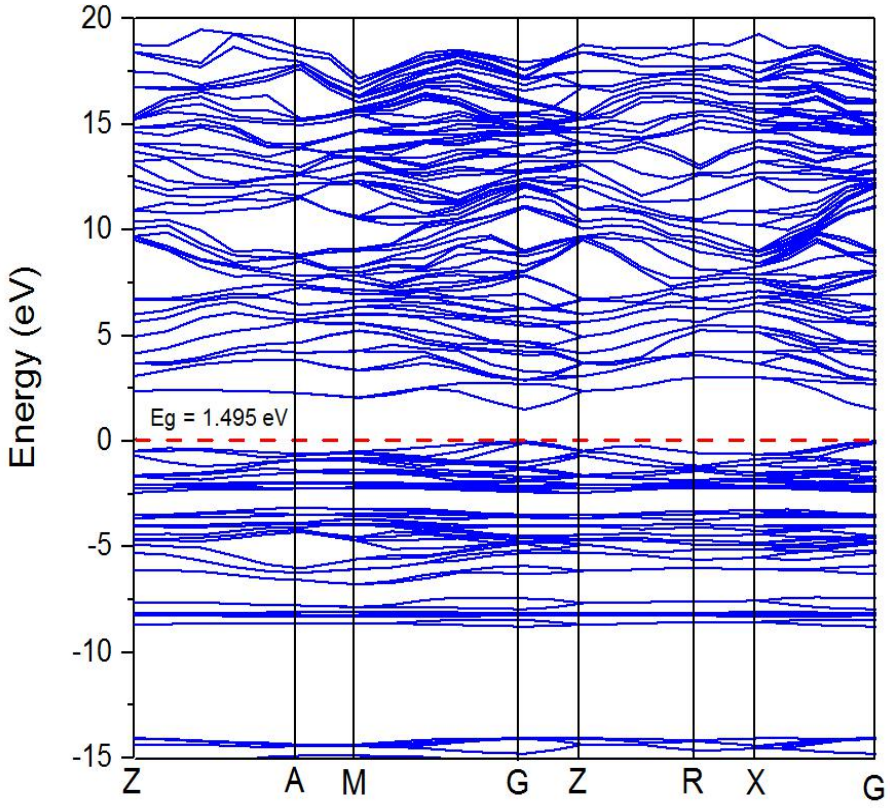


Figure 16. Band structure for bulk CZTS obtained by using HSE06 functional.

The conduction band is made of a single band while the valence band has several bandwidths. One bandwidth is observed at energies from -2 to -3 eV, which is dominated by the Cu-3d states and another one at energies from -6 to -7 eV, which is dominated by S-3p states. From -8 eV there is a huge bandwidth of about 4 eV on the valence band, which is due to the S-3s state. There are few short energy gaps on the valence band lying from -2 eV to -3 eV and -6 eV to -7 eV which are closest to the Fermi region. The conduction band has energy gap from 2 eV to 3 eV matching the energy gap on the valence band.

The valence atomic configurations of CZTS structure is $3d^{10}4s^1$ for Cu, $3d^{10}4s^2$ for Zn, $5s^25p^2$ for Sn and $3s^23p^4$ for S. The valence band is composed mostly of the S-3p and Cu-3d states while the conduction band is composed mostly of the Sn-5s and Sn-5p states respectively as indicated in the density of states in Figure 17.

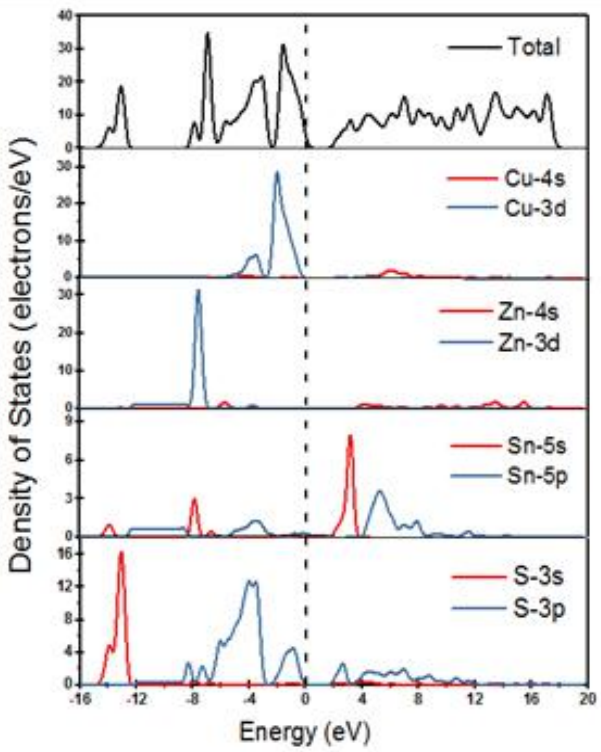


Figure 17. Partial density of states of CZTS bulk structure indicating contributions to the band gap by the last two occupied orbitals per atom.

The Cu-4s and Zn-4s states are almost vanishing with a slight appearance on energy range from 4 to 8 eV, they have the lowest density of states on both the valence and the conduction band. The s-states for Cu, Zn and S are the lowest available states on the valence and conduction bands respectively. The valence band of CZTS is mainly composed of the hybridization between Cu-3d states and S-3p states. The Zn-4s state is very low on both the valence and conduction bands, there are no states available to be occupied by the dopant elements. There is a strong presence of S-3s and 3p states on the valence band.

### 4.1.3. Optical properties

Optical properties involve a more detailed analysis of reflectivity, conductivity, dielectric constant, absorption, refractive index and the loss function of semiconductors for applications in solar cell technologies. Understanding the optical properties of semiconductors is one way to improve the efficiency of many solar-electrical energy devices. Although there are numerous experimental and theoretical studies on the electronic structures of CZTS, there are only a few studies on its optical properties [26].

All frequencies of visible light are absorbed by metal because of the continuously available empty states, which allow electron transitions since they don't allow any light to pass through, however that is not the case for semiconductors. The near surface electron absorbs visible light. When light waves strike the surface of materials, some of the waves are reflected by the material while the other portion is either absorbed or transmitted through the material. Bombardment of semiconductors by photons, with energy equal to or greater than that of the band gap results in a creation of electron-hole pairs that can be used to generate current. The absorption coefficient $\alpha(\omega)$ can also be obtained directly from the dielectric function through the equation:

$$\alpha(\omega) = \frac{\sqrt{2\omega}}{c}\left[\sqrt{\varepsilon_1(\omega)^2 + \varepsilon_2(\omega)^2} - \varepsilon_1(\omega)^2\right]^{1/2} \quad \ldots\ldots\ldots\ldots\ldots\ldots (4.1)$$

where $c$ is the speed of light and $\varepsilon_1(\omega)$, $\varepsilon_2(\omega)$ are the real and imaginary parts of the dielectric function respectively [90].

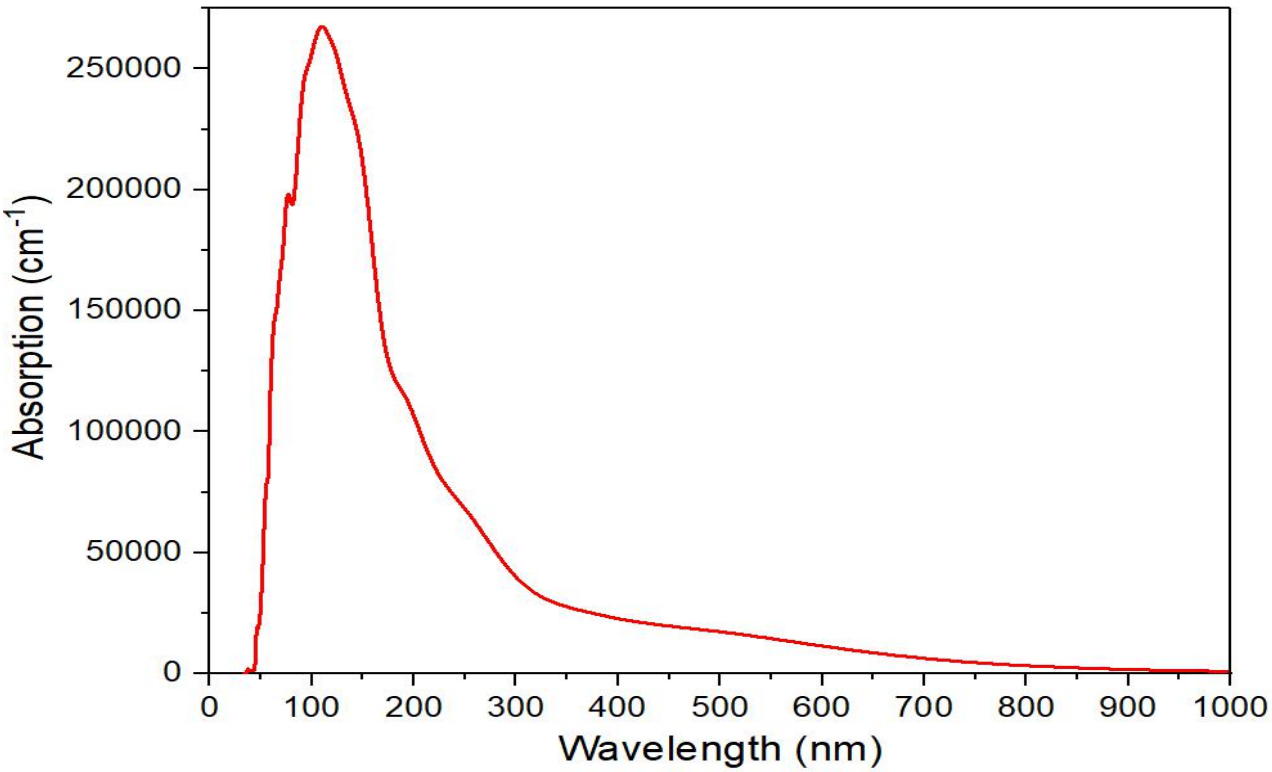


Figure 18. Absorption spectrum of bulk CZTS.

Figure 18 indicates the absorption spectrum for bulk CZTS. Optical absorption shows exactly where in the electromagnetic spectrum is the photocatalytic activity of a given semiconducting material. The visible region lies between 400 and 700 nm per the solar spectrum, calculated curve shows that CZTS has a very high absorption activity on wavelengths 50-400 nm which is the ultra-violent region. The highest absorption peak is obtained at 150 nm of the wavelength. Achieving a shift of the peak towards the visible region is ideal for application in photovoltaic solar cells. This is because most of the solar energy falling on earth has wavelengths of 250-2500 nm which is closest to the visible region and covers the infrared region, hence high absorption is desirable on the visible region for a higher conversion efficiency of solar cells.

CZTS has a high absorption coefficient of $10^4$ $cm^{-1}$ and it matches very well with the solar spectrum, it is desirable to obtain the highest peak corresponding to the absorption coefficient for CZTS. Absorption coefficient defines the amount of light absorbed by the material. Figure 18 shows that most of the light is absorbed on the

wavelengths ranging between 50 and 250 nm. A low absorption coefficient results in the carrier generation throughout the semiconducting material. To achieve the desirable results for CZTS and chalcopyrite in general, the response to visible light needs to be enhanced using various methods and one of which is doping with foreign elements that have very high optical and electrolytic response.

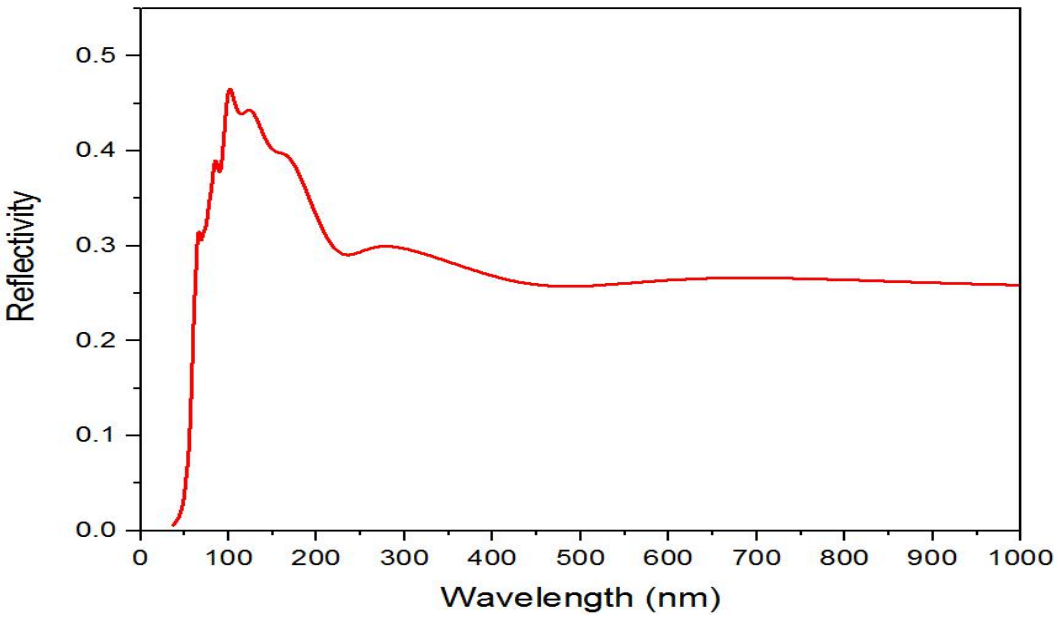


Figure 19. Reflection spectrum of bulk CZTS.

Reflectivity is the ratio of the light wave reflected from a surface. The reflectivity spectrum is displayed in figure 19 as a function of wavelength. The highest reflectivity is at wavelength of 100 nm, thereafter it drops from 110-200 nm with a slight occurrence of two shoulder peaks. There is an indication of lower reflectivity at wavelengths 400-500 nm as the spectrum seems to be skewed downwards. The maximum reflectivity occurs in the ultra-violent region. The reflectivity maintains a constant lowest value for wavelengths ranging from 500 to 1000 nm.

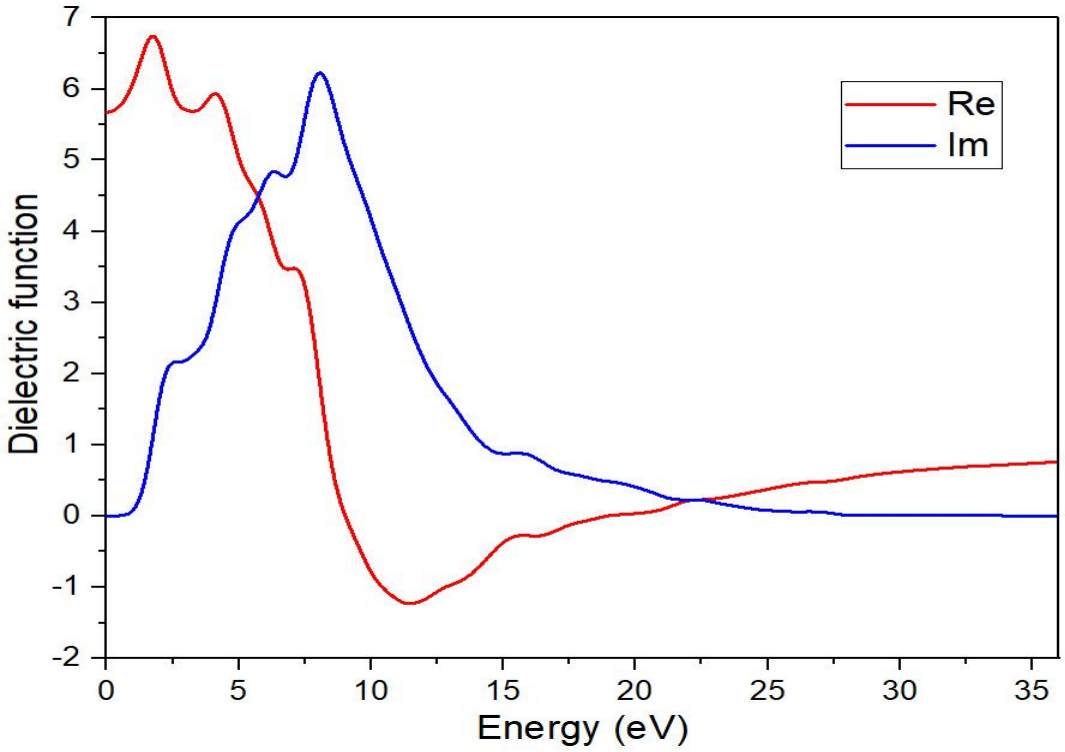


Figure 20. Dielectric function of bulk CZTS.

The real and imaginary parts of the dielectric function against the frequency are shown in figure 20, one main aspect of the characteristics of solids is the dielectric function. The dielectric function of any material describes the electrical and optical properties by focusing on the polarization and absorption properties of that material. It consists of two parts, the real and imaginary parts thus making it a complex function. The frequency dependent dielectric function is given by the equation:

$$\varepsilon(\omega) = \varepsilon_1(\omega) + i\varepsilon_2(\omega) \quad \ldots\ldots\ldots\ldots\ldots\ldots\ldots\ldots \quad (4.2)$$

The imaginary part of the curve denoted by $\varepsilon_2(\omega)$ is evaluated first from the direct inter-band transition and the real part of the curve $\varepsilon_1(\omega)$ is obtained from the imaginary part by Kramers-Kronig conversion [26]. The electronic band structure is the main underlying property for analyzing the polarization response because the dielectric function is related to the joint density of states [91]. The polarizability, which represents the deformability of the electronic distribution is to be connected with the shape of the valence charge density [92].

The imaginary part shows one main peak at 8 eV and it adopts a constant value as the frequency increases. As the frequency decreases from 8 eV, there are few minor peaks and the noticeable ones are located at 2 eV and 6 eV. The dielectric function for the real part decreases as the frequency increases, major peaks are located at 1 eV, 3 eV and 4.5 eV with the lowest peak located at 11 eV. The real and imaginary parts of the dielectric function have the same value of frequency at 5 eV. The highest peak of the real part is located at energies favorable to many semiconductors for application in solar cells and corresponds to the band gap of 1.5 eV for CZTS.

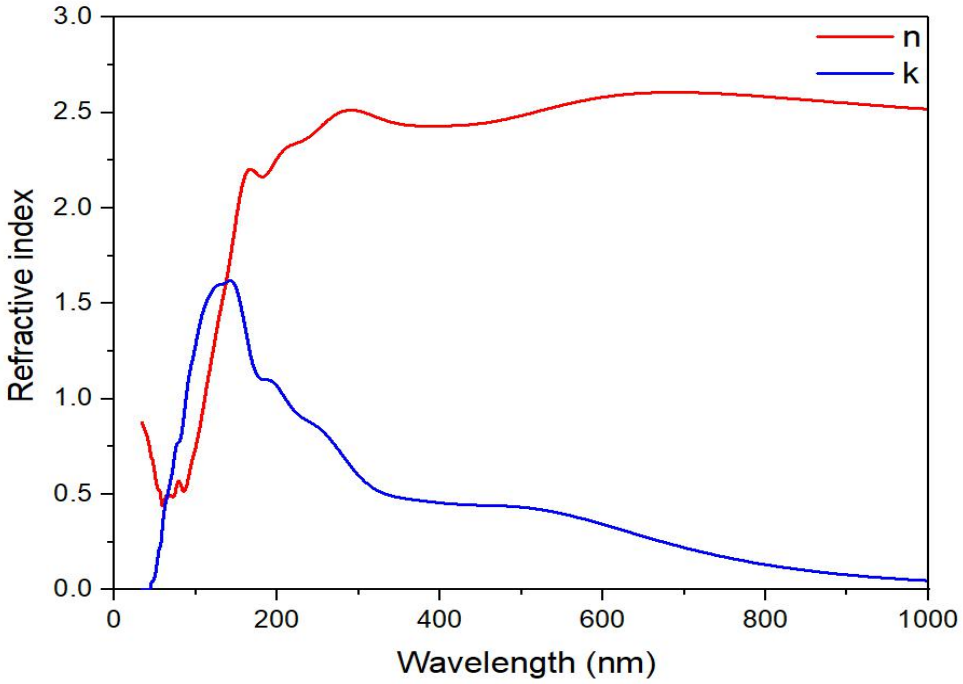


Figure 21. Refractive index of bulk CZTS.

The refractive index spectrum is presented in Figure 21. The refractive index in a semiconductor is the measure of its transparency to incident spectral radiation. We can be able to tell how much of light is refracted or reflected upon falling on a material by analyzing the refractive index. The refractive index is closely related to the band gap. The relation is represented by the Moss relation equation with a conclusion that the narrow absorption band of semiconductors in the ultra-violent region is the factor which

determines the refractive index [93]. The refractive index is directly related to the fundamental energy gap by the Moss relation equation:

$$E_g n^4 = k \quad \ldots\ldots\ldots\ldots\ldots\ldots\ldots\ldots\ldots\ldots\ldots\ldots \quad (4.3)$$

where k is a constant with a value of 108 eV. The band gap obtained for the current study is 1.413 eV, using the above equation we obtain the refractive index of 1.400, compared to the experimental value of 2.323 [94].

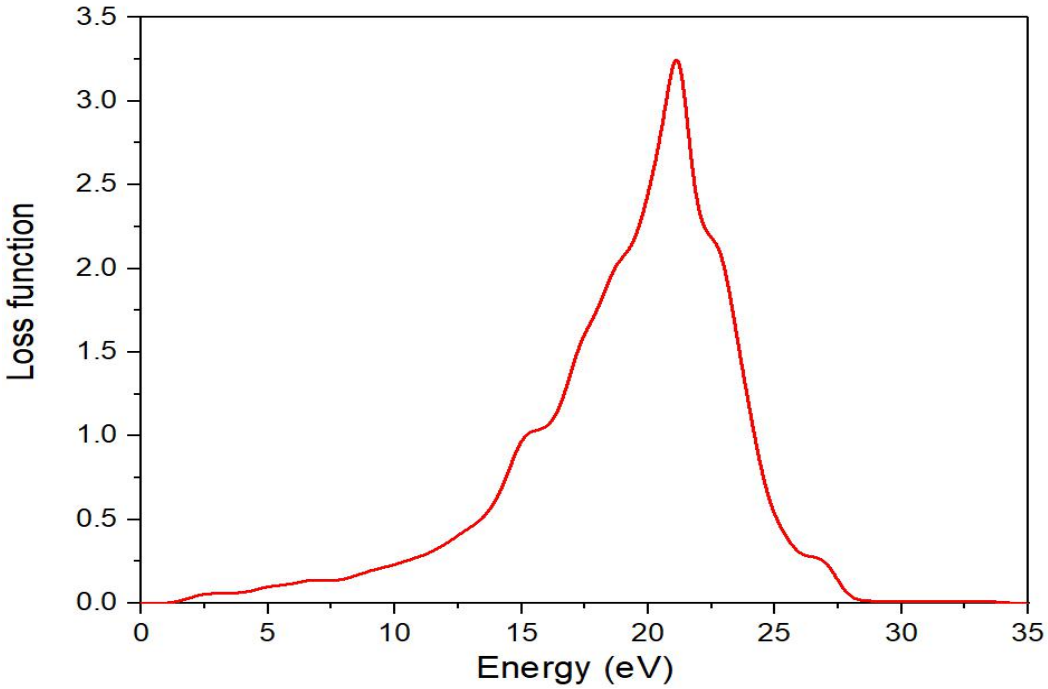


Figure 22. Energy loss function of bulk CZTS.

The energy loss function represents the energy loss of electrons when passing through a material. The band gap of CZTS obtained is 1.447 eV, energy loss function is expected to be lower in energy values around 1.447 eV. The spectrum suggests that CZTS loses very little of energy for the band gap as the spectrum lies flat on energies from 0 to 2 eV and increases from there. Achieving low energy loss function corresponding to the band gap energy is favorable for CZTS base photovoltaic solar cells.

The energy loss function shows a sharp peak at 21 eV. There is a smooth increase of energy lost from 2 to 10 eV, thereafter there is an exponential increase for energies ranging from 10 to 21 eV. A drop of loss function is observed for a very short range of energies from 21 to 25 eV. This is due to the very high reflectivity around the energies in that range. The energy loss function adopts a constant value for energies starting from 28 eV. This indicates no energy lost from energies beyond 28 eV.

### 4.2. CZTS (112) surface

The (112) surface was cleaved from the bulk CZTS system and is shown in Figure 23. The literature suggests that (112) surface is the most dominant and stable surface of CZTS [95]. The surface thickness was set to 8.596 Å to allow all atoms on the structure to be accounted for and visible on the surface. The vacuum thickness was set to 10.00 Å so that the atom can be restricted to be as close as possible to the surface. To expose more of the CZTS surface, a 2x2x2 supercell was employed. This allowed more doping regions as well as a larger plane to expose more of the surface.

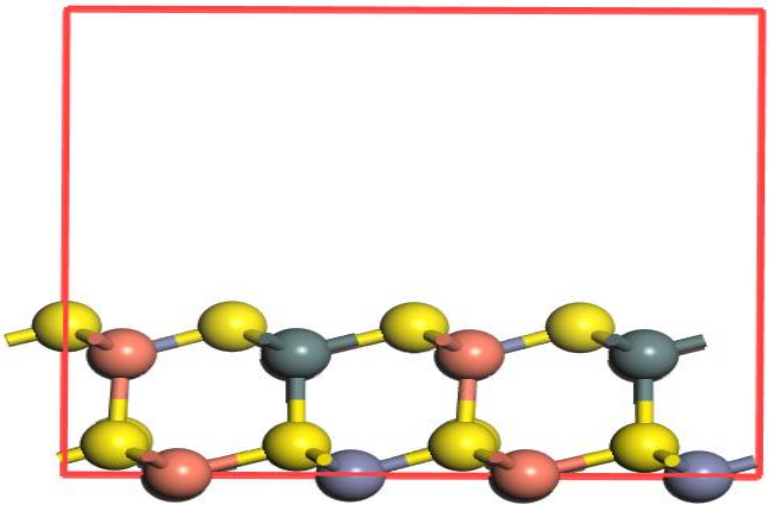

Figure 23. CZTS (112) pure surface.

The surface is dominated by sulphur and copper atoms as they are the most central atoms in the bulk structure. Tin and zinc are the least appearing atoms in the bulk structure, hence it is still the case even on the surface.

### 4.2.1. Electronic properties

The band structure for CZTS (112) plane gives a band gap of 1.2 eV. It exhibits properties of a flat energy gap that is desirable for semiconductors. Flat band topology cancels out the formation of electron traps in the band gap resulting in an even distribution of electrons along the band. Clas *et al.* in reviewing the electronic and optical properties of CZTS and CZTSe stated that the flat CB and VB dispersions are more pronounced in the CZTS and CZTSe compared with the chalcopyrite CIGS and CIGSe [91]. This results in electrons easily moving from the valence band to the conduction band with the same energy and cancels any possible electron traps that might arise in the energy gap.

There is one strongly visible band width in the conduction band which is very close to the Fermi level. The energy gap for the band width is 0.5 eV and it creates a boundary for electrons to migrate easily into the conduction band. An additional energy of 0.5 eV will be required to allow electrons to reach the conduction band from the valence band. There is no available data from literature to compare the band structures of the surface.

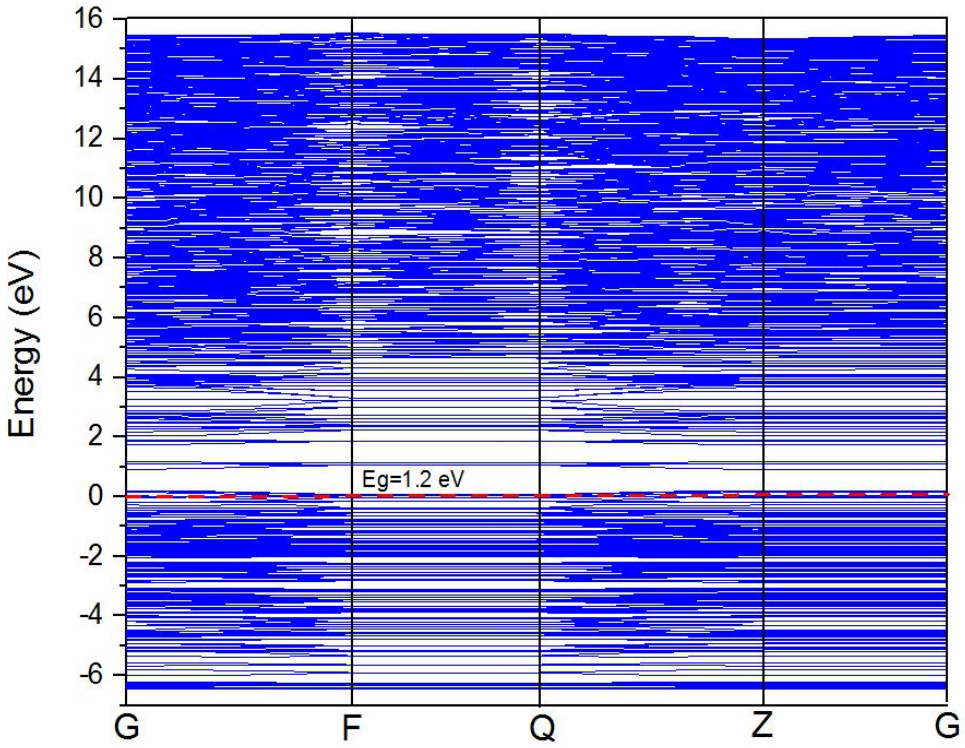


Figure 24. Band structure of pure CZTS (112) surface.

There are no literature results on electronic and optical properties for the CZTS (112) surface to compare with. Most studies focused on absorption, substitution and addition of dopants on the bulk CZTS structure. Additional information on electronic properties can be obtained from the density of states and is presented in Figure 25. The total density of states for the surface is dominated by the Cu-3d, Zn-3d and S-3p states on the valence band while the conduction band is dominated by the Sn-5s and Sn-5p states.

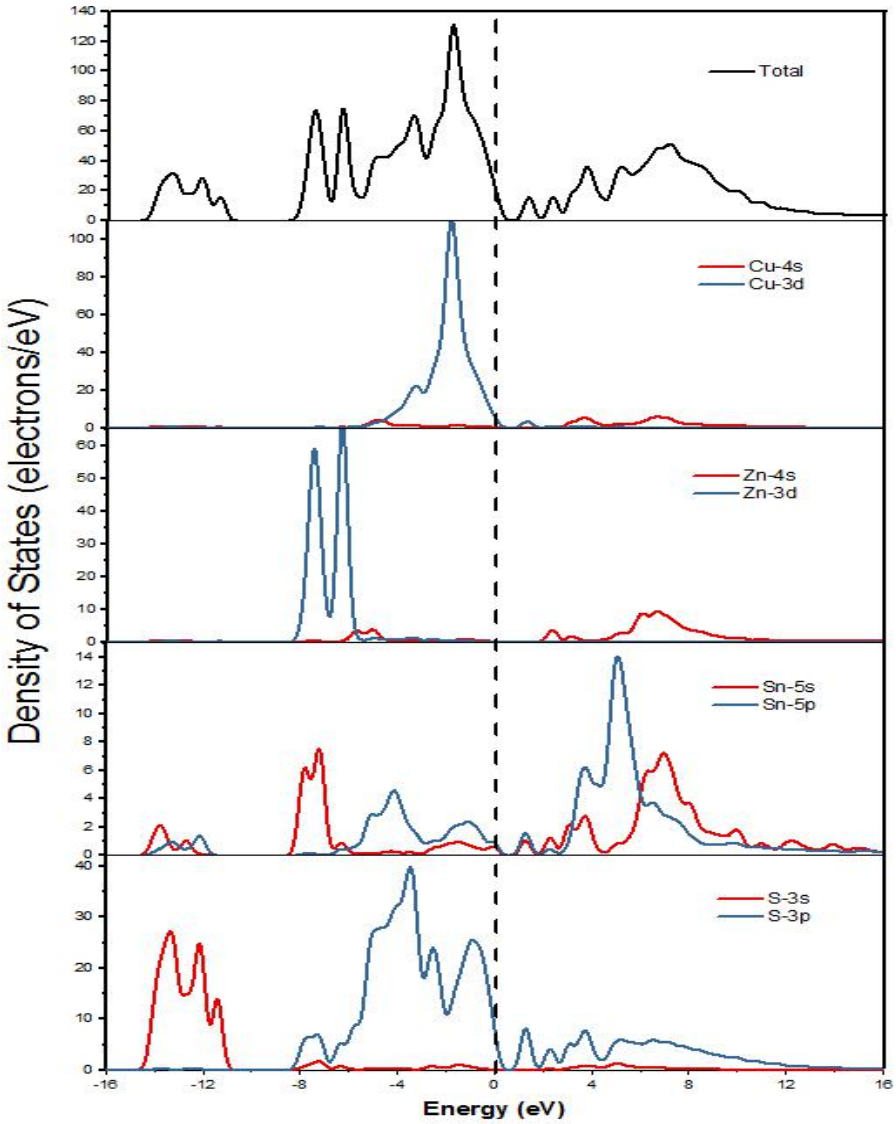


Figure 25. Density of states for CZTS (112) surface.

The peak for the total energy on the valence band is due to the hybridization between the S-3p and Cu-3d states. The Zn-4s state has a very little contribution to both the valence and conduction bands. For very low energies, the valence band consists mostly of S-3p states. The peak for the total energy on the conduction band is due to the hybridization of Sn-5p and S-3p states. The Cu-3d and Zn-3d states are dominant on the valence band.

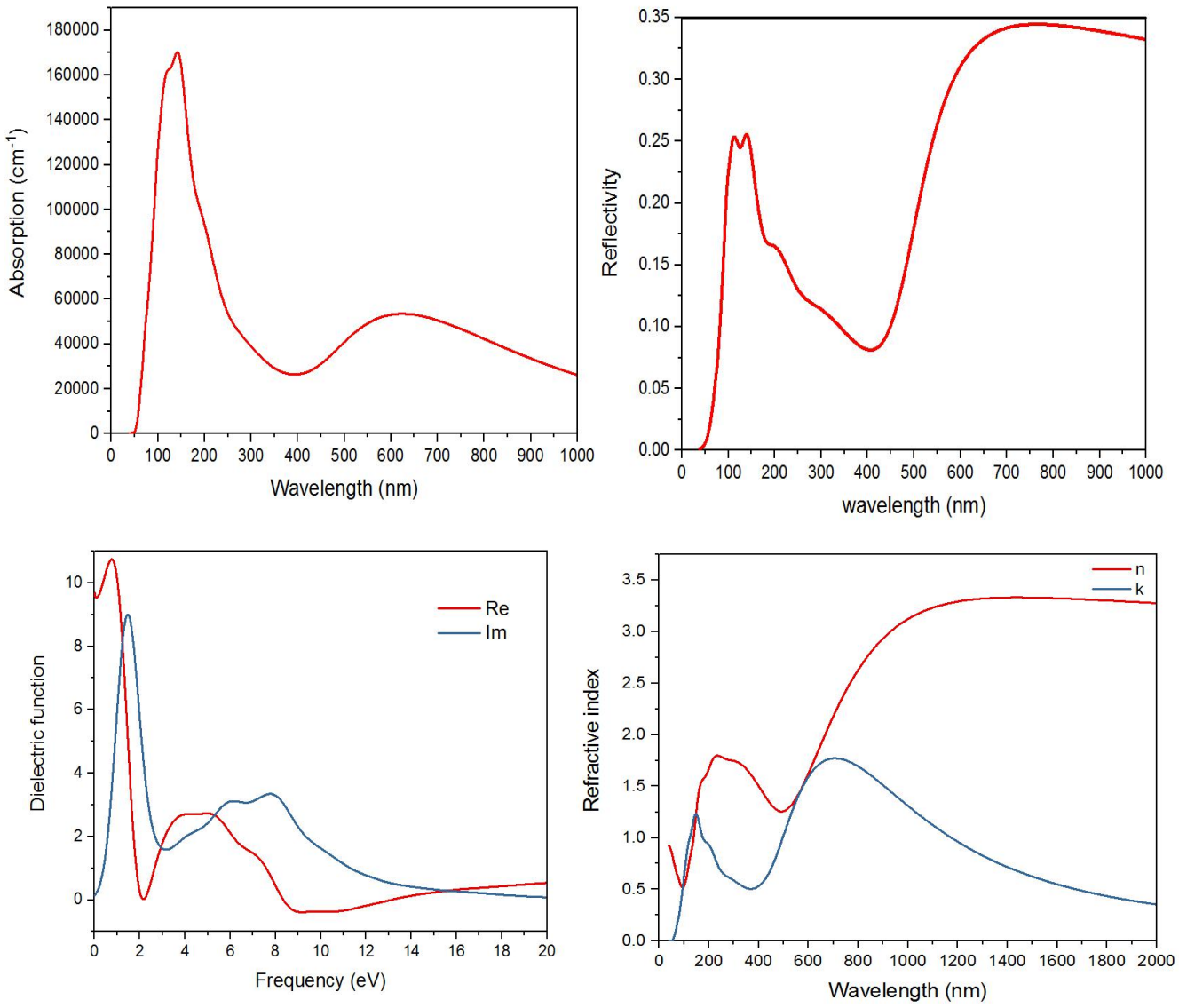


Figure 26. Absorption, reflectivity, dielectric function and refractive index for CZTS (112) surface.

The CTZS (112) surface shows an increase in absorption compared to the bulk CZST over the visible region, however it has maximum absorption in the ultra-violet (UV) region as indicated in Figure 26. The reflectivity curve shows an increase in reflectivity in the visible region. The maximum peak is directly at 700 nm and the increase is triggered at 400 nm. The real part of the dielectric function has a maximum peak at 1.5 eV and a sharp drop to a low peak at 2 eV. The imaginary part has a high peak at 2 eV

corresponding to the real part minimum. The curves indicate points where the real and imaginary curves have the same values such as at 2.5 and 4.5 eV.

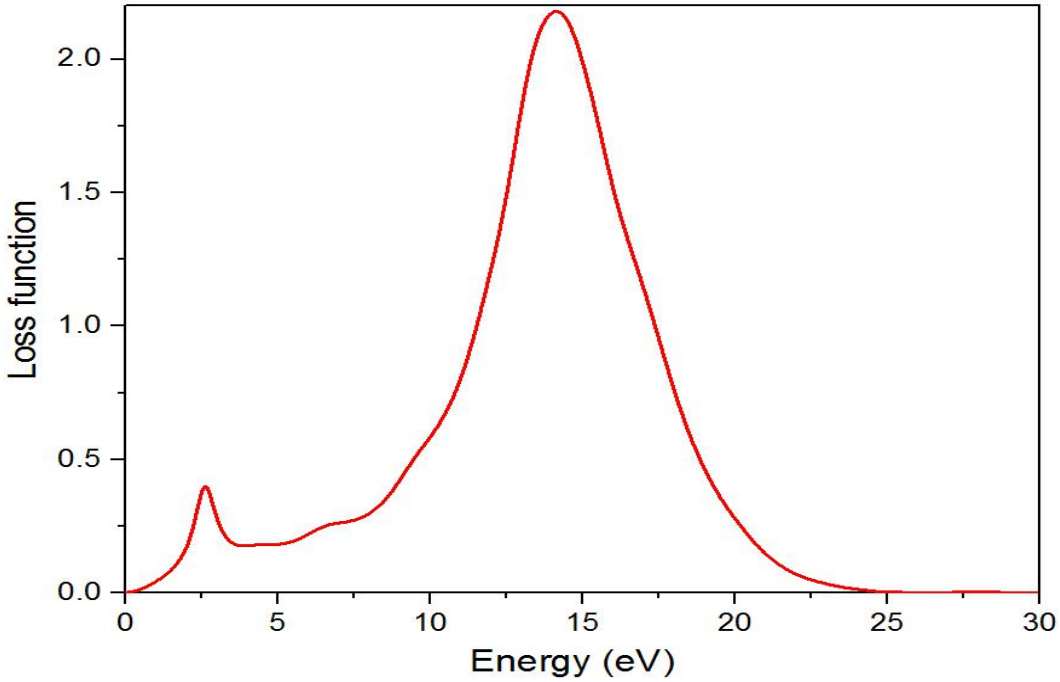


Figure 27. Energy loss function for CZTS (112) surface.

The energy loss function has a maximum peak at around 15 eV and a smaller peak located at 2.5 eV in Figure 27. There is a constant increase and decline of the curve to and from the maximum peak. The loss function spectrum adopts a constant lowest value at points beyond 25 eV. This is typical for CZTS as observed from the results obtained on the bulk structure. The energy loss function gives information about the transparency of the material, for a very high loss function the material is expected to be transparent. CZTS requires energies far lower than 13 eV for electrons to be ejected from the valence to conduction band.

### 4.3. Doped CZTS (112) surface

To investigate the effect of doping, (112) surface was cleaved from the bulk CZTS system as discussed in section 4.2. After a full geometry optimization of the surface, sodium, barium and calcium atoms were adsorbed onto (112) surface and predicted

both the electronic and optical properties. The Adsorption Locator module of Materials Studio was used to determine the optimum doping site and preferred attachment of the atom onto the surface. The module identifies the adsorption areas with low energies, which are preferred as the doping regions on the surface.

### 4.3.1. Na-doped CZTS

The Adsorption Locator module gives regions for the lowest energy on the surface where the dopant is to be adsorbed. It uses the force-field method to obtain a ranking of the energies for each generated configuration, thereby indicating the preferred adsorption sites. The number of low energy regions also depend on the surface area of the plane, with larger surfaces producing more regions of low energy on the surface. Another contribution to the number of regions is the atom that is being adsorbed onto the surface. For this study, only the first lowest energy region is considered, i.e. Na-doped - 1 with an adsorption energy -0.510 eV as listed in Table 2. The low energy regions in the table are indicated by the shaded areas on the surface of the plane.

The energies are generated automatically by the Adsorption Locator module for all the calculations. The lowest energy regions have energies starting from -0.510 eV to the highest possible being -0.286 eV. For Na to be attached or removed from the surface, it will need a minimum of -0.510 eV in energy. These energies correspond to the shaded fields indicated in Figure 28 with the lowest being pointed with an arrow and highest being lightly red and smaller in size. The highest energy regions appear very weak, small and almost disappearing from the surface, while the lowest energy regions appear big and strongly shaded.

Table 2. Adsorption energies for Na doped regions on the CZTS (112) surface

| **Structures** | **Adsorption energy (eV)** |
|---|---|
| Na-doped – 1 | -0.510 |
| Na-doped – 2 | -0.460 |

| | |
|---|---|
| Na-doped – 3 | -0.448 |
| Na-doped – 4 | -0.448 |
| Na-doped – 5 | -0.429 |
| Na-doped – 6 | -0.424 |
| Na-doped – 7 | -0.415 |
| Na-doped – 8 | -0.415 |
| Na-doped – 9 | -0.414 |
| Na-doped – 10 | -0.311 |
| Na-doped – 11 | -0.286 |

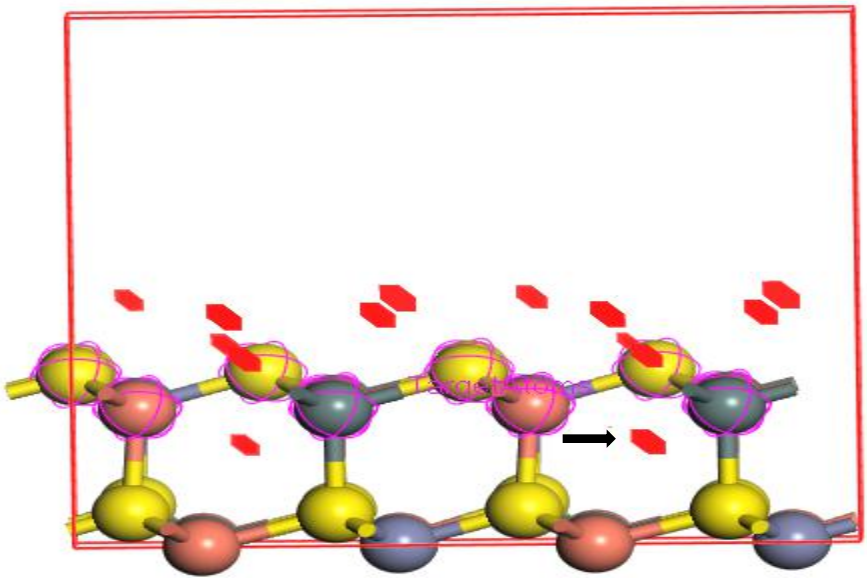

Figure 28. CZTS (112) surface indicating adsorption volume fields for low energies for Na.

Figure 28 shows strong fields for sodium adsorption on the surface. These fields are associated with very low energies preferred for adsorption. The sodium atom is to be adsorbed at these regions and preference is given to the strongly reddish and bigger regions as they indicate areas of lowest energy on the surface. The lowest energy region is indicated by the black arrow in Figure 28. There are other strongest fields of adsorption visible with two around the center and another two on the right side of the surface.

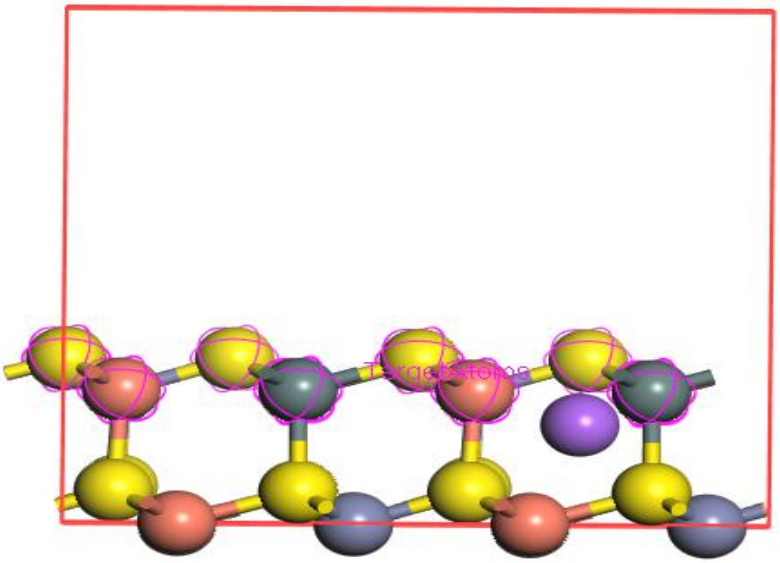

Figure 29. Na-doped CZTS (112) surface, adsorbed atom indicted by purple ball.

Figure 29 shows the position of sodium (in purple) adsorbed onto the (112) surface. The sodium atom is mostly adsorbed by the sulfur atoms on the surface. This is due to the strong presence of sulphur on the (112) surface than any other atom of CZTS. Na atom is imbedded within the structure rather than a distance from the surface. The position corresponds to the adsorption energy of -0.510 eV. Sulphur and tin are closest to the sodium atom.

The band structure for sodium doped CZTS (112) surface is shown in Figure 30. The band gap was found to be 1.016 eV, which is very close to 1 eV. There are visible bandwidths on the conduction band. The first bandwidth is located at energies between 1 and 2 eV, which is about 0.5 eV. Another bandwidth on the conduction band is located at 5 to 6 eV, which also is around 0.5 eV. Sodium doped CZTS (112) surface creates bandwidths that are 0.5 eV or lower closest to the band gap and increase for higher energies.

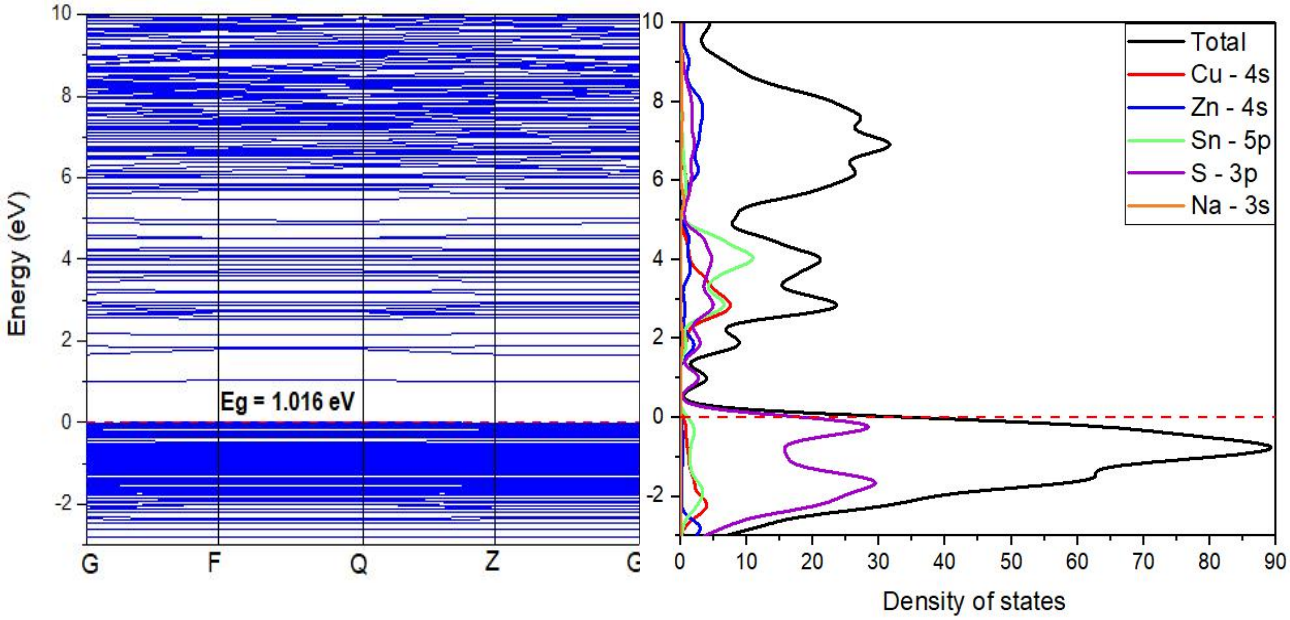


Figure 30. Na-doped CZTS (112) surface band structure and density of states.

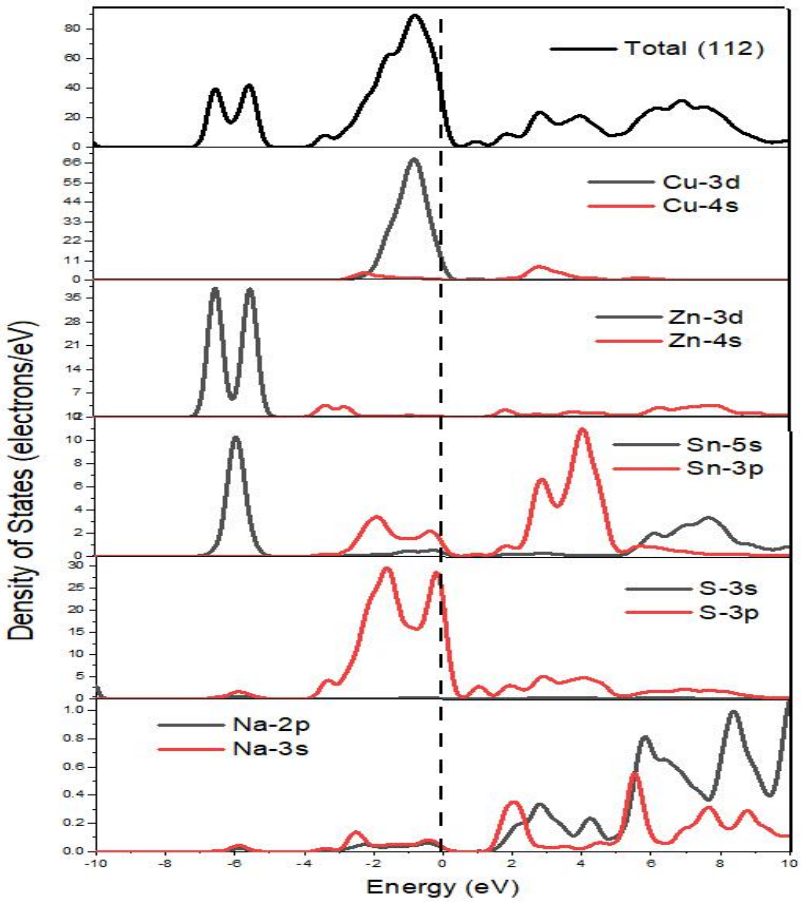


Figure 31. Partial density of states for Na-doped (112) surface, the highest two occupied orbitals are indicated.

The partial density of states show a significant contribution from the sodium atom on the conduction band as shown by Figure 31. The most active state is the 2p state. The valence and conduction bands are showing strong presence of the Na-2p state. The Na-3s peak is located at around 3 eV on the conduction band. The band gap is mostly composed of Cu-3d, S-3p and Na-2p states respectively. The greatest contribution to the total density of states on the valence band is mostly due to Cu-3d, S-3p and Na-2p and the conduction band is mostly Sn-5p and Na-2p states.

Xia *et al*. [24] showed that the upper valence band of Na doped CZTS mainly consists of Cu-d and S-p states; this is supported by the greater presence of Cu-3d and S-3p as major contributors to the valence band from Figure 31. A noticeable reduction in the band gap is one property expected for Na-doped CZTS. This suggests that our results correlate literature results obtained for Na-doped systems.

### 4.3.2. Ca-doped CZTS

There are five possible regions of low energy on the (112) surface of CZTS for the Ca atom adsorption. The only considered adsorption configuration is for Ca-doped-1. It is expected to give the best results since they are ordered accordingly arranged starting from the lowest to highest possible energy for the adsorption.

Table 3. Adsorption energies of Ca on CZTS (112) surface

| Structures | Adsorption energy (eV) |
|---|---|
| Ca-doped – 1 | -1.417 |
| Ca-doped – 2 | -1.354 |
| Ca-doped – 3 | -1.307 |
| Ca-doped – 4 | -1.287 |
| Ca-doped – 5 | -1.226 |

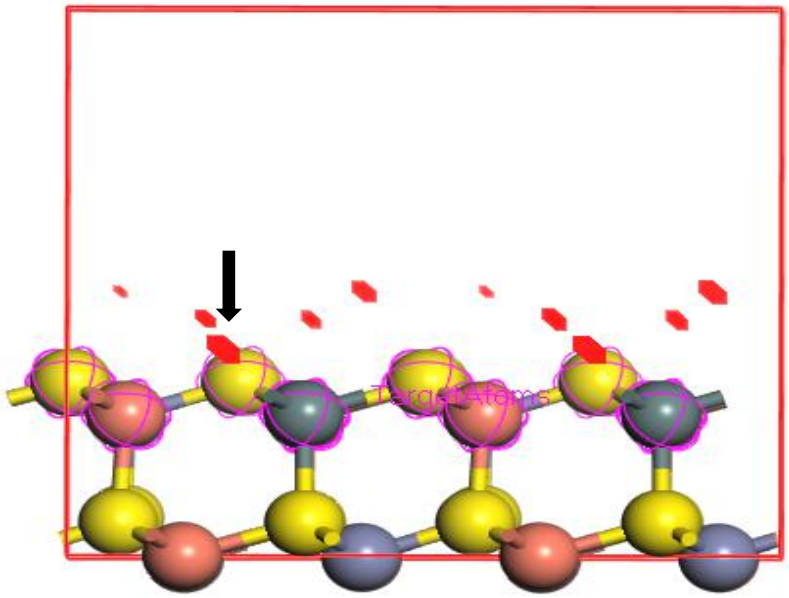

Figure 32. CZTS (112) surface indicating adsorption volume fields for low energies for Ca.

There is a strong presence of adsorption regions on most parts of the surface with the dominant ones indicated by bigger shapes and shaded strongly red. Figure 32 suggests that Ca can be adsorbed closer to sulphur atom as indicated by the biggest shaded regions located very close to sulphur. The lowest energy region is indicated by the black arrow in Figure 32.

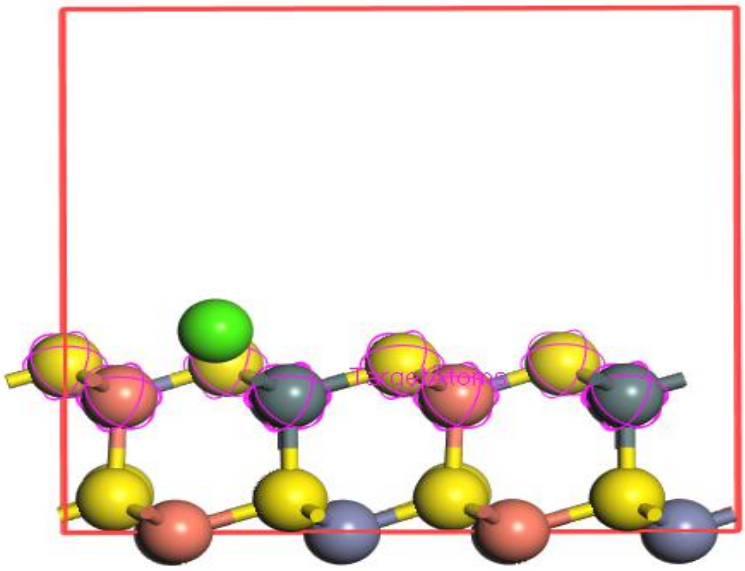

Figure 33. Ca-doped CZTS (112) surface, adsorbed atom indicated by green ball.

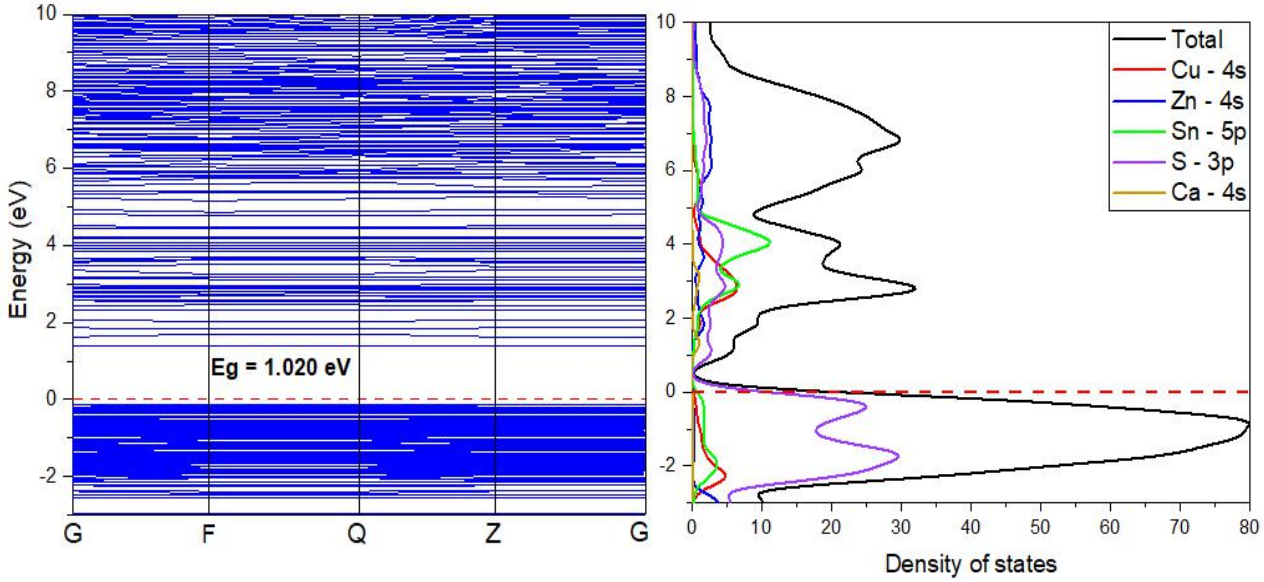


Figure 34. Ca-doped CZTS (112) surface band structure and density of states.

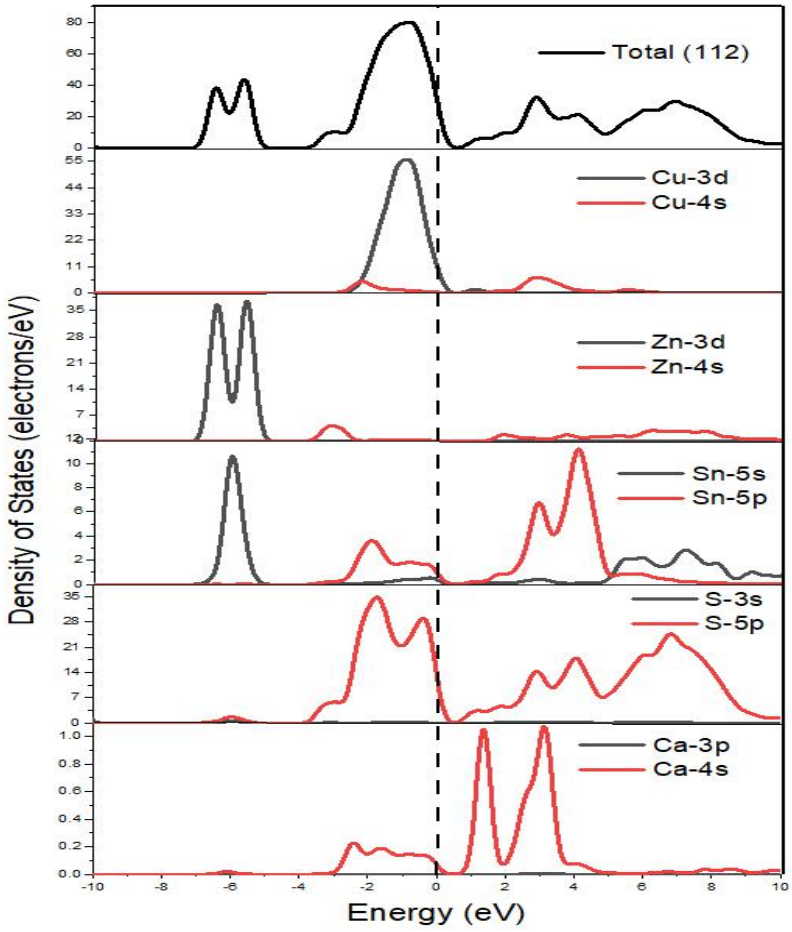


Figure 35. Partial density of states for Ca-doped (112) surface, the highest two occupied orbitals are indicated.

The band gap is 1.020 eV for the Ca-doped surface. There is a presence of very small and noticeable bandwidths between 1.3 and 3 eV, this serves as an electron trap region. The valence band has bandwidths furthest to the band gap.

There is a strong presence of the S-5p and Cu-3d state on the band gap region. The states closest to the Fermi level are due to Cu-3d and S-5p orbitals as indicated by Figure 35. Zinc is very weak with only the Zn-3d state appearing on the valence band at lower energy from -4 eV to -8e V and Cu-4s orbital with almost no contribution to both the valence and conduction bands. The contribution of calcium is mostly due to the Ca-4s state and is dominant on the conduction band.

### 4.3.3. Ba-doped CZTS

The Adsorption Locator module gives four possible locations on the CZTS (112) surface where the Ba can be adsorbed as indicated by the red regions. The possible locations are ranked per their energies starting from the lowest (most favorable) to the highest (less favorable) adsorption site.

Table 4. Adsorption energies for Ba atom on the CZTS (1 1 2) surface

| Structures | Adsorption energy (eV) |
|---|---|
| Ba-doped – 1 | -1.957 |
| Ba-doped – 2 | -1.740 |
| Ba-doped – 3 | -1.721 |
| Ba-doped – 4 | -1.585 |

The fields represent areas on the surface where it has the lowest energy and thus favorable for adsorption. The bigger the shaded region, the more likely is the atom to be adsorbed in the location. The preferred areas of low energy for the atom attachment are indicated by the volume of the regions inside the red hexagonal shapes. There are two dominant low energy regions indicated in Figure 36. Both these locations are very close to the sulphur atom indicated by the yellow colour. The lowest energy region is indicated by the black arrow in Figure 36.

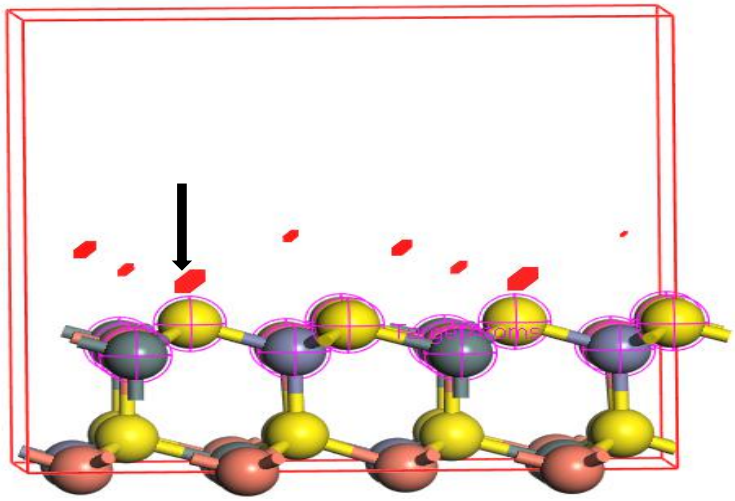

Figure 36. CZTS (112) surface indicating adsorption volume fields for low energies for Ba.

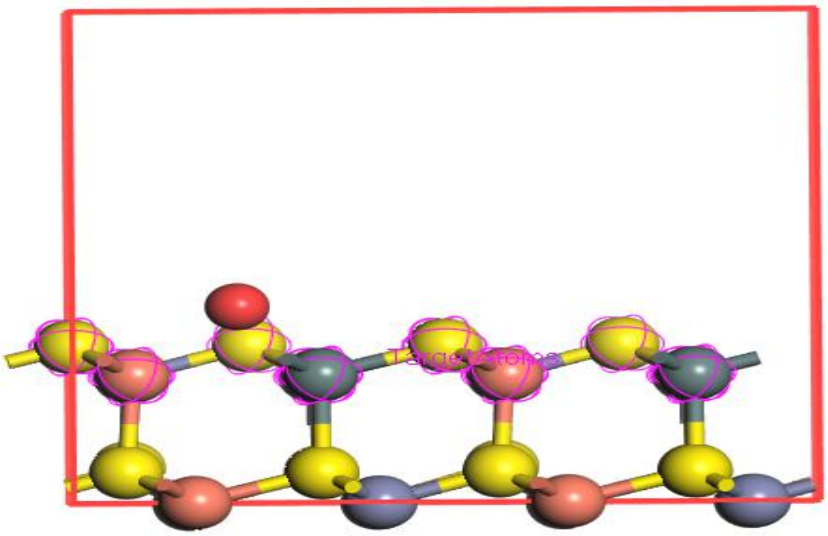

Figure 37. Ba-doped CZTS (112) surface, absorbed atom indicated by red ball.

There are two possible locations for the barium atom to be adsorbed on the (112) plane, these are indicated Table 4. The current study focuses only on one of the possibe locations indicated as Ba-doped-1. The Ba-doped structure is given in Figure 37 showing the location of the barium atom (red coloured) on the (112) plane. The barium atom is adsorbed slightly above the sulphur atom on the plane.

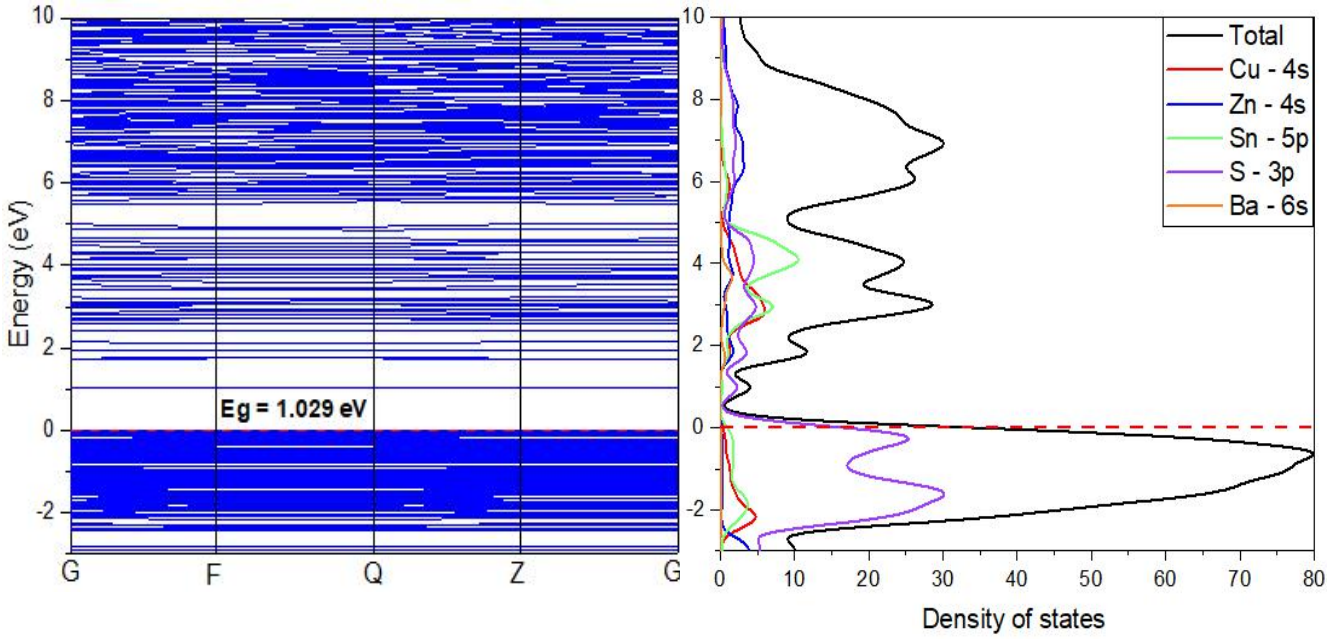


Figure 38. Ba-doped CZTS (112) surface band structure and density of states.

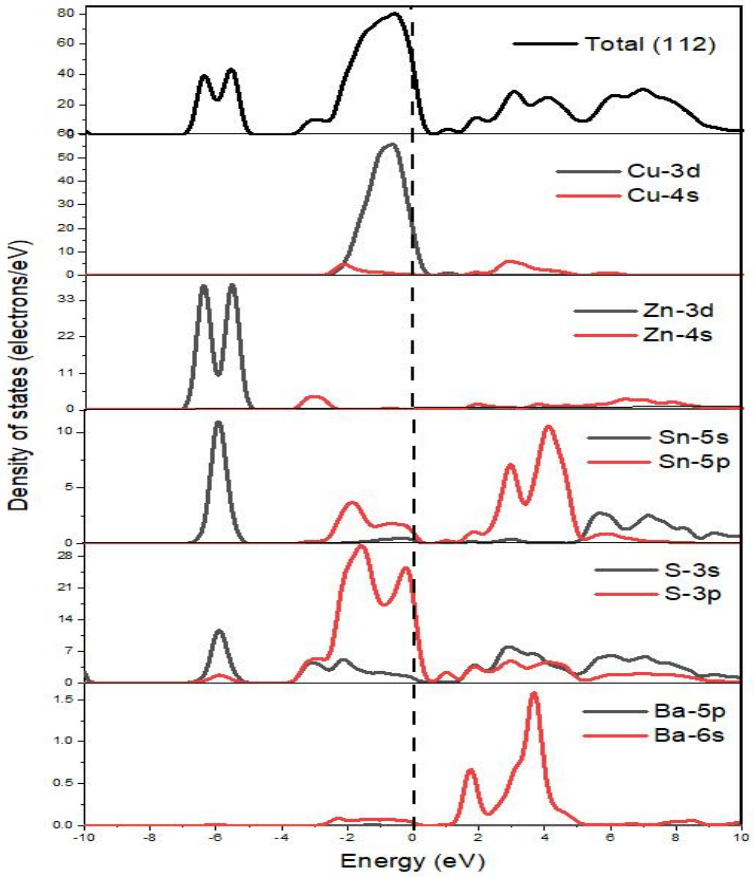


Figure 39. Partial density of states for Ba-doped (112) surface, the highest two occupied orbitals are indicated.

The band structure for Ba-doped CZTS (112) surface is presented above. The band gap is 1.209 eV. There are observable bandwidths from both the valence and conduction bands with the conduction band being the dominant. The valence band has three bandwidths on the energies ranging from -8 eV to 0 eV. Most of them are attributed to the flat states for Cu-4s, Zn-3s and S-3s respectively. Ba has no contribution to the valence band with any states.

The density of states for Ba-doped CZTS on the (112) plane shows a very strong presence of the Sn-5p and S-3p states around the band gap, this indicates that there is hybridization of the p-orbitals for tin and sulphur. The Cu-4s, Zn-4s and S-3s orbitals are showing no signs of activity around the band gap, hence they are less involved in the band structure adjustments. It indicates that knowing properties of tin can bring a huge change to the properties of CZTS doped with barium. There is a very small contribution to the overall density of states coming from barium. The only active state is located at the conduction band for the Ba-6s state.

### 4.4. CZTS (112) surface optical properties

The application of CZTS in photovoltaics requires very high performance of its optical properties in the visible region. Countless factors such as absorption and reflectivity take great influence to the performance of semiconductors.

Absorption coefficient gives information about the solar energy conversion of material and how far light of specific frequency can penetrate the material before being absorbed. The absorption against wavelength spectra is given in Figure 40. The undoped CZTS surface' absorption curve is compared with Na-, Ca- and Ba-doped CZTS (112) absorption spectra. The visible region indicates more absorption activity for the spectra with barium being the highest and sodium taking the lowest other than the total (total being for the pure surface). There is an impressive improvement of absorption from the total CZTS (112) surface for Na-, Ca- and Ba-doped surface on the visible region with the differences clearly visible.

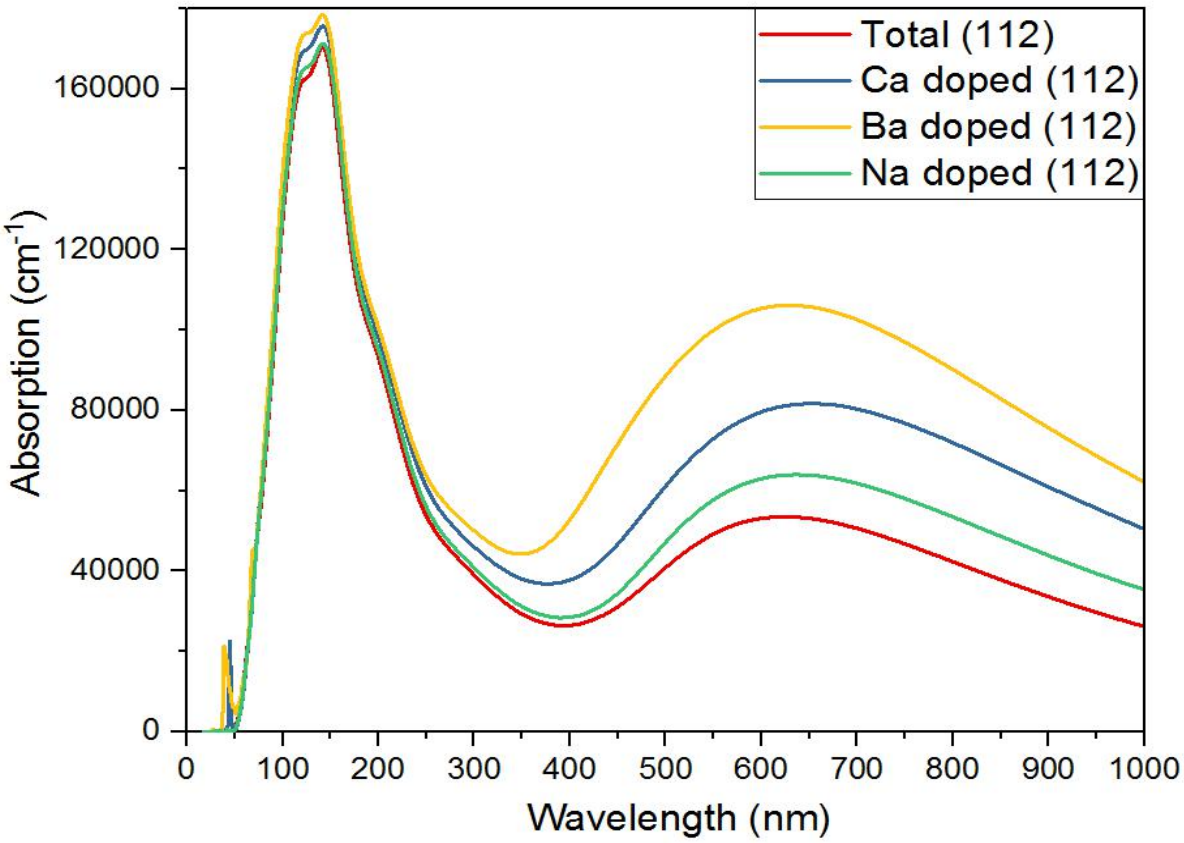


Figure 40. Absorption spectra of pure (total) and doped CZTS (112) surface.

CZTS was identified as kesterite type and it is said to have a direct band gap of 1.51 eV with an optical absorption coefficient of $1x10^4$ $cm^{-1}$ [96]. The highest absorption coefficient for the doped surface structures is for barium with $10x10^4$ $cm^{-1}$. Calcium and sodium have absorption coefficients of $8x10^4$ $cm^{-1}$ and $6x10^4$ $cm^{-1}$ respectively. Ba-doped surface gives the highest absorption peak on the visible region followed by the calcium and sodium. These peaks can be credited to the position of the elements on the periodic table and their photo-electrolytic properties. Doping of CZTS with Ba can improve the absorption coefficient of CZTS-based solar cells for application in renewable energy.

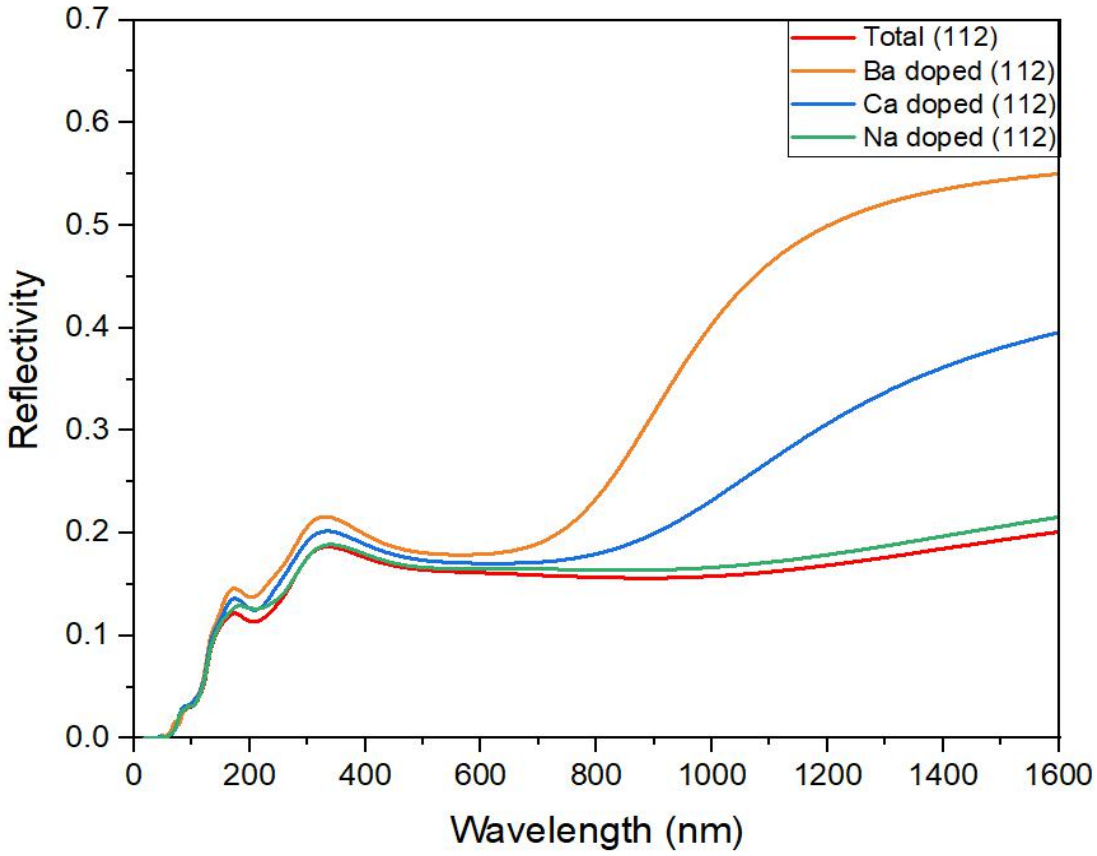


Figure 41. Reflectivity function of pure (total) and doped CZTS (112) surface.

Reflectivity in terms of wavelength is presented in Figure 41. The pure and doped (112) surfaces are tightly matched in the infrared region. Significant variations of the reflectivity spectra are observed in the visible region. Ba has the highest peak in both the infrared and visible regions. The Ba-doped spectrum shows an increase of reflectivity starting from the infrared moving into the visible region and a similar increase is observed in the visible region for undoped, Ca-doped and Na-doped curves. The reflectivity for Ba-doped curve is much higher in the visible region as expected.

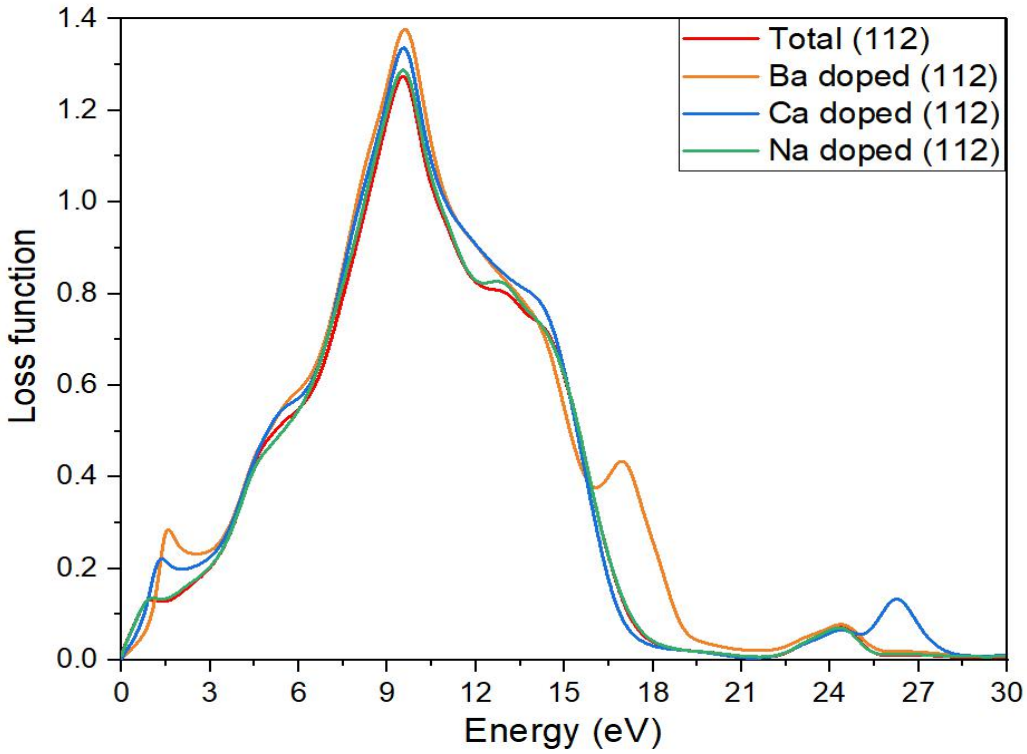


Figure 42. Energy loss function of pure (total) and doped CZTS (112) surface.

The energy loss function has one major peak for the pure and doped (112) surface. The peak occurs at 9-10 eV, this is the region of high reflectivity of the surface. There are two more visible peaks, one from 1.5 eV and another one between 25 and 27.5 eV, which is dominated by the presence of barium. At 1.5 eV there is evident for very low reflectivity as shown by the energy loss function peak. There is one shoulder peak due to the Ba doped curve on energies ranging from 15 to 20 eV. For energies greater than 33 eV, the graph is flat hence this may result in the material being transparent. There is a smaller peak for the Ca doped curve at 26.5 eV and a sudden drop to the Ba doped peak at 25 eV.

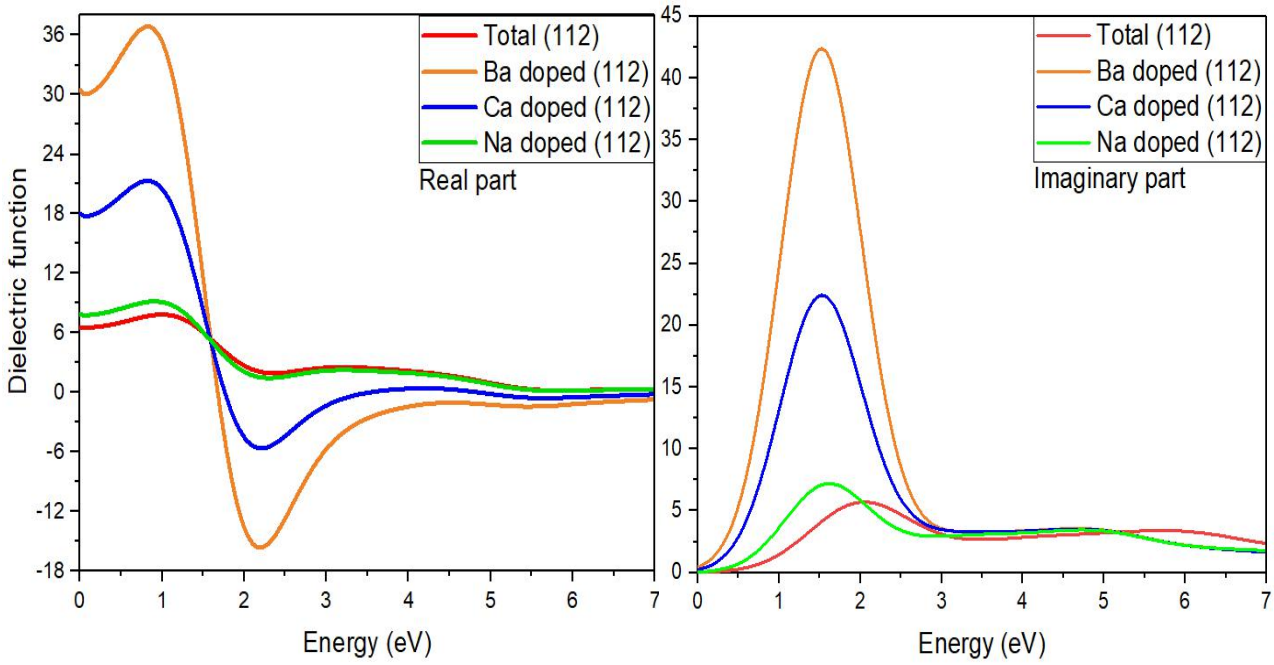


Figure 43. Dielectric function of pure (total) and doped CZTS (112) surface.

The real and the imaginary parts of the dielectric function against photon energy change are shown in Figure 43. The dielectric function describes the polarization and absorption of a material. The real part gives information about how much is the material polarized by an applied electric field and the imaginary part is for the absorption of photon in the material. The real part of the dielectric function falls below zero from 1.5-3.2 eV for Na-, Ca- and Ba-doped surface. The Ba-doped surface has a downward maximum peak at around 2 eV while the second peak is for Ca-doped at this energy. The difference between the peaks is largely noticeable for Ba- and Ca-doped surface, which is closely matched with the undoped (112) surface curve. The imaginary part has the highest peak for Ba-doped surface at approximately 1.5 eV, this corresponds to the band gap of CZTS.

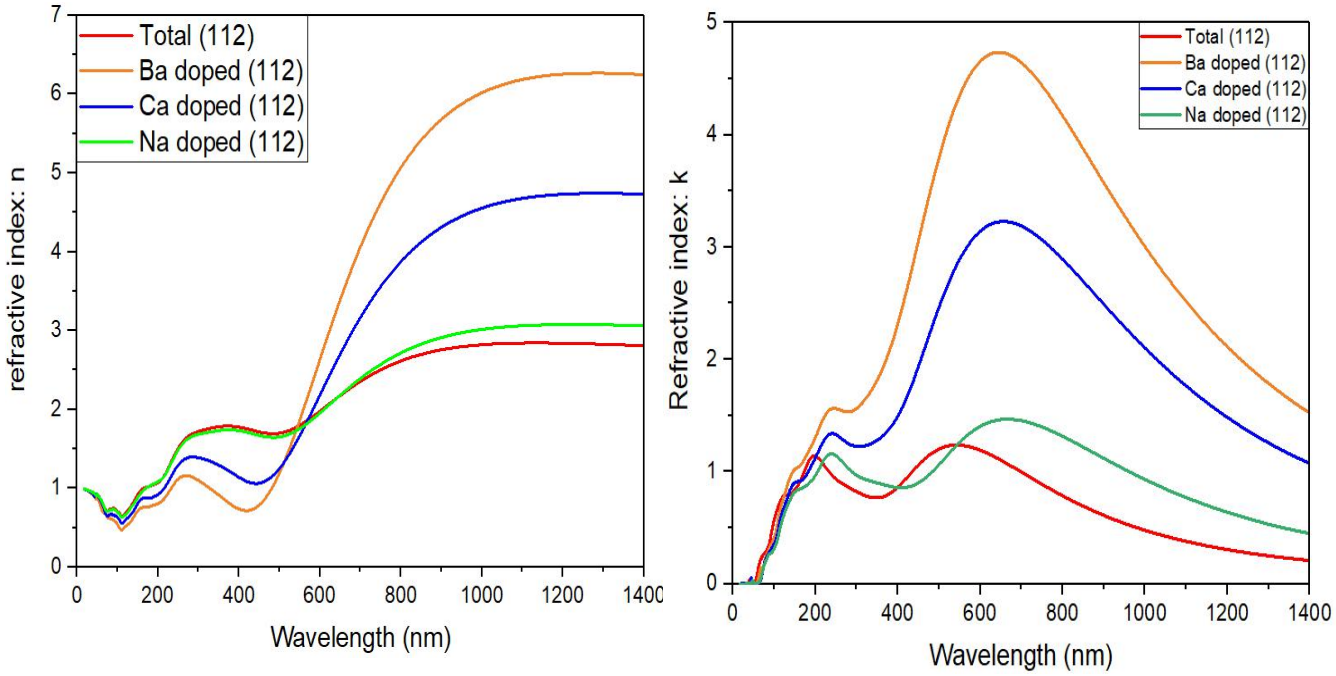


Figure 44. Refractive index of pure (total) and doped CZTS (112) surface.

Graphs of refractive index for doped CZTS (112) surface are presented in Figure 44. For the refractive index n, the Ba-doped spectrum is dominant over the Ca- and Na-doped spectra. The refractive index increases steadily for Ba doped on the visible region form being the lowest to the highest. The Ca- and Na-doped curves are closely matched with the pure (112) surface. At wavelengths of 600-700 nm, the curves are matched perfectly with the same refractive index. Below the wavelength range, Ba-doped spectrum indicates the lowest refractive index while the pure (112) surface spectrum maintains the highest. Above 750 nm, the curve for Ba-doped has the highest refractive index while the undoped plane is at the lowest. The extinction coefficient refractive index k has a sharp curve in the visible region leading to the infrared region.

# CHAPTER FIVE

## 5. Conclusion

In this work, we studied the optical and electronic properties of bulk CZTS and (112) surface using first principle calculations. The ground state conditions for the bulk structure were successfully determined and were comparable with literature results. The ground state energy was found to be 400 eV and the reciprocal space was 4x4x2 for the bulk CZTS. The calculated lattice parameters are found to be a = b = 5.470 Å and c = 10.920 Å. The band gap obtained with the assistance of scissors operator is 1.445 eV through calculations with the GGA functional and it is a direct band gap. Since the GGA functional underestimates the band gap, HSE06 functional was also used to verify the accuracy of the band gap calculations and energy band gap of 1.495 eV was found.

Semiconductors having band gap of ~ 1.5 eV can create electron-hole pairs in the visible region; most of the solar light falls on the infrared and visible regions and has maximum value in the visible region. CZTS film is a tetragonal structure with preferential orientation along the (112) plane. The CZTS (112) plane band gap is lower than the bulk CZTS structure, it indicates the existence of flat band and eliminates chances of having electron traps on the band gap. It is evident that doping CZTS (112) surface with either Ca, Ba or Na reduces the band gap and this could improve the efficiency of CZTS-based solar cells. The density of states showing the contribution of atomic states on the structure as well as the doped surfaces depict that sulphur dominates the valence band while tin dominates the conduction band. Copper and zinc have the lowest contribution towards the band gap in the conduction band. These findings showed that best CZTS solar cells are Cu-poor and Zn-rich.

Barium-doped CZTS (112) surface has the highest absorption and reflectivity on the valence band over calcium and sodium. The lowest adsorption energies for Na, Ca and Ba are -0.510 eV, -1.417 eV and -1.957 eV respectively. The band gap energies for the doped structures are 1.016 eV for Na, 1.020 eV for Ca and 1.029 eV for Ba with Na-

doped structure having the lowest yet very close to the others. The loss function spectrum is tightly matched with the maximum point located at 12.5 eV with Ba-doped spectra visibly the highest at this point. The dielectric function is at the highest for Ba-doped spectrum at low energies. The refractive index is also the highest spectrum on the visible region for Ba-doped CZTS curve. Ba-doped (112) surface present better results than calcium doped surface for improved CZTS-based solar cells, hence it could improve the efficiency of such photovoltaics.

The material class of kesterite, which CZTS belongs to, has crystal structure similar to that of chalcopyrite's, therefore similar electronic properties were expected. CZTS shows a p-type semiconducting behavior with a carrier concentration ~$10^{17}$ $cm^{-3}$, optical absorption coefficient ~ $10^{4}$ $cm^{-1}$ and direct band gap ~1.4 eV. These results suggest that doping with barium rather than calcium could improve the photocatalytic activity on the CZTS-based solar cells. High absorption and low reflectivity on the visible region are some of the ideal factors for an improved efficiency in solar cells. Reduced band gap to optimal values is also contributing to improvements in the efficiency of solar cells.

New thin-film solar cell materials and a greater understanding of their properties are needed to meet the urgent demand for sustainable, lower cost and scalable photovoltaics. Doping of semiconductors is expected to decrease the bandgap and improve its optical response for application in renewable energy technologies. The decrease of the bandgap size can be understood from the orbital hybrid interactions. For kesterite solar cells to present a commercially viable solution it will certainly be necessary to reach 15% efficiency. The results obtained from this study shared insights on how can researchers design better CZTS based solar cells.

## References

[1] R. Sen and S. C. Bhattacharyya, “Off-grid electricity generation with renewable energy technologies in India : An application of HOMER,” *Renew. Energy*, vol. 62, pp. 388–398, 2014.

[2] A. V. Herzog, T. E. Lipman, and D. M. Kammen, “Renewable energy sources,” *Encycl. Life*, pp. 1–63, 2001.

[3] R. Haas, G. Resch, C. Panzer, S. Busch, M. Ragwitz, and A. Held, “Efficiency and effectiveness of promotion systems for electricity generation from renewable energy sources - Lessons from EU countries,” *Energy*, vol. 36, pp. 2186–2193, 2011.

[4] B. A. M. A. Wadud, M. T. Zaman, F. Rabbee, and M. R. Rahman, “Renewable Energy: An Ideal Solution of Energy Crisis and Economic Development in Bangladesh,” *Glob. J. Res. Eng. Electr. Electron. Eng.*, vol. 13, 2013.

[5] J. A. Turner, “A Realizable Renewable Energy Future,” *Science New Series*, vol. 285, pp. 687–689, 2016.

[6] M. Jiang and X. Yan, “$Cu_2ZnSnS_4$ Thin Film Solar Cells : Present Status and Future Prospects,” *Sol. cells - Res. Appl. Perspect.*, pp. 107-141, 2013.

[7] S. Wenham, M. Green, M. Watt, R. Corkish, and A. Sproul, “Applied Photovoltaics - Google Books.” 2007.

[8] Department of Minerals and Energy/Republic of South Africa and Department of Minerals and Energy of the Republic of South Africa, “White Paper on Renewable Energy,” *Unfccc*, November, 2003.

[9] Department of Energy, “State of Renewable Energy in South Africa,” Pretoria, 2015.

[10] M. Maleka, L. Mashimbyane, and P. Goyns, *South african energy synopsis 2010*. pretoria: Department of Energy, 2010.

[11] S. Shauddin, “Comparison among Various Emerging PV Cells with History,

Current Status and Future Challenges," *Energy and Power*, vol. 3, pp. 91–105, 2013.

[12] W. Shockley and H. J. Queisser, "Detailed balance limit of efficiency of p-n junction solar cells," *J. Appl. Phys.*, vol. 32, pp. 510–519, 1961.

[13] S. R. Forrest, "The limits to organic photovoltaic cell efficiency," *MRS Bull.*, vol. 30, pp. 28–32, 2005.

[14] "Solar Panel Building DC Energy Systems." available at https://learn.libre.solar/system/solar_panel.html.

[15] "P-N Junction Diode Applications." available at https://en.wikipedia.org/wiki/P-n_junction.

[16] E. F. Feo, "The Future of Renewable Energy Financing," *Renewable Energy Features, Biomass*, January, pp. 1–13, 2008.

[17] Solar Tech USA, "Types of Solar Cells," available at https://fas.org/sgp/crs/misc/R42509.pdf, 2014.

[18] M. Green and X. Hao, "UNSW develops world-leading thin-film solar cells," *Australian Centre for Advanced Photovoltaics*, 2006.

[19] S. Mason, "Researchers use liquid inks to create better solar cells (layers)." University of California, Los Angeles, 2014.

[20] N. Bristow and J. Kettle, "Outdoor performance of organic photovoltaics: Diurnal analysis, dependence on temperature, irradiance, and degradation," *J. Renew. Sustain. Energy*, vol. 7, 2015.

[21] G. M. Ford, Q. Guo, R. Agrawal, and H. W. Hillhouse, "Earth Abundant Element $Cu_2ZnSnS_4$," *Chem. Mater.*, vol. 23, pp. 8–11, 2011.

[22] S. Ji and C. Ye, "$Cu_2ZnSnS_4$ as a New Solar Cell Material: The History and the Future," *Rev. Adv. Sci. Eng.*, vol. 1, pp. 42–58, 2012.

[23] A. Ritscher, J. Just, O. Dolotko, S. Schorr, and M. Lerch, "A mechanochemical route to single phase $Cu_2ZnSnS_4$ powder," *J. Alloys Compd.*, vol. 670, pp. 289-

296, 2016.

[24] W. Xiao, J.N Wang, X.S Xhao, J.W Wang, G.J Huang, L Cheng, L.J Jiang and L.G Wang, “Intrinsic defects and Na doping in CZTS: A density-functional theory study,” *Sol. Energy*, vol. 116, pp. 125–132, 2015.

[25] Online article, “CZTS - Wikipedia.” available at https://en.wikipedia.org/wiki/CZTS#:~:text=Copper%20zinc%20tin%20sulfide%20(CZTS,the%20sulfur%2Dselenium%20alloy%20CZTSSe.

[26] Z. Zhao and X. Zhao, “Electronic, optical, and mechanical properties of $Cu_2ZnSnS_4$ with four crystal structures,” *J. Semicond.*, vol. 36, pp. 083004, 2015.

[27] H. Katagiri, K Jimbo, W.S Maw, K Oishi, M Yamazaki, H Araki and A Takeuchi,, “Development of CZTS-based thin film solar cells,” *Thin Solid Films*, vol. 517, pp. 2455–2460, 2009.

[28] S. Byungha, G. Oki, Z. Yu, B. Nestor, C. Jay, and G. Supratik, “Thin film solar cell with 8.4% power conversion efficiency using an earth-abundant $Cu_2ZnSnS_4$ absorber,” *J. Optoelectron. Adv. Mater.*, vol. 21, pp. 72–76, 2013.

[29] Z. Y, Y.F Li, B Yao, R Deng, Z.H Ding, T Wu, G Yang, C.R Li, Z.Y Dong, L Liu, L.G Zhang and H.F Zhao, “Bandgap engineering of $Cu_2Cd_xZn_{1-x}SnS_4$ alloy for photovoltaic applications: A complementary experimental and first-principles study,” *J. Appl. Phys.*, vol. 114, pp. 183506, 2013.

[30] S. R. Hall, J. T. Szymanski, and J. M. Stewart, “Kesterite, $Cu_2(Zn,Fe)SnS_4$ and Stannite $Cu_2(Fe,Zn)SnS_2$, structurally similar but distinct minerals,” *Can. Mineral.*, vol. 16, pp. 131–137, 1978.

[31] I. Camps, J. Coutinho, M. Mir, A. da Cunha, M. Rayson, and P. Briddon, “Elastic and optical properties of $Cu_2ZnSn(Se_xS_{1-x})_4$ alloys : density functional calculations,” *Semicond. Sci. Technol*, vol. 115001, pp. 1–8, 2012.

[32] US DOE, “Solar Performance and Efficiency | Department of Energy,” *Washington DC*. 2013.

[33] P. Srivastava, P. Gupta, and A. Singh, “Critical Factors Affecting Efficiency of Maximum Power Point Tracking in Solar Cells,” vol. 7, pp. 2010–2015, 2015.

[34] A. E. Green, T. Sawada, and E. Shettle, “The middle ultraviolent reaching the ground,” *Photochem. Photobiol.*, vol. 19, pp. 251–259, 1974.

[35] “Electromagnetic Spectrum - Principles of Structural Chemistry.” available at https://www.quora.com/What-are-the-different-types-of-electromagnetic-waves-and-its-uses .

[36] D. B. Mitzi, O. Gunawan, T. K. Todorov, K. Wang, and S. Guha, “The path towards a high-performance solution-processed kesterite solar cell,” *Sol. Energy Mater. Sol. Cells*, vol. 95, pp. 1421–1436, 2011.

[37] C. G. Granqvist, “Transparent conductors as solar energy materials: A panoramic review,” *Sol. Energy Mater. Sol. Cells*, vol. 91, pp. 1529–1598, 2007.

[38] Z. Zongyan and Z. Xiang, “Electronic , optical , and mechanical properties of $Cu_2ZnSnS_4$ with four crystal structures,” *journal of semiconductors*, vol. 36, pp. 0–13, 2015.

[39] R. J. Deokate, A. D. Adsool, N. S. Shinde, S. M. Pawar, and C. D. Lokhande, “Structural and optical properties of spray-deposited $Cu_2ZnSnS_4$ thin films,” *Energy Procedia*, vol. 54, pp. 627–633, 2014.

[40] H. S. Min, “Optical properties of ternary thin films ( $Ni_3Pb_2S_2$) prepared by chemical bath deposition technique,” *Res. J. Chem. Environ.*, vol. 20, pp. 29-33, 2016.

[41] C. Wan, J. Zhao, S. Member, and Y. Song, “Photovoltaic and Solar Power Forecasting for Smart Grid Energy Management,” *J. Power Energy Syst.*, vol. 1, pp. 38–46, 2015.

[42] M. Kumar and C. Persson, “Absorber Materials : A Density Functional Theory Study,”*Int. J. of Theo. App. Sci.*, vol. 5, pp. 1–8, 2013.

[43] S. Schorr, “The crystal structure of kesterite type compounds: A neutron and X-

ray diffraction study," *Sol. Energy Mater. Sol. Cells*, vol. 95, pp. 1482–1488, 2011.

[44] J. P. Leitão, N. M. Santos, and P. A. Fernandes, "Study of optical and structural properties of CZTS thin films." *Thin Solid Films*, vol. 519, pp. 7390–7393, 2011.

[45] A. V. Kumar, N. K. Park, and E. T. Kim, "A simple chemical approach for the deposition of $Cu_2ZnSnS_4$ thin films," *Phys. Status Solidi*, vol. 211, pp. 1857–1859, 2014.

[46] Z. Y. Zhao and X. Zhao, "First-Principles Study on Doping Effects of Sodium in Kesterite $Cu_2ZnSnS_4$," *Inorganic Chemistry*, vol. 53, pp. 9235–9241, 2014.

[47] S. Chen, A. Walsh, X. G. Gong, and S. H. Wei, "Classification of lattice defects in the kesterite $Cu_2ZnSnS_4$ and $Cu_2ZnSnSe_4$ earth-abundant solar cell absorbers," *Adv. Mater.*, vol. 25, pp. 1522–1539, 2013.

[48] A. Nagaoka, H. Miyake, T Taniyama, K Kakimoto, Y Nose, M Scarpulla and K Yoshino, "Effects of sodium on electrical properties in $Cu_2ZnSnS_4$ single crystal," *Appl. Phys. Lett.*, vol. 104, pp. 152101, 2014.

[49] S. Siebentritt, M. Igalson, C. Persson, and S. Lany, "The electronic structure of chalcopyrites - Bands, point defects and grain boundaries," *Prog. Photovoltaics Res. Appl.*, vol. 18, pp. 390–410, 2010.

[50] L. Yalçin and R. Öztürk, "Performance comparison of c-Si, mc-Si and a-Si thin film PV by PVsyst simulation," *J. Optoelectron. Adv. Mater.*, vol. 15, pp. 326–334, 2013.

[51] W. Kohn and L. J. Sham, "Self-consistent equations including exchange and correlation effects," *Phys. Rev.*, vol. 140, pp. 1133-1138,1965.

[52] C. J. Bosson, M.T. Birch, D.P. Halliday, K.S Knight, C.C Tang, A.K. Kleppe and P.D.Hatton, "Crystal Structure and Cation Disorder in Bulk $Cu_2ZnSnS_4$ Using Neutron Diffraction and X-Ray Anomalous Scattering," *IEEE*, vol. 8, pp. 0405–0410, 2016.

[53] P. Xu, S. Chen, B. Huang, H. J. Xiang, X. Gong, and S. Wei, "Stability and

electronic structure of $Cu_2ZnSnS_4$ surfaces : First-principles study,"*Phys. Rev B.*, vol. 88,, pp. 1–8, 2013.

[54] S. K. Swami, A. Kumar, and V. Dutta, "Deposition of Kesterite $Cu_2ZnSnS_4$ (CZTS) Thin Films by Spin Coating Technique for Solar Cell Application," *Energy Procedia*, vol. 33, pp. 198–202, 2013.

[55] R. Seshadri, "Doping of semiconductors," in *Mrl.Ucsb.Edu*, pp. 1–4. avalable at https://www.mrl.ucsb.edu/~seshadri/old/MATRL100A/class12.pdf

[56] "Doping techniques - Waferfabrication - Semiconductor Technology from A to Z - Halbleiter." available at https://www.halbleiter.org/en/waferfabrication/doping/

[57] S. Meenakshi, "Pressure induced phase transition in defect chalcopyrite compounds," *J. Phys. Conf. Ser.*, vol. 377, pp. 1-6, 2012.

[58] S. Chen, J. H. Yang, X. G. Gong, A. Walsh, and S. H. Wei, "Intrinsic point defects and complexes in the quaternary kesterite semiconductor $Cu_2ZnSnS_4$," *Phys. Rev. B - Condens. Matter Mater. Phys.*, vol. 81, pp. 35–37, 2010.

[59] T. Maeda, S. Nakamura, and T. Wada, "First-Principles Study on Cd Doping in $Cu_2ZnSnS_4$ and $Cu_2ZnSnSe_4$," *Jpn. J. Appl. Phys.*, vol. 51, pp. 10NC11, 2012.

[60] O. P. Singh, A. Sharma, K. S. Gour, S. Husale, and V. N. Singh, "Fast switching response of Na-doped CZTS photodetector from visible to NIR range," *Sol. Energy Mater. Sol. Cells*, vol. 157, pp. 28–34, 2016.

[61] C. Tablero, "Electronic and photon absorber properties of cr-doped $Cu_2ZnSnS_4$," *J. Phys. Chem. C*, vol. 116, pp. 23224–23230, 2012.

[62] C. Tablero, "Effect of the oxygen isoelectronic substitution in $Cu_2ZnSnS_4$ and its photovoltaic application," *Thin Solid Films*, vol. 520, pp. 5011–5013, 2012.

[63] X. L. Zhang, M. M. Han, Z. Zeng, and Y. Duan, "The role of Sb in solar cell material $Cu_2ZnSnS_4$," *J. Mater. Chem. A.,* pp. 1–22, 2017.

[64] H. S. Craft, R. Collazo, Z. Sitar, and J. P. Maria, "A novel strategy to control defects and secondary phases of CZTS by surfactant Potassium," vol. 4, pp.

2105–2110, 2006.

[65] M. M. I. Sapeli, M. T. Ferdaous, S. A. Shahahmadi, K. Sopian, P. Chelvanathan, and N. Amin, “Effects of Cr doping in the structural and optoelectronic properties of $Cu_2ZnSnS_4$ (CZTS) thin film by magnetron co-sputtering,” *Mater. Lett.*, vol. 221, pp. 22–25, 2018.

[66] H. Dixit, N. Tandon, S, Cotteinier, R. Saniz, D. Lamoen, B. Partoens, V. Van speybroeck and M. Waroquier, “Electronic structure and band gap of zinc spinel oxides beyond LDA: $ZnAl_2O_4$, $ZnGa_2O_4$ and $ZnIn_2O_2$,” *New J. Phys.*, vol. 13, pp. 1–11, 2011.

[67] C. Malerba, F. Biccari, C. L. A. Ricardo, M. Valentini, R. Chierchia, M. Muller, A. Santori, E. Esposito, P. Mangiapane, P. Scardi and A. Mittiga, “CZTS stoichiometry effects on the band gap energy,” *J. Alloys Compd.*, pp. 1–32, 2013.

[68] S. J. Clark, M. D segall, C. J. Pickard, P. J. Hasnip, M. I. J. Probert, K. Refson and M. C. Payne, “First principles methods using CASTEP,” *Zeitschrift für Krist.*, vol. 220, pp. 567–570, 2005.

[69] D. M. Brink, “Density functional theory,” *Nucl. Phys. News*, vol. 12 , pp. 27–32, 2002.

[70] Payne M. C., M. P. Teter, D. C. Allan, T. A. Arias, and J. D. Joannopoulos, “Iterative minization techniques for ab initio total-energy calculations: molecular dynamics and conjugate gradient,” *Rev. Mod. Phys.*, vol. 64, pp. 1045–1097, 1992.

[71] J. Riess and W. Münch, “The theorem of hohenberg and kohn for subdomains of a quantum system,” *Theor. Chim. Acta*, vol. 58, pp. 295–300, 1981.

[72] W. Kohn, A. Savin, and C. A. Ullrich, “Hohenberg-Kohn theory including spin magnetism and magnetic fields,” *Int. J. Quantum Chem.*, vol. 100, pp. 20–21, 2004.

[73] A. F. Oliveira, G. Seifert, T. Heine, and H. A. Duarte, “Density-functional based tight-binding: An approximate DFT method,” *J. Braz. Chem. Soc.*, vol. 20, pp.

1193–1205, 2009.

[74] A. Stan, N. E. Dahlen, and R. Van Leeuwen, “Levels of self-consistency in the GW approximation,” *J. Chem. Phys.*, vol. 130, pp. 1–11, 2009.

[75] S. Kurth, M. Marques, M. Lüders, and E. K. U. Gross, “Local Density Approximation for Superconductors,” *Physical review Letters*, vol. 83, pp. 2628-2631, 1999.

[76] E. W. Brown, B. K. Clark, J. L. Dubois, and D. M. Ceperley, “Path-Integral Monte Carlo Simulation of the Warm Dense Homogeneous Electron Gas,” *Physical Review Letters*, vol. 110, , pp. 1–5, 2013.

[77] J. Toulouse, “Introduction to density-functional theory,” pp. 1-58, 2019.

http://www.lct.jussieu.fr/pagesperso/toulouse/enseignement/introduction_dft.pdf

[78] J. R. Yates, C. J. Pickard, and F. Mauri, “Calculation of NMR chemical shifts for extended systems using ultrasoft pseudopotentials,” *Phys. Rev. B - Condens. Matter Mater. Phys.*, vol. 76, pp. 1–11, 2007.

[79] P. Schwerdtfeger, “The Pseudopotential Approximation in Electronic Structure Theory,” *ChemPhysChem*, Vol. 12, pp. 3143–3155, 2011.

[80] M. Payne, M. Teter, D. Allan, T. Arias, and J. Joannopoulos, “Iterative minimisation techniques for ab inito total energy calculations MD and CG,” *Rev. Mod. Phys.*, vol. 64, pp. 1045, 1992.

[81] M. Eder, J. Hafner, and E. G. Moroni, “Structural, electronic, and magnetic properties of thin Mn/Cu (100) films,” *Phys. Rev. B*, vol. 61, pp. 11492, 2000.

[82] Computational results obtained using software programs from Dassault Systemes BIOVA. The *ab initio* calculations were performed with the CASTEP program, and graphical display generated with BIOVA Materials Studio, “Modules Tutorials,” 2017.

[83] J. P. Perdew, J. A. Chevary, S. H. Vosko, K. A. Jackson, M. R. Pederson, D. J. Singh and C. Fiolhais, “Atoms, molecules, solids, and surfaces: Applications of

the generalized gradient approximation for exchange and correlation," *Physical Review B*, vol. 46,pp. 6671-6687, 1992.

[84] J. D. Pack and H. J. Monkhorst, "'special points for Brillouin-zone integrations'-a reply," *Phys. Rev. B*, vol. 16, pp. 1748-1749, 1977.

[85] S. Kim, J. Park, S. N. Hood, and A. Walsh, "Lone-pair effect on carrier capture in $Cu_2ZnSnS_4$ solar cells," *J. Mater. Chem. A*, vol. 1, pp. 1-8, 2019.

[86] C. Dun, N. A. W. Holzwarth, Y. Li, W. Huang and D. L. Carrol, "$Cu_2ZnSnS_xO_{4x}$ and $Cu_2ZnSnS_xSe_{4x}$: First principle simulations of optimal alloy configurations and their energies," vol. 193513, pp. 1-12, 2014.

[87] X. D. Chen, L. Chen, Q. Q. Sun, P. Zhou, and D. W. Zhang, "Hybrid density functional theory study of $Cu(In_{1-x}Ga_x)Se_2$ band structure for solar cell application," *AIP Adv.*, vol. 4, pp. 087118, 2014.

[88] J. L. Shay and J. H. Wernick, *Chapter 1-introduction - Ternary Chalcopyrite Semiconductors: Growth, Electronic Properties, and Applications*, vol. 7, pp. 1-3,1975.

[89] K. N. Basri, N. A. Zabidi, H. Abu Kassim, and A. N. Rosli, "Density Functional Theory (DFT) Calculation of Band Structure of Kesterite," *Adv. Mater. Res.*, vol. 1107, pp. 491-495, 2015.

[90] M. Kumar and C. Persson, "$Cu_2ZnSnS_4$ and $Cu_2ZnSnSe_4$ as Potential Earth-Abundant Thin-Film Absorber Materials: A Density Functional Theory Study," *Int. J. Theor. Appl. Sci.*, vol. 5, pp. 1-8, 2013.

[91] C. Persson, "Electronic and optical properties of $Cu_2ZnSnS_4$ and $Cu_2ZnSnSe_4$," *J. Appl. Phys.*, vol. 107, pp. 053710, 2010.

[92] H. He, R. Orlando, M. A Blanco, R. Pandey, E. Amzallag, I. Baraille and M. Rérat, "First-principles study of the structural, electronic, and optical properties of $Ga_2O_3$ in its monoclinic and hexagonal phases," *Phys. Rev. B - Condens. Matter Mater. Phys.*, vol. 74, pp. 1-8, 2006.

[93] N. M. Ravindra, P. Ganapathy, and J. Choi, “Energy gap-refractive index relations in semiconductors - An overview,” *Infrared Phys. Technol.*, vol. 50, pp. 21-29, 2007.

[94] W. Li, K Jiang, J Zhang, X Chen, Z Hu, S Chen, L Sun and J Chu., “Temperature dependence of phonon modes, dielectric functions, and interband electronic transitions in $Cu_2ZnSnS_4$ semiconductor films,” *Phys. Chem. Chem. Phys.*, vol. 14, pp. 9936, 2012.

[95] P. Xu, S. Chen, B. Huang, H. J. Xiang, X. G. Gong, and S. H. Wei, “Stability and electronic structure of $Cu_2ZnSnS_4$ surfaces: First-principles study,” *Phys. Rev. B - Condens. Matter Mater. Phys.*, vol. 88, pp. 1-8, 2013.

[96] S. Das, K. C. Mandal, and R. N. Bhattacharya, “Earth-Abundant $Cu_2ZnSn(S,Se)_4$ (CZTSSe) Solar Cells,” pp 25-41, 2016.